



**HAL**  
open science

# Hydrogen-Bonded Open-Framework with Pyridyl-Decorated Channels: Straightforward Preparation and Insight into its Affinity for Acidic Molecules in Solution

Georges Mouchaham, Nans Roques, Walid Khodja, Carine Guyard-Duhayon,  
Yannick Coppel, Stéphane Brandès, Tamás Fodor, Michel Meyer, Jean-Pascal  
Sutter

► **To cite this version:**

Georges Mouchaham, Nans Roques, Walid Khodja, Carine Guyard-Duhayon, Yannick Coppel, et al.. Hydrogen-Bonded Open-Framework with Pyridyl-Decorated Channels: Straightforward Preparation and Insight into its Affinity for Acidic Molecules in Solution. *Chemistry - A European Journal*, 2017, 23 (49), pp.11818-11826. 10.1002/chem.201701732 . hal-01563184

**HAL Id: hal-01563184**

**<https://u-bourgogne.hal.science/hal-01563184>**

Submitted on 17 Dec 2021

**HAL** is a multi-disciplinary open access archive for the deposit and dissemination of scientific research documents, whether they are published or not. The documents may come from teaching and research institutions in France or abroad, or from public or private research centers.

L'archive ouverte pluridisciplinaire **HAL**, est destinée au dépôt et à la diffusion de documents scientifiques de niveau recherche, publiés ou non, émanant des établissements d'enseignement et de recherche français ou étrangers, des laboratoires publics ou privés.

# Hydrogen-bonded open-framework with pyridyl-decorated channels: Straightforward preparation and insight into its affinity for acidic molecules in solution

Georges Mouchaham,<sup>a,b</sup> Nans Roques,<sup>\*a,b</sup> Walid Khodja,<sup>a,b</sup> Carine Duhayon,<sup>a,b</sup> Yannick Coppel,<sup>a,b</sup> Stéphane Brandès,<sup>c</sup> Tamás Fodor,<sup>c</sup> Michel Meyer,<sup>c</sup> and Jean-Pascal Sutter <sup>\*a,b</sup>

<sup>a</sup> CNRS, LCC (Laboratoire de Chimie de Coordination), 205 route de Narbonne, F-31077 Toulouse, France.

<sup>b</sup> Université de Toulouse, UPS, INPT, F-31077, Toulouse, France.

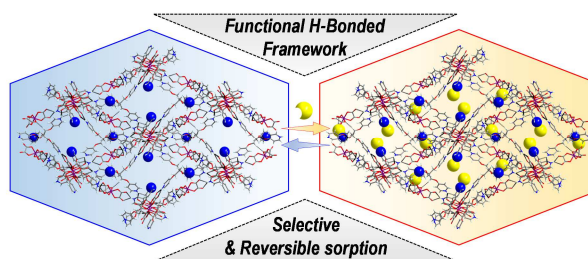
<sup>c</sup> Institut de Chimie Moléculaire de l'Université de Bourgogne (ICMUB), UMR 6302 CNRS, Université de Bourgogne–Franche-Comté, 9 avenue Alain Savary, BP 47870, F-21078 Dijon Cedex, France.

\* e-mail : [sutter@lcc-toulouse.fr](mailto:sutter@lcc-toulouse.fr) ORCID : [orcid.org/0000-0003-4960-0579](https://orcid.org/0000-0003-4960-0579)

[Nans.roques@lcc-toulouse.fr](mailto:Nans.roques@lcc-toulouse.fr)

## Table of content entry

A hydrogen-bonded open framework (53% of accessible void) with pores decorated by pyridyl groups, shows remarkable affinity for acidic organic molecules in solution.



**Abstract :**

An hydrogen-bonded open framework with pores decorated by pyridyl groups has been constructed following an off-charge-stoichiometry assemblage of protonated tetrakis(4-pyridyl-oxymethyl)methane and  $[\text{Al}(\text{oxalate})_3]^{3-}$ , respectively the H-bond donor and acceptor of the ionic H-bond interactions. This supramolecular porous architecture (**SPA-2**) possesses 1 nm-large pores interconnected in 3D with high solvent accessible void (53%). It demonstrated remarkable affinity for acidic organic molecules in solution, which was investigated by the means of various carboxylic acids including larger drug molecules. Noteworthy, competing sorption between acetic acid and its halogenated homologues evidenced good selectivity of the porous material for the halogenated acids. The gathered results, including a series of guest@**SPA-2** crystal structures and HRMAS-NMR, suggest that the efficient sorption exhibited by the material not just relies on an acid-base interaction. The facile release of these guests' molecules in neutral conditions makes this SPA a carrier of acidic molecules.

## INTRODUCTION

Microporous hydrogen-bonded frameworks are an emerging class of materials<sup>[1]</sup> reminiscent to MOFs (Metal-Organic Frameworks) and COFs (Covalent Organic Frameworks) for which high surface area and potential in the fields of gas sorption/separation have been highlighted only in recent years.<sup>[2]</sup> To date, very little attention has been given to their sorption properties in liquid media,<sup>[2d, 2e, 2g, 3]</sup> however selective sequestration, chemical transformation, sorption and sensing in solutions represent huge domains of use for microporous materials.<sup>[4]</sup> Such functionalities rely heavily on specific chemical groups decorating the inner channels, thereby imparting selective sorption, catalytic activity, detection, etc. to the microporous materials.<sup>[2d, 2e, 2g, 5]</sup> For instance, basic sites play an essential role in recognition of acidic molecules and metal ions.<sup>[6]</sup>

The building-blocks design<sup>[7]</sup> and/or post-synthetic modification<sup>[8]</sup> are widely used strategies to implant specific chemical functions in molecule-based materials. However, the construction of H-bonded frameworks displaying basic sites in their channels is particularly challenging because of the propensity of such groups to act as H-bond acceptors leading them to be involved in the H-bonded network during the assembling procedure.

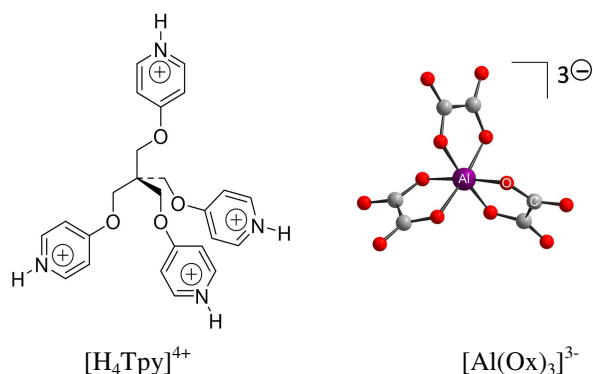
Our design of supramolecular porous architectures (SPA)<sup>[9]</sup> follows a bimolecular approach,<sup>[2h, 2p, 10]</sup> involving anionic metal-oxalato complexes and protonated amine derivatives (typically pyridine or imidazole), respectively acting as H-bond acceptor  $[A]^{x-}$  and donor  $[D-H]^{y+}$  units, assembled by strong ionic H-bonds.<sup>[11]</sup> Following this approach, hybrid frameworks characterized by permanent porosity, large pore size (1 nm), and remarkable thermal and chemical robustness can be achieved.<sup>[12]</sup> These supramolecular architectures usually result from a charge-stoichiometry assemblage between the cationic and anionic units (e.g.  $2 [D-H]^{3+} / [A]^{6-}$  in **SPA-1**<sup>[12]</sup>), yielding neutral networks in which all the cationic D-H moieties are involved in H-bonding with the anionic metal complexes. We are now

considering the possibility to achieve off-charge-stoichiometry associations, reasoning that this would leave the D-H group with the charge in excess untouched by the cation-anion association and thus provide direct access to porous supramolecular materials decorated by basic groups. This original approach proved successful yielding the unprecedented microporous supramolecular architecture **SPA-2** reported herein. This crystalline solid exhibits large 3D pores with high solvent accessible voids and channels decorated by pyridyl groups. The **SPA-2** material demonstrates high affinity toward various carboxylic acids, including larger drug molecules. The gathered results, including a series of guest@**SPA-2** crystal structures, suggest that the efficient sorption properties exhibited by the material do not rely solely on an acid-base interaction. Interestingly, the facile release of these guest molecules in neutral conditions makes this SPA a possible acid carrier material.

## RESULTS AND DISCUSSION

**Synthesis of the SPA-2 Material.** The hydrogen-bonded supramolecular architecture of formula  $[(H_3Tpy)Al(Ox)_3]$ , **SPA-2** in the following, was obtained by reacting aluminum(III)-oxalate complex  $[Al(Ox)_3]^{3-}$  and protonated tetrakis(4-pyridyl-oxymethyl)methane,  $[H_4Tpy]^{4+}$ , in a 1:1 ratio in  $H_2O$  (Scheme 1). The tetrapyridinium cation was generated *in-situ* by imposing an acidic medium ( $pH \approx 2$ ) with  $HNO_3$ . Upon addition of EtOH to the reaction mixture, octahedron-shaped single crystals of the protonated material **SPA-2**· $HNO_3$  were formed in good yields. The  $HNO_3$ -free material, **SPA-2**, was generated subsequently by washing the crystals with a diluted solution of pyridine in ethanol or simply washing thoroughly the crystals of **SPA-2**· $HNO_3$  with an EtOH/ $H_2O$  (3:1 v/v) solution.  $HNO_3$  removal was confirmed by IR (the nitrate characteristic band at  $1385\text{ cm}^{-1}$  disappears during the washing step), thermogravimetric analyses (the bump ascribed to the formation of  $NO_2$  from  $NO_3^-$  upon heating **SPA-2**· $HNO_3$  is missing in the TGA trace of **SPA-2**),<sup>[13]</sup> and by

compositional analyses (EA) (see experimental section and ESI). Powder X-ray diffraction (Figure S9) confirmed that the crystallinity of the material remained unaffected by removal of HNO<sub>3</sub>. The facile elimination of HNO<sub>3</sub> upon washing can be related to the relatively weak basicity of the pyridyl units of Tpy in **SPA-2**. The detailed investigation of the acid-base properties of the conjugated free-base Tpy revealed stepwise protonation constants ranging from log  $K_{011} = 5.8(2)$  to log  $K_{014} = 4.3(1)$ , for mono- to tetra-protonation (in MeOH/H<sub>2</sub>O 8:2 v/v solution,  $I = 0.2$  M KCl,  $T = 298.2(1)$  K). As a matter of comparison, in same conditions the protonation constant of pyridine was log  $K_{011} = 3.87(1)$ , whereas for 4-methoxypyridine a log  $K_{011}$  of ca 5.2 is estimated. A detailed discussion on the physico-chemical investigation for Tpy can be found in the Supporting Information.



**Scheme 1.** Molecular building units involved in the formation of **SPA-2**: (*left*) tetrakis(4-pyridinium-oxymethyl)methane ( $H_4Tpy^{4+}$ ) and (*right*) aluminum trisoxalate complex  $[Al(Ox)_3]^{3-}$  ( $NO_3^-$  and  $K^+$  counter-ions are omitted).

**Crystal Structure and Physical Properties of the SPA-2 Material.** The robustness of the framework applied also to single crystals, which allowed to investigate the structures for both **SPA-2·HNO<sub>3</sub>** and **SPA-2** by single crystal diffraction studies. **SPA-2·HNO<sub>3</sub>** indifferently crystallized in the complementary chiral space groups  $P4_12_12$  or  $P4_32_12$ ; both were systematically found in a crystal batch. Its asymmetric unit comprises one  $[H_4Tpy]^{4+}$ , one

$[\text{Al}(\text{Ox})_3]^{3-}$ , and one  $\text{NO}_3^-$  together with 14.75  $\text{H}_2\text{O}$  found over 30 crystallographic positions (for additional information see ESI). The supramolecular architecture of **SPA-2**· $\text{HNO}_3$  (Figure 1a) results from H-bond linkages between the organic cations and the metal-complex anions. Each organic cation is bound to three different  $[\text{Al}(\text{Ox})_3]^{3-}$  and each metal-complex unit reciprocally connects three different  $[\text{H}_4\text{Tpy}]^{4+}$  (Figure S2). In this arrangement, three pyridinium moieties of an organic unit are involved in H-bonds with metal-oxalates, whereas the fourth stays outside this network. This latter group is found in close proximity of an  $\text{NO}_3^-$  ( $d_{\text{Npyridinium}\cdots\text{O}^-\text{nitrate}} = 2.77 \text{ \AA}$ ), suggesting H-bonding between them.

The H-bonded network formed by  $[\text{H}_4\text{Tpy}]^{4+}$  and  $[\text{Al}(\text{Ox})_3]^{3-}$  generates 2D corrugated honeycomb-like layers, whose folds are decorated by dangling pyridinium groups (Figure S3). Such layers develop both in the *ac* and *bc* crystallographic planes leading to mutual interpenetration that generates the overall 3D framework structure shown by **SPA-2**· $\text{HNO}_3$  (Figure 1a and Figure S4 and S5). In this inclined polycatenated framework,<sup>[14]</sup> two sets of interlocked honeycomb layers are almost perpendicular to each other with an angle of  $89.98^\circ$  between their mean planes (see Figure S4). This arrangement yields infinite crisscrossed channels running along *b* and *c* crystallographic directions. The pyridinium- $\text{NO}_3$  moieties are located at the intersections of the channels, which accounts for the reduced apparent aperture of the channels (*ca*  $6 \times 4 \text{ \AA}^2$ , when van der Waals radii are considered). The volume within the channels is occupied by guest solvent molecules but only *ca* twelve  $\text{H}_2\text{O}$  could be localized in the asymmetric unit by crystallography. When these are neglected, a potential void volume of 49.7% is determined using PLATON,<sup>[15]</sup> this represents a volume of  $6175 \text{ \AA}^3$  per  $12437 \text{ \AA}^3$  of the unit cell. Additional information on the guests composition was supplied by  $^1\text{H-NMR}$  spectroscopy, TGA, and EA (see ESI) leading to the formulation  $[(\text{H}_4\text{Tpy})\text{NO}_3\text{Al}(\text{Ox})_3] \cdot 23 \text{ H}_2\text{O} \cdot 2\text{EtOH}$  for **SPA-2**· $\text{HNO}_3$ .

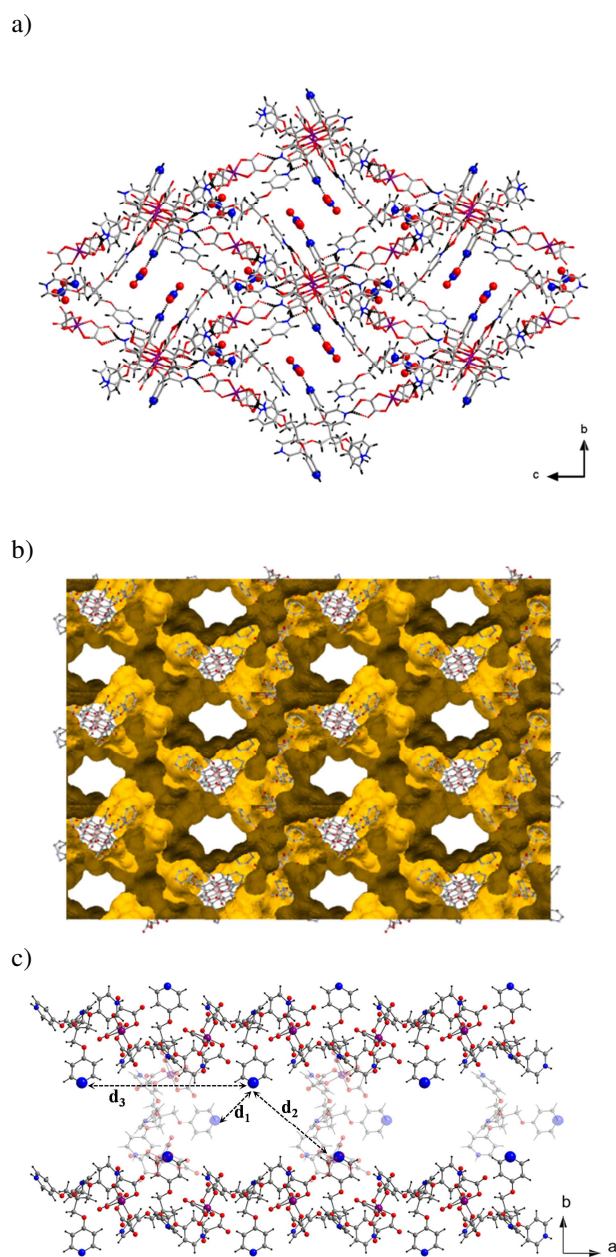


**Figure 1.** Supramolecular architectures of **SPA-2·HNO<sub>3</sub>** and **SPA-2**. (a) Ball and stick representation for the supramolecular framework of **SPA-2·HNO<sub>3</sub>**; the NO<sub>3</sub><sup>-</sup> units and the N-atoms of the pyridyl groups linked to them are highlighted; (b) representation for **SPA-2** highlighting the voids within the framework, the yellow skin is the contact surface of a spherical probe of 1.2 Å radius with the channels' walls; (c) Sectional pore view along *c* highlighting the arrangement of the free-pyridyl groups within a channel,  $d_1 = 11.4 \text{ \AA}$ ,  $d_2 = 12.0 \text{ \AA}$  and  $d_3 = 18.0 \text{ \AA}$ . Color codes: C, grey; H, black, N, blue; O, red; solvent molecules are not shown.

The crystal structure for **SPA-2** confirmed the elimination of HNO<sub>3</sub> and an unchanged supramolecular organization with respect to **SPA-2**·HNO<sub>3</sub> (Figure 1b and S11). Removal of HNO<sub>3</sub> leads to enlarged pore apertures (*ca* 7.5 × 6 Å<sup>2</sup>), while potential void volume is concomitantly increased to 53%.<sup>[15]</sup> Structure examination also reveals additional smaller channels (*ca* 6 × 3 Å<sup>2</sup>) along the [111] crystallographic direction (Figure S12), which are partly occluded in **SPA-2**·HNO<sub>3</sub>. The pyridyl groups decorating the main channels have a helical arrangement with separations to the first neighbors of 11.4, 12.0, and 18.0 Å (N<sub>py</sub>···N<sub>py</sub> distances, Figure 1c). Diffraction data allowed to localize 10.5 H<sub>2</sub>O in the asymmetric unit but full guest composition was deduced from <sup>1</sup>H-NMR, TGA and EA (see ESI) leading to the formulation [(H<sub>3</sub>Tpy)Al(Ox)<sub>3</sub>]·17.7H<sub>2</sub>O·0.6EtOH for **SPA-2**.

**SPA-2** loses part of its guest molecules at 298 K when crystals are removed from their mother liquors but its crystallinity is not affected over a period of 24 h (Figure S14). Diffraction data, both for a single crystal and for a powder sample, indicate a slight change of cell parameters. For longer times, the solid turns progressively amorphous and the same occurs when the solid is activated at 298 K in vacuum. This activated material did not adsorb gases such as N<sub>2</sub> or CO<sub>2</sub>, suggesting a flexible architecture that compacts upon guest release. The lack of gas adsorption is then ascribed to a reduced aperture of the channels during the activation process, and their pore size probably falls in the same order of magnitude than the guest size itself (CO<sub>2</sub>, 3.3 Å and N<sub>2</sub>, 3.64 Å). However, its crystallinity was fully regenerated in a few minutes when the amorphous solid was soaked in a 4:1 v/v EtOH/H<sub>2</sub>O mixture (Figure S14). The **SPA-2** belongs to the type I compound of the third generation of porous solvated solids as defined by Kitagawa.<sup>[16]</sup>

**SPA-2** proved very stable in common organic solvents (alcohols, acetone, chloroform, THF, acetonitrile, etc.) and was found to exchange guest molecules with the liquid media (Figure S15-S16). Solution <sup>1</sup>H-NMR spectroscopy in D<sub>2</sub>O performed on crystals dissolved after being

soaked in a given liquid allowed to evaluate the amount of adsorbed molecule per  $[(\text{H}_3\text{Tpy})\text{Al}(\text{Ox})_3]$  formula unit to 10.7 for MeOH, 7 for EtOH, 6 for *i*PrOH, 4 for acetone, 2.3 for THF, and 4.6 for MeCN (Figure S17), in addition to residual H<sub>2</sub>O that was not quantified. Guest exchange in absolute EtOH was found to be fast with an increase from 0.6 molecules in as-synthesized **SPA-2** to 7 EtOH in only 4 h with concomitant reduction of the H<sub>2</sub>O contents to 3.5 molecules (ESI). In the following, EtOH@**SPA-2** will refer to such crystals of **SPA-2** kept in absolute EtOH.

**Sorption Properties of the SPA-2 Material.** The capability for **SPA-2** to adsorb acidic organic molecules in solution was investigated with acetic acid and a series of its halogenated derivatives (experimental procedure and details of the compositional characterizations can be found in the SI). <sup>1</sup>H-NMR of acid@**SPA-2** crystals dissolved in D<sub>2</sub>O and elemental analysis have been used to quantify the number of guest molecules; the results discussed below, and gathered in Table 1, are given with respect to the SPA formula unit,  $[(\text{H}_3\text{Tpy})\text{Al}(\text{Ox})_3]$ . All experiments have been repeated at least three times with results showing less than 10% of deviation. When EtOH@**SPA-2** was soaked in a 3 M solution of CH<sub>3</sub>COOH in EtOH, an uptake of three molecules of acetic acid was observed in less than 15 minutes (Figure 2) and this amount remained unchanged for longer immersion times. Halogenated derivatives showed the same behavior with a number of adsorbed molecules depending on their steric demand rather than on their p*K*<sub>a</sub> (Table 1). For instance, for CCl<sub>3</sub>COOH, the bulkiest acid of the series, the adsorption curve saturates for 1.5 molecules while it is a stronger acid than CH<sub>3</sub>COOH. It can be noticed that for all the carboxylic acids the number of adsorbed molecules is larger than what would be expected for just an acid-base interaction with the pyridyl site (i.e. uptake of one equivalent).

Reducing the acid concentration to 0.3 M hardly changed the sorption feature with an uptake of 2.8 CH<sub>3</sub>COOH molecules, although the time to reach saturation was slightly increasing

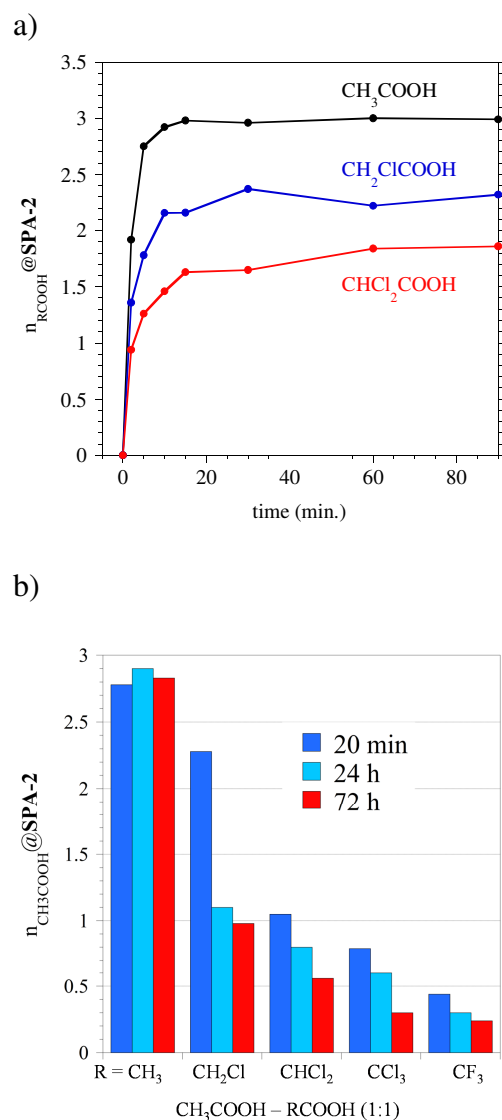


**Figure 2.** Sorption of acid molecules as a function of sorption time for crystals soaked in 3 M ethanol solutions of  $\text{CH}_3\text{COOH}$  (black),  $\text{ClCH}_2\text{COOH}$  (blue) and  $\text{Cl}_2\text{CHCOOH}$  (red); (b) acetic acid guest in competing  $\text{CH}_3\text{COOH}/\text{RCOOH}$  sorption as a function of R and time (20 min, blue; 1 day, light-blue; 3 days, red)

(Figure S24a). Reducing further the concentration to 0.03 M lead to a much slower adsorption with only 0.7 molecules adsorbed after 90 min but saturation was not reached. Such a behavior shows that the interaction between **SPA-2** and the carboxylic acid is not strong and release is possible. Indeed, rinsing thoroughly  $\text{CH}_3\text{COOH}@SPA-2$  crystals with EtOH was sufficient to remove most of the acetic acid hosted in the channels (Figure S24b and S25), much like for  $\text{HNO}_3$ . This release was found less efficient for  $\text{CF}_3\text{COOH}@SPA-2$  that still

exhibited a characteristic IR band for C-F ( $1130\text{ cm}^{-1}$ , Figure S26) after the crystals have been rinsed with EtOH, though its intensity was reduced. Addition of some pyridine (0.01 M) to EtOH was required to reach a complete removal of  $\text{CF}_3\text{COOH}$ . This stronger retention for  $\text{CF}_3\text{COOH}$  indicated that the strength of the interactions with the supramolecular frameworks may vary significantly depending on the characteristics of the carboxylic acids and suggested a possible discrimination between the acids by **SPA-2**.

**Table 1.**  $\text{RCOOH}@$ **SPA-2** : Number ( $n$ ) of Carboxylic Acid Molecules Adsorbed by **SPA-2**.

	$\text{p}K_{\text{a}}^{[17]}$	$n^a$	<i>Competitive sorption: <math>n_{\text{CH}_3\text{COOH}}</math> versus <math>n_{\text{RCOOH}}^b</math></i>				
$\text{CH}_3\text{COOH}$	4.76	3.0	2.8 <sup>c</sup>	1.0	0.6	0.3	0.3
$\text{CH}_2\text{ClCOOH}$	2.87	2.4		2.0			
$\text{CHCl}_2\text{COOH}$	1.35	2.0			1.5		
$\text{CCl}_3\text{COOH}$	0.66	1.5				not quantified	
$\text{CF}_3\text{COOH}$	0.52	1.65					not quantified

<sup>a</sup> For EtOH@**SPA-2** soaked for 90 min in a 3 M solution of the considered carboxylic acid in EtOH at 293 K. <sup>b</sup> For competitive sorption after 72 h, each column indicates the composition in  $\text{CH}_3\text{COOH}$  and second acid as deduced by  $^1\text{H}$  NMR, see Figures S29-30. <sup>c</sup> Blank experiment with only  $\text{CH}_3\text{COOH}$ . Based on solution  $^1\text{H}$  NMR data except for the trihalogenated derivatives. For additional guest content (EtOH and  $\text{H}_2\text{O}$ ) content, see SI.

This was confirmed by competitive sorption experiments performed with equimolar amounts of  $\text{CH}_3\text{COOH}$  and one of the halogenated acids. For the chlorinated derivatives, a clear decrease of the number of acetic acid in **SPA-2** was observed with the increase of the halogen substituents of the competing acid (Figure 2b). For instance, while for the blank experiment (i.e. only acetic acid) 2.80  $\text{CH}_3\text{COOH}$  were found in **SPA-2** after 20 min immersion, this value was reduced to 1.20, 1.05 and 0.79 in the presence of chloro-, dichloro- and trichloro-acetic acid, respectively. This result clearly disclosed a direct correlation between the interaction strength of **SPA-2** and the carboxylic acids with their  $\text{p}K_{\text{a}}$ . Longer soaking times (24 h and 72 h) lead to progressive exchange of adsorbed acetic acid for the halogenated acid (Table 1, Figures S29-S30), while the amount of adsorbed  $\text{CH}_3\text{COOH}$  remained constant in the reference experiment. The affinity of **SPA-2** for halogenated acids was further confirmed

with trifluoroacetic acid in the presence of which only 0.44/0.3 (after 20 min/72 h) acetic acid molecule were retained by the porous material. It can be noticed that the selectivity of the sorption increases with the strength of the acid but also with the number of halogen substituents.

The crystal structures of host-guest compounds  $\text{CH}_3\text{COOH}@$ **SPA-2**,  $\text{CF}_3\text{COOH}@$ **SPA-2**, and  $\text{CCl}_3\text{COOH}@$ **SPA-2** have been investigated, revealing some information on the host-guest interactions. The single crystal diffraction studies have been performed on crystals of **SPA-2** after immersion in the respective acid solution (see ESI for additional information). For  $\text{CH}_3\text{COOH}@$ **SPA-2** and  $\text{CF}_3\text{COOH}@$ **SPA-2** respectively, 0.5 and 0.25 acid molecules could be localized in the channels (for effective composition see ESI) and the positioning of the carboxylic moieties close to the N atom of the free-pyridyl units ( $d_{\text{N-O}} = 2.993$  and  $2.58 \text{ \AA}$ , respectively) strongly suggests H-bond interaction between them (Figure 3a and S20).  $\pi \cdots \pi$  interactions and  $\text{F} \cdots \pi$  contacts are also evidenced between the crystallized guests and the supramolecular scaffold. A notably different situation was found for the crystallized trichloroacetic acid guests. The  $\text{CCl}_3\text{COOH}$  seen by X-ray is not in the vicinity of a pyridyl unit but localized close to oxalate units and facing them by the Cl atoms. Obviously these trichloroacetic acid molecules interact with the supramolecular framework through  $\text{Cl} \cdots \pi$  and  $\text{Cl} \cdots \text{O}$  contacts with oxalates (Figure 3c,d) and these interactions are strong enough to lead to an organized arrangement of  $\text{CCl}_3\text{COOH}$  all through the crystal. For this compound too, only a part of the  $\text{CCl}_3\text{COOH}$  (0.25 versus effective content of 1.25) located in the channels was detected by X-ray diffraction, suggesting that other interactions with the framework may take place. This structural information on the host-guest interactions points out that the affinity of the framework for acidic molecules does not just come down to an acid-base association. Other interactions, such as the halogen interactions evidenced for  $\text{CCl}_3\text{COOH}$ , may play an

important role and certainly account for an acid uptake exceeding in all cases the 1:1 stoichiometry with the pyridyl unit.

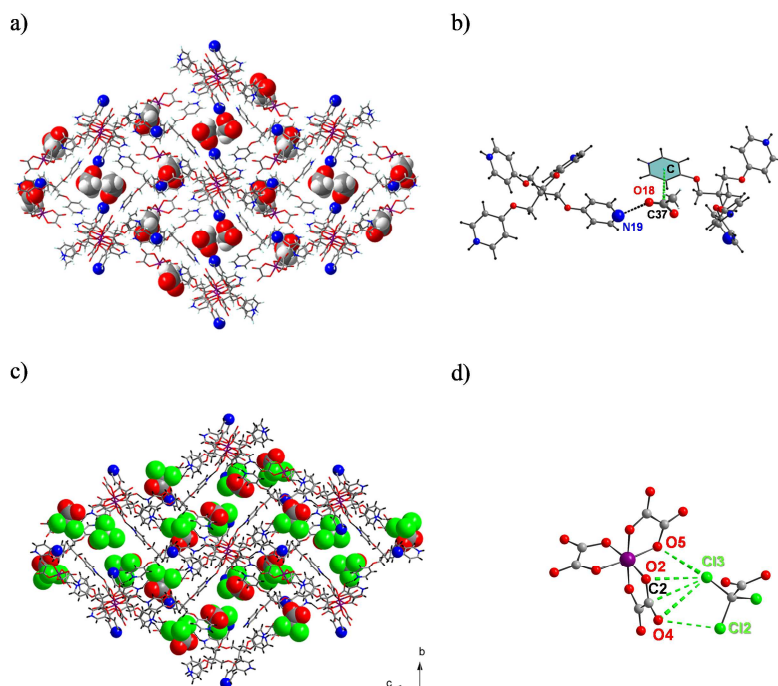


**Figure 3.** Crystal structure of CH<sub>3</sub>COOH@SPA-2 and CCl<sub>3</sub>COOH@SPA-2: (a) Ball and stick view of CH<sub>3</sub>COOH@SPA-2 showing the crystallized acetic acid guests (space filling view) in the channels; (b) detail of the supramolecular interactions (dashed lines) of an acetic acid molecule with the host framework ( $d(\text{N19}\cdots\text{O18}) = 2.99 \text{ \AA}$ ;  $d(\text{C37}\cdots\text{C}) = 3.36 \text{ \AA}$ ); (c) view of CCl<sub>3</sub>COOH@SPA-2 showing the crystallized CCl<sub>3</sub>COOH in space filling view; and (d) detail of the supramolecular contacts of CCl<sub>3</sub>COOH with the oxalate units. The crystallized H<sub>2</sub>O are omitted for clarity in all cases. Color codes: C, grey; H, black; N, blue; O, red.

Solid-state MAS NMR spectroscopy provided a deeper insight into the behaviors of the guest molecules within the channels. The <sup>13</sup>C MAS spectrum acquired with direct polarization for SPA-2 (Figure 4a) shows well-resolved signals for the components of the framework as well as for the EtOH located in the channels. For CH<sub>3</sub>COOH@SPA-2 (Figure 4b, top) two additional peaks corresponding to acetic acid (at 20.7 and 175.3 ppm, respectively) are observed with a very small signal from EtOH as compared to SPA-2. The molecular dynamics was probed by <sup>13</sup>C CP (cross polarization) and INEPT (insensitive nuclei enhanced

by polarization transfer) polarization experiments. The  $^{13}\text{C}$  CP spectra (central parts of Figure 4a,b) exhibit only the signals of the molecules involved in the supramolecular framework (i.e., oxalates and Tpy molecules), which correspond to the rigid part of the material. The signals of EtOH and  $\text{CH}_3\text{COOH}$  appear in the INEPT spectra (Figure 4a,b bottom), indicating that these molecules are highly mobile in the channels at NMR time scale,<sup>[18]</sup> much like in a liquid-like state rather than in a solid state. The fact that all  $\text{CH}_3\text{COOH}$  molecules are found to be mobile

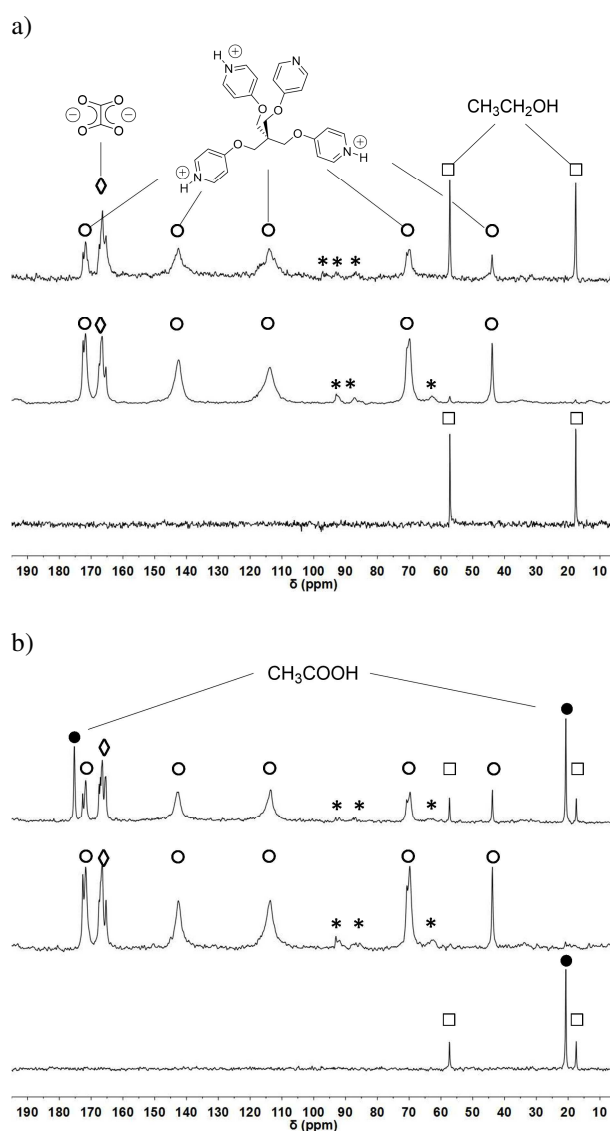


**Figure 4.** Solid-state  $^{13}\text{C}$ -MAS spectra for single crystals of (a) SPA-2 and (b)  $\text{CH}_3\text{COOH}@$ SPA-2 with on top the direct polarization, in the middle the CP polarization, and at the bottom the INEPT polarization (quaternary  $^{13}\text{C}$  atoms are not detected in INEPT experiments). Signals marked by \* are rotation bands. Pick attributions:  $\diamond$ , oxalates;  $\circ$ ,  $\text{H}_3\text{Tpy}^{3+}$ ;  $\square$ , EtOH;  $\bullet$ , acetic acid.

by NMR while a fraction of them was localized by X-ray diffraction can be ascribed to the different temperature at which each experiment has been performed, i.e. 293 K and 100 K, respectively.

Further insight in the motional characteristics of the guest molecules was provided by high resolution magic angle spinning (HRMAS)  $^1\text{H}$  NMR spectroscopy.<sup>[19]</sup> The HRMAS  $^1\text{H}$  spectrum recorded at 293 K shows four sets of well resolved resonances attributed to  $\text{H}_2\text{O}$ , EtOH, and  $\text{CH}_3\text{COOH}$  (Figure S38) in a ratio of 1–1.5\*/1/1 (\*  $\text{H}_3\text{O}^+/\text{H}_2\text{O}$  ratio is unknown), in agreement with the ratio anticipated for  $\text{CH}_3\text{COOH}@$ **SPA-2**. The lack of signals from the Tpy groups confirms that the dangling pyridyl moieties are not mobile. Two different chemical environments can be clearly observed for the EtOH and  $\text{CH}_3\text{COOH}$  molecules with a ratio for the two contributions of 15/85 (A-E/B-F) for EtOH and 10/90 (C/D) for  $\text{CH}_3\text{COOH}$ . Pulsed field gradient (PFG)  $^1\text{H}$  HRMAS experiments<sup>[20]</sup> indicated that different diffusion characteristics are associated to these signals (Table 2 and Figure 5). The major signal of  $\text{CH}_3\text{COOH}$  (resonance D) is characterized by a very small and a larger diffusion coefficient ( $0.15 \times 10^{-10}$  and  $6.9 \times 10^{-10} \text{ m}^2.\text{s}^{-1}$ ), the latter being already below the rate measured in a 1.5/1/1  $\text{H}_2\text{O}/\text{EtOH}/\text{CH}_3\text{COOH}$  solution,<sup>[21]</sup> while for the minor resonance (C) a single but intermediate diffusion coefficient is found. The values found for the diffusion coefficients support the occurrence of interactions between the carboxylic acids and their surrounding in the channels. The different coefficients also confirm that acetic acid experiences diverse interaction sites with the framework. The same conclusion can be drawn for EtOH. Related experiments with **SPA-2** yielded a single set of signals for  $\text{H}_2\text{O}$  and EtOH found in a ratio 1/0.08 (Figure S39). For the water resonance, two diffusion coefficients are obtained that are significantly smaller than for a 1/0.08  $\text{H}_2\text{O}/\text{EtOH}$  solution.<sup>[22]</sup> Ethanol revealed also two diffusion components similar to that found for  $\text{CH}_3\text{COOH}@$ **SPA-2**. These diffusion coefficient values were consistent and reproducible over a period of several hours.

The mobility evidenced for the guest molecules within the channels allows understanding why only very few guest molecules are detected by X-ray diffraction analyses. Obviously, even for temperatures as low as 100 K a large part of the guests remain mobile and only those with stronger interactions with the channels' atoms are then crystallized.

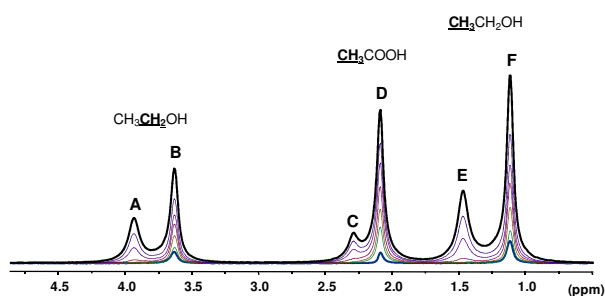
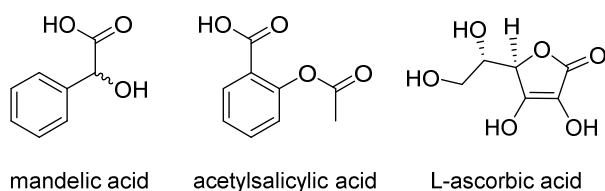


**Figure 5.**  $^1\text{H}$  PFG HRMAS NMR spectra (293 K, 4 kHz) for  $\text{CH}_3\text{COOH}@$ SPA-2 showing the intensity variation of the signals for EtOH (A-E and B-F) and for  $\text{CH}_3\text{COOH}$  (C and D) with the gradient strength

**Table 2.**  $^1\text{H}$  HRMAS PFG NMR Data for SPA-2 and  $\text{CH}_3\text{COOH}@$ SPA-2.

	Chemical shift (ppm)	Diffusion coefficient ( $\times 10^{-10} \text{ m}^2 \cdot \text{s}^{-1}$ ) <sup>a</sup>			
		fast component	relative ratio (%)	slow component	relative ratio (%)
<b><math>\text{CH}_3\text{COOH}@</math>SPA-2</b>					
EtOH (A-E)	3.94–1.47	8.7 $\pm$ 1.5	70 $\pm$ 10	1.0 $\pm$ 0.3	30 $\pm$ 10
EtOH (B-F)	3.64–1.12	11.3 $\pm$ 1.5	70 $\pm$ 10	0.15 $\pm$ 0.05	30 $\pm$ 10
$\text{CH}_3\text{COOH}$ (C)	2.29	5.3 $\pm$ 0.4	100	–	–
$\text{CH}_3\text{COOH}$ (D)	2.09	6.9 $\pm$ 1.2	50 $\pm$ 10	0.15 $\pm$ 0.1	50 $\pm$ 10
<b>SPA-2</b>					
$\text{H}_2\text{O}$	4.94	8.0 $\pm$ 2.0	20 $\pm$ 10	2.2 $\pm$ 0.4	80 $\pm$ 10
EtOH (A-E)	3.60–1.12	13 $\pm$ 4.0	50 $\pm$ 30	1.1 $\pm$ 0.3	50 $\pm$ 30

<sup>a</sup> PFG data were best analyzed with a bi-exponential fitting (except for C), yielding a fast and a slow diffusion coefficient of weighted ratio.



**Scheme 2.** Larger acidic molecules envisioned as guests for **SPA-2**.

Finally, the possibility for **SPA-2** to host larger acidic guests is illustrated by the sorption of a series of simple drug molecules: mandelic acid ( $pK_a = 3.41$ ), L-ascorbic acid (vitamin C,  $pK_a = 4.2$ ), and acetylsalicylic acid (aspirin,  $pK_a = 3.49$ ) (Scheme 2). For ascorbic acid and mandelic acid, respectively 1.25 and 1.4 molecules have been found in **SPA-2** when sorption was performed from solutions in EtOH. This amount was enhanced to 2.2 for mandelic acid using acetone solutions, a solvent with no competing H-bond interactions with the framework. Same condition could not be applied to ascorbic acid because of its insolubility but for acetylsalicylic acid, the bulkiest molecule of the series, the sorption of 1 molecule could be achieved using acetone (Figures S31-32) while no uptake was found in EtOH. Solid state  $^{13}\text{C}$ -MAS NMR experiments (Figure S33-35) indicated that these larger acid molecules are not very mobile (no signal in the  $^{13}\text{C}$  INEPT MAS experiment), but none could not be localized by single crystal diffraction studies despite the high crystallinity of the materials (Figure S36). In all cases the sorption process is reversible. Just soaking these acid@**SPA-2** crystals in EtOH leads to the release of the acid molecules from their hosting framework in very smooth conditions.

It is interesting to compare the time course of the adsorption of mandelic acid for each solvent (Figures 6 and S37). From both EtOH and acetone solutions the uptake of a first molecule is fast and takes place within minutes, afterwards the behavior significantly depends on the solvent. In EtOH, the loading rapidly saturates with 1.4 molecules, whereas in acetone the sorption reaches a plateau value of 2.3 molecules within 2 h of soaking. These behaviors are

consistent with the occurrence of different interactions between the guests and the hosting framework, as highlighted above for the simpler carboxylic acid. The uptake of a first molecule of mandelic acid is likely to be driven by the acid-base interactions with the basic pyridine sites located in the channels. The accommodation of further molecules obviously involves weaker interactions that can be compromised by protic solvents such as alcohols able to behave as H-bond donors with the hosting framework at the detriment of the carboxylic units. Hence, a more efficient uptake both in guest amount and in speed is achieved with acetone, which has poor supramolecular interactions with the framework.

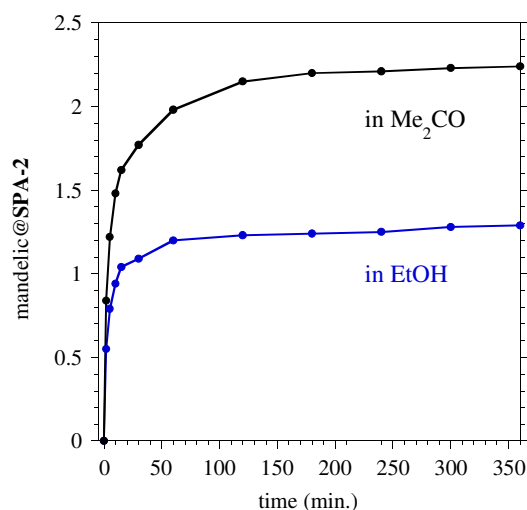


**Figure 6.** Sorption of mandelic acid in the supramolecular framework of **SPA-2** (up to 10 h) from 0.3 M ethanol solution (blue) and from 0.3 M acetone solution (black).

## CONCLUDING REMARKS

The results gathered herein demonstrate that microporous H-bonded frameworks with pores decorated by basic sites can be readily obtained using a quite simple and versatile design strategy. This is illustrated by **SPA-2**, the first microporous H-bonded framework with pores decorated by pyridyl groups. These groups endow the crystalline solid with remarkable

sorption capabilities towards acidic molecules in solution even for larger molecules that are accommodated in 1 nm-large channels.

In most of the examples considered here the acid-to-pyridine ratio exceeded one, revealing that, though the acid-base association is decisive in the efficiency of the sorption process, several other supramolecular interactions contribute to the accommodation of the guests. These include H-bonding involving the carboxylic groups but also weaker interactions such as halogen bonding with the oxalate units as revealed by crystal structure investigations. This variety of host-guests interactions points to the importance of the overall composition of the channels' walls in the uptake capacity of the porous material.

Last but not least is the nature of the solvent.<sup>[23]</sup> Whereas loading acid guest molecules is efficiently performed in a solvent with poor supramolecular interactions with the framework and with the substrate, their spontaneous release in smooth mild is obtained just by soaking the solid material in a protic solvent such as alcohol. This suggests the possibility to use **SPA-2** as carrier-material for acidic molecules.

## **EXPERIMENTAL SECTION:**

**General Methods.** All chemicals were purchased from commercial sources and used as received. Infrared spectra were recorded in transmission mode on KBr pellets with a Perkin-Elmer Spectrum 100 FT-IR spectrometer in the range 4000–600  $\text{cm}^{-1}$ . Elemental analyses (EA) were performed using a Perkin-Elmer 2400 II, CHNS/O analyzer. Thermogravimetric analyses (TGA) measurements have been done on a Perkin-Elmer Diamond TG/DTA instrument; the compounds were heated using a 10  $^{\circ}\text{C}\cdot\text{min}^{-1}$  heating rate, under a  $\text{N}_2$  flow, in the 25–600 $^{\circ}\text{C}$  temperature range. Routine  $^1\text{H}$ - and  $^{13}\text{C}$ - NMR were performed on a Bruker Advance 400 spectrometer.

**Crystallographic Studies:** Data were collected at 100 K on a Bruker Apex2 diffractometer equipped with a Mo microfocus source (for **SPA-2**) or on a GEMINI diffractometer using Cu- $K\alpha$  radiation ( $\lambda = 1.54180 \text{ \AA}$ ). The structures were solved by SUPERFLIP or by direct methods using SIR92 or SHELXS86, and refined by means of least-squares procedures on  $F$  using the programs of the PC version of CRYSTALS. Atomic scattering factors were taken from the International tables for X-ray Crystallography.<sup>[24]</sup> Hydrogen atoms were refined using a riding model. Guest molecules (i.e., water molecules and/or acid molecules) were often located in partial occupancy. Moreover, several disorders (especially on pyridyl groups) were treated for the host framework; refinement of the final models led to imperfect but reasonable solutions. For **SPA-2**·HNO<sub>3</sub>, the NO<sub>3</sub><sup>-</sup> is located on a unique position with occupancy 1. For CH<sub>3</sub>COOH@**SPA-2** and CCl<sub>3</sub>COOH@**SPA-2**, the acid molecule was found on a unique position in occupancy 0.5 and 0.25, respectively; in CF<sub>3</sub>COOH@**SPA-2**, the acid molecule was found disordered over two positions with 0.125/0.125 occupancies, leading to a global occupancy of 0.25. For the three acid@**SPA-2** structures, an hydrogen atom could not be located neither on N(12), nor on the carboxylic moieties but it was included in the given formula. The absolute configurations of the compounds were determined by Flack parameter refinement. The result is unambiguous for structures collected at Cu radiation. For the structure of **SPA-2**, which data were collected using Mo radiation, the s.u. value for the Flack parameter is greater than the value of 0.10 suggested as the upper limit for being confidently.<sup>[25]</sup> However, the Hooft parameter 'y',<sup>[26]</sup> calculated using CRYSTALS, was  $y = -0.001(26)$  indicating that the absolute structure has been determined correctly.

The powder X-ray diffraction (PXRD) patterns were recorded in transmission mode (using a capillary setup) on a XPert Pro ( $\theta$ - $\theta$  mode) Panalytical diffractometer with  $\lambda(\text{Cu}_{K\alpha 1, K\alpha 2}) = 1.54059, 1.54439 \text{ \AA}$ . All data were collected in the  $5^\circ < 2\theta < 50^\circ$  range, with 0.02 steps and 10 s of exposure.

**NMR spectroscopy.** Solid-state MAS and High Resolution (HR) MAS NMR experiments were recorded on a Bruker Avance 400 and 500 MHz spectrometers. All chemical shifts are relative to TMS. Samples were packed into 4 mm zirconia rotors and spun at 10 and 4 kHz for solid MAS and HRMAS, respectively. For  $^1\text{H}$  MAS and  $^{13}\text{C}$  MAS with direct polarization, small flip angle of  $30^\circ$  were used with recycle delays of 3 s and 10 s, respectively.  $^{13}\text{C}$  MAS spectra with Cross polarization (CP) were recorded with a recycle delay of 2 s and contact times of 2 ms.  $^{13}\text{C}$  MAS with INEPT polarization were recorded with a recycle delay of 3 s. All pulsed field gradient HRMAS measurements were collected at 293 K with a stimulated echo sequence with bipolar and spoil gradient pulses. Different diffusion delays between 80 to 500 ms and gradient pulse duration between 1.6 to 4 ms were used in order to measure the high, intermediate and low diffusion coefficients.

**Synthesis.**  $\text{K}_3[\text{Al}(\text{C}_2\text{O}_4)_4]\cdot 3\text{H}_2\text{O}$ <sup>[27]</sup> and Tpy<sup>[28]</sup> have been prepared following described procedures.

**SPA-2·HNO<sub>3</sub>.** An aqueous solution (3 mL) of  $\text{K}_3[\text{Al}(\text{C}_2\text{O}_4)_3]\cdot 3\text{H}_2\text{O}$  (75 mg, 0.162 mmol) is slowly added to an acidic aqueous solution (2 mL; pH ~ 2 adjusted with concentrated  $\text{HNO}_3$ ) of Tpy (72 mg, 0.162 mmol) under continuous stirring. EtOH (4 mL) is added to the resulting solution and the beaker is placed in a vessel containing 50 mL of EtOH. The vessel is sealed and is kept undisturbed. Crystals of SPA-2·HNO<sub>3</sub> (145 mg, 0.112 mmol, 69 %) are formed over 48 h, these crystals are suitable for X-ray diffraction experiments.  $^1\text{H}$ -NMR (400 MHz, D<sub>2</sub>O,  $\delta$  ppm): 8.52 – 8.45 (m, 8H; H<sub>ar</sub>-Tpy), 7.51 – 7.42 (m, 8H; H<sub>ar</sub>-Tpy), 4.80 (s, 8H; CH<sub>2</sub>-Tpy), 3.57 (q, 4H; CH<sub>3</sub>CH<sub>2</sub>OH), 1.10 (t, 6H; CH<sub>3</sub>CH<sub>2</sub>OH).  $^{13}\text{C}$ -NMR (400 MHz, D<sub>2</sub>O,  $\delta$  ppm): 170.9 (C<sub>ar</sub>-Tpy), 165.7 (C-oxalate), 142.7 (C<sub>ar</sub>-Tpy), 113.2 (C<sub>ar</sub>-Tpy), 67.6 (CH<sub>2</sub>-Tpy), 57.4 (CH<sub>3</sub>CH<sub>2</sub>OH), 43.9 (C<sub>quat</sub>-Tpy), 16.8 (CH<sub>3</sub>CH<sub>2</sub>OH). IR (KBr, cm<sup>-1</sup>): 3418(m), 3086(m), 2955(m), 1716(m), 1666(s), 1634(s), 1506(s), 1466(m), 1403(s), 1385(m, NO<sub>3</sub><sup>-</sup>), 1319(s), 1293(s), 1194(s), 1100(w), 1028(m), 1015(m), 995(m), 947(w), 906 (m), 800(s), 722(w),

676(w). Elemental Anal. (%) calcd. for  $[(\text{H}_4\text{Tpy})\text{NO}_3\text{Al}(\text{Ox})_3]\cdot 23\text{H}_2\text{O}\cdot 2\text{EtOH}$  ( $\text{C}_{35.00}\text{H}_{86.00}\text{N}_5\text{O}_{44.00}\text{Al}_{1.00}$ ): C, 32.14; H, 6.63; N, 5.35; Found: C, 32.20; H, 6.26; N, 4.97. TGA: Calculated weight loss for (1  $\text{HNO}_3$  + 23  $\text{H}_2\text{O}$  + 2  $\text{EtOH}$ ): 43.5%; Found: 29.1% between 25–145°C (15  $\text{H}_2\text{O}$  + 2 $\text{EtOH}$ ), 7.3% between 145–245°C (loss of  $\text{HNO}_3$  + 2  $\text{H}_2\text{O}$ ). Expected weight loss is observed at 290°C. See Figure S8 for TGA trace.

**SPA-2:** Careful washing of *ca* 150 mg of single crystals of **SPA-2**· $\text{HNO}_3$  with 3×5 mL of a 0.01M solution of pyridine in  $\text{EtOH}$  over 15 min, followed by 5 min washing with absolute ethanol yields **SPA-2** as single crystals suitable for X-ray diffraction (quantitative yield).  $^1\text{H}$ -NMR (400 MHz,  $\text{D}_2\text{O}$ ,  $\delta$  ppm): 8.52 – 8.45 (m, 8H;  $\text{H}_{\text{ar}}\text{-Tpy}$ ), 7.51 – 7.42 (m, 8H;  $\text{H}_{\text{ar}}\text{-Tpy}$ ), 4.80 (s, 8H;  $\text{CH}_2\text{-Tpy}$ ); 3.57 (q, 1.2H;  $\text{CH}_3\text{CH}_2\text{OH}$ ), 1.10 (t, 1.8H;  $\text{CH}_3\text{CH}_2\text{OH}$ ).  $^{13}\text{C}$ -NMR (400 MHz,  $\text{D}_2\text{O}$ ,  $\delta$  ppm): 170.8 ( $\text{C}_{\text{ar}}\text{-Tpy}$ ), 165.4 (C-oxalate), 142.6 ( $\text{C}_{\text{ar}}\text{-Tpy}$ ), 113.4 ( $\text{C}_{\text{ar}}\text{-Tpy}$ ), 67.5 ( $\text{CH}_2\text{-Tpy}$ ), 57.4 ( $\text{CH}_3\text{CH}_2\text{OH}$ ), 43.8 ( $\text{C}_{\text{quat}}\text{-Tpy}$ ), 16.8 ( $\text{CH}_3\text{CH}_2\text{OH}$ ). Solid  $^{13}\text{C}$ -NMR HPDec  $^{13}\text{C}/1\text{H}$ / (400 MHz,  $\delta$  ppm): 171.8 ( $\text{C}_{\text{ar}}\text{-Tpy}$ ), 166.6 (C-oxalate), 142.8 ( $\text{C}_{\text{ar}}\text{-Tpy}$ ), 114.3 ( $\text{C}_{\text{ar}}\text{-Tpy}$ ), 69.9 ( $\text{CH}_2\text{-Tpy}$ ), 57.2 ( $\text{CH}_3\text{CH}_2\text{OH}$ ), 43.8 ( $\text{C}_{\text{quat}}\text{-Tpy}$ ), 16.7 ( $\text{CH}_3\text{CH}_2\text{OH}$ ). IR (KBr,  $\text{cm}^{-1}$ ): 3418(m), 3086(m), 2955(m), 1716(m), 1666(s), 1634(s), 1506(s), 1466(m), 1403(s), 1319(s), 1293(s), 1194(s), 1100(w), 1028(m), 1015(m), 995(m), 947(w), 906 (m), 800(s), 722(w), 676(w). Elemental Anal. (%) calcd. for  $[(\text{H}_3\text{-Tpy})\text{Al}(\text{Ox})_3]\cdot 17.7\text{H}_2\text{O}\cdot 0.6\text{EtOH}$  ( $\text{C}_{32.20}\text{H}_{66.00}\text{N}_4\text{O}_{34.30}\text{Al}_{1.00}$ ): C, 35.64; H, 6.13; N, 5.16; Found: C, 35.48; H, 5.91; N, 4.77. TGA: Calculated weight loss for (17.7  $\text{H}_2\text{O}$  + 0.6  $\text{EtOH}$ ): 31.9%; Found: 30.0% between 25–145°C. Expected weight loss is observed at 230°C. See Figure S8 for TGA trace.

**Supporting information.** Complementary figures and experimental procedures, ORTEP plots, SC and PXRD data, TGA, details on sorption procedures and guest@**SPA-2** characterizations (IR,  $^1\text{H}$ -NMR,  $^{13}\text{C}$ -NMR in  $\text{D}_2\text{O}$  solution and in solid state) are included in

the Supporting Information. CCDC-1537662 (SPA-2·HNO<sub>3</sub>), CCDC-1537663 (SPA-2), CCDC-1537661 (CH<sub>3</sub>COOH@SPA-2), CCDC-1537660 (CF<sub>3</sub>COOH@SPA-2) and CCDC-1537659 (CCl<sub>3</sub>COOH@SPA-2) contains the supplementary crystallographic data for this paper. These data can be obtained free of charge from The Cambridge Crystallographic Data Centre via [www.ccdc.cam.ac.uk/data\\_request/cif](http://www.ccdc.cam.ac.uk/data_request/cif).

**ACKNOWLEDGEMENTS.** This work was supported by the French Ministry for Education and Research by a grant for G.M., and by the French research agency ANR under project ANR-15-CE29-0013. T.F. thanks also the Conseil Regional de Bourgogne for a post-doctoral fellowship awarded in the frame of the PARI II CDEA program. Authors are grateful to the Integrated Screening Platform of Toulouse (PICT, IBiSA) for providing access to the Bruker Avance500 NMR spectrometer with HRMAS equipment.

## References:

- [1] a) A. I. Cooper, *Angew. Chem. Int. Ed.* **2012**, *51*, 7892-7894; b) J. Lü, R. Cao, *Angew. Chem. Int. Ed.* **2016**, *55*, 9474-9480.
- [2] a) M. Mastalerz, I. M. Oppel, *Angew. Chem. Int. Ed.* **2012**, *51*, 5252-5255; b) Y. He, S. Xiang, B. Chen, *J. Am. Chem. Soc.* **2011**, *133*, 14570-14573; c) S. Dalapati, R. Saha, S. Jana, A. K. Patra, A. Bhaumik, S. Kumar, N. Guchhait, *Angew. Chem. Int. Ed.* **2012**, *51*, 12534-12537; d) X.-Z. Luo, X.-J. Jia, J.-H. Deng, J.-L. Zhong, H.-J. Liu, K.-J. Wang, D.-C. Zhong, *J. Am. Chem. Soc.* **2013**, *135*, 11684-11687; e) T. H. Chen, I. Popov, W. Kaveevivitchai, Y. C. Chuang, Y. S. Chen, O. Daugulis, A. J. Jacobson, O. S. Miljanic, *Nature Commun.* **2014**, *5*; f) P. Li, Y. He, H. D. Arman, R. Krishna, H. Wang, L. Weng, B. Chen, *Chem. Commun.* **2014**, *50*, 13081-13084; g) P. Li, Y. He, J. Guang, L. Weng, J. C.-G. Zhao, S. Xiang, B. Chen, *J. Am. Chem. Soc.* **2014**, *136*, 547-549; h) J. Lu, C. Perez-Krap, M. Suyetin, N. H. Alsmail, Y. Yan, S. H. Yang, W. Lewis, E. Bichoutskaia, C. C. Tang, A. J. Blake, R. Cao, M. Schroder, *J. Am. Chem. Soc.* **2014**, *136*, 12828-12831; i) P. Li, Y. He, Y. Zhao, L. Weng, H. Wang, R. Krishna, H. Wu, W. Zhou, M. O'Keeffe, Y. Han, B. Chen, *Angew. Chem. Int. Ed.* **2015**, *54*, 574-577; j) H. Wang, B. Li, H. Wu, T.-L. Hu, Z. Yao, W. Zhou, S. Xiang, B. Chen, *J. Am. Chem. Soc.* **2015**, *137*, 9963-9970; k) W. Yang, B. Li, H. Wang, O. Alduhaish, K. Alfooty, M. A. Zayed, P. Li, H. D. Arman, B. Chen, *Cryst. Growth Des.* **2015**, *15*, 2000-2004; l) P. F. Li, C. X. Qian, A. J. Lough, G. A. Ozin, D. S. Seferos, *Dalton Trans.* **2016**, *45*, 9754-9757; m) S. Nandi, D. Chakraborty, R. Vaidhyanathan, *Chem. Commun.* **2016**, *52*, 7249-7252; n) D. D. Zhou, Y. T. Xu, R. B. Lin, Z. W. Mo, W. X. Zhang, J. P. Zhang, *Chem. Commun.* **2016**, *52*, 4991-4994; o) F. Hu, C. Liu, M. Wu, J. Pang, F. Jiang, D. Yuan, M. Hong, *Angew. Chem. Int. Ed.* **2017**, *56*, 2101-2104; p) T. Adachi, M. D. Ward, *Acc. Chem. Res.* **2016**, *49*, 2669-2679.
- [3] R. Natarajan, L. Bridgland, A. Sirilculkajorn, J. H. Lee, M. F. Haddow, G. Magro, B. Ali, S. Narayanan, P. Strickland, J. P. H. Charmant, A. G. Orpen, N. B. McKeown, C. G. Bezzu, A. P. Davis, *J. Am. Chem. Soc.* **2013**, *135*, 16912-16925.
- [4] a) B. Van de Voorde, B. Bueken, J. Denayer, D. De Vos, *Chem. Soc. Rev.* **2014**, *43*, 5766-5788; b) A. Samokhvalov, *Chem. Eur. J.* **2015**, *21*, 16726-16742.
- [5] J. F. Van Humbeck, T. M. McDonald, X. Jing, B. M. Wiers, G. Zhu, J. R. Long, *J. Am. Chem. Soc.* **2014**, *136*, 2432-2440.
- [6] Z. Yan, G. Li, L. Mu, S. Tao, *J. Mater. Chem.* **2006**, *16*, 1717-1725.
- [7] a) B. Chen, L. Wang, Y. Xiao, F. R. Fronczek, M. Xue, Y. Cui, G. Qian, *Angew. Chem. Int. Ed.* **2009**, *48*, 500-503; b) J. S. Seo, D. Whang, H. Lee, S. I. Jun, J. Oh, Y. J. Jeon, K. Kim, *Nature* **2000**, *404*, 982-986.
- [8] a) A. Demessence, D. M. D'Alessandro, M. L. Foo, J. R. Long, *J. Am. Chem. Soc.* **2009**, *131*, 8784-8785; b) M. Savonnet, S. Aguado, U. Ravon, D. Bazer-Bachi, V. Lecocq, N. Bats, C. Pinel, D. Farrusseng, *Green Chem.* **2009**, *11*, 1729-1732; c) S. M. Cohen, *Chem. Sci.* **2010**, *1*, 32-36.
- [9] a) F. Thétiot, C. Duhayon, T. S. Venkatakrishnan, J.-P. Sutter, *Cryst. Growth Des.* **2008**, *8*, 1870-1877; b) G. Mouchaham, N. Roques, S. Brandes, C. Duhayon, J. P. Sutter, *Cryst. Growth Des.* **2011**, *11*, 5424-5433; c) G. Mouchaham, N. Roques, C. Duhayon, I. Imaz, J. P. Sutter, *New J. Chem.* **2013**, *37*, 3476-3487; d) G. Mouchaham, N. Roques, I. Imaz, C. Duhayon, J. P. Sutter, *Cryst. Growth Des.* **2010**, *10*, 4906-4919; e) G. Mouchaham, N. Roques, A. Kaiba, P. Guionneau, J. P. Sutter, *CrystEngComm*

- 2010**, *12*, 3496-3498; f) G. Mouchaham, M. Gualino, N. Roques, C. Duhayon, S. Brandes, J. P. Sutter, *CrystEngComm* **2015**, *17*, 8906-8914.
- [10] a) S. A. Dalrymple, G. K. H. Shimizu, *J. Am. Chem. Soc.* **2007**, *129*, 12114-12116; b) P. Dechambenoit, S. Ferlay, N. Kyritsakas, M. W. Hosseini, *J. Am. Chem. Soc.* **2008**, *130*, 17106-17113; c) I. Imaz, A. Thillet, J.-P. Sutter, *Cryst. Growth Des.* **2007**, *7*, 1753-1761; d) B. R. Bhogala, S. Basavoju, A. Nangia, *Cryst. Growth Des.* **2005**, *5*, 1683-1686; e) A. M. Beatty, *Coord. Chem. Rev.* **2003**, *246*, 131-143; f) K. T. Holman, A. M. Pivovar, J. A. Swift, M. D. Ward, *Acc. Chem. Res.* **2001**, *34*, 107-118; g) A. D. Burrows, C. W. Chan, M. M. Chowdhry, J. E. McGrady, D. M. P. Mingos, *Chem. Soc. Rev.* **1995**, *24*, 329-339; h) Y. Liu, W. Xiao, J. J. Yi, C. Hu, S.-J. Park, M. D. Ward, *J. Am. Chem. Soc.* **2015**, *137*, 3386-3392; i) M. Morshedi, M. Thomas, A. Tarzia, C. J. Doonan, N. G. White, *Chem. Sci.* **2017**, *8*, 3019-3025.
- [11] M. Meot-Ner, *Chem. Rev.* **2012**, *112*, PR22-PR103.
- [12] N. Roques, G. Mouchaham, C. Duhayon, S. Brandes, A. Tachon, G. Weber, J. P. Bellat, J. P. Sutter, *Chem. Eur. J.* **2014**, *20*, 11690-11694.
- [13] J. Mu, D. D. Perlmutter, *Thermochim. Acta* **1982**, *56*, 253-260.
- [14] L. Carlucci, G. Ciani, D. M. Proserpio, *Coord. Chem. Rev.* **2003**, *246*, 247-289.
- [15] A. L. Spek, *PLATON, A Multipurpose Crystallographic Tool*, Utrecht (The Netherlands), Utrecht University, **2001**.
- [16] S. Kitagawa, K. Uemura, *Chem. Soc. Rev.* **2005**, *34*, 109-119.
- [17] D. R. Lide, *Handbook of Chemistry and Physics*, 85 ed., CRC Press, Boca Raton, **2005**.
- [18] A. Nowacka, P. C. Mohr, J. Norrman, R. W. Martin, D. Topgaard, *Langmuir* **2010**, *26*, 16848-16856.
- [19] a) S. P. Brown, *Solid State Nucl. Magn. Reson.* **2012**, *41*, 1-27; b) A. Nowacka, P. C. Mohr, J. Norrman, R. W. Martin, D. Topgaard, *Langmuir* **2010**, *26*, 16848-16856
- [20] a) S. Viel, F. Ziarelli, G. Pagès, C. Carrara, S. Caldarelli, *J. Magn. Res.* **2008**, *190*, 113-123; b) J. E. Jenkins, M. R. Hibbs, T. M. Alam, *ACS Macro Letters* **2012**, *1*, 910-914.
- [21] **Note** : The diffusion rates measured for a 1.5/1/1 H<sub>2</sub>O/EtOH/CH<sub>3</sub>COOH solution at 20°C are 9.5±1.0 ×10<sup>-10</sup> m<sup>2</sup>.s<sup>-1</sup> for CH<sub>3</sub>COOH, 10.8±1.0×10<sup>-10</sup> m<sup>2</sup>.s<sup>-1</sup> for EtOH, and 12.5±1.5×10<sup>-10</sup> m<sup>2</sup>.s<sup>-1</sup> for H<sub>2</sub>O.
- [22] **Note** : The diffusion rates measured for a 1/0.08 H<sub>2</sub>O/EtOH solution at 20°C are 10.9±1.0×10<sup>-10</sup> m<sup>2</sup>.s<sup>-1</sup> for EtOH and 19.3±2.0×10<sup>-10</sup> m<sup>2</sup>.s<sup>-1</sup> for H<sub>2</sub>O.
- [23] A. Henschel, I. Senkovska, S. Kaskel, *Adsorption* **2011**, *17*, 219-226.
- [24] A. J. C. Wilson, *International Tables for X-ray Crystallography Vol. C*, Kluwer Academic, Dordrecht, **1992**.
- [25] H. D. Flack, G. Bernardinelli, *J. Appl. Cryst.* **2000**, *33*, 1143-1148.
- [26] R. W. W. Hooft, L. H. Straver, A. L. Spek, *J. Appl. Cryst.* **2008**, *41*, 96-103.
- [27] J. C. Bailar, E. M. Jones, H. S. Booth, M. Grennert, in *Inorg. Synth.*, John Wiley & Sons, Inc., **2007**, p. 35.
- [28] P. E. Ryan, C. Lescop, D. Laliberté, T. Hamilton, T. Maris, J. D. Wuest, *Inorg. Chem.* **2009**, *48*, 2793-2807.

## Hydrogen-bonded open-framework with pyridyl-decorated channels: Straightforward preparation and insight into its affinity for acidic molecules in solution

Georges Mouchaham,<sup>a,b</sup> Nans Roques,<sup>\*a,b</sup> Walid Khodja,<sup>a,b</sup> Carine Duhayon,<sup>a,b</sup> Yannick Coppel,<sup>a,b</sup> Stéphane Brandès,<sup>c</sup> Tamás Fodor,<sup>c</sup> Michel Meyer,<sup>c</sup> and Jean-Pascal Sutter <sup>\*a,b</sup>

### SUMMARY

#### **A. guest@SPA-2: Experimental procedures and characterizations**

- 1) Sorption of acetic acid/halogenated analogues from as-synthesized **SPA-2** (p. 2)
- 2) Sorption kinetics for acetic acid and halogenated analogues (p. 3)
- 3) Competitive sorption of acetic acid and halogenated analogues (p. 6)
- 4) Sorption of other acid molecules sorption (p. 7)

#### **B. Figures** (p. 10)

#### **C. Tables** (p. 39)

#### **D. HRMAS <sup>1</sup>H NMR** (p. 42)

#### **E. Acid-Base Properties of the Tpy** (p. 45)

#### **References** (p. 47)

## A. Experimental procedures and characterizations

### 1) CH<sub>3</sub>COOH@SPA-2, CCl<sub>3</sub>COOH@SPA-2, and CF<sub>3</sub>COOH@SPA-2 for crystal structure characterization.

**General experimental procedure:** Freshly prepared as-synthesized SPA-2 crystals are removed from their mother liquor and immediately soaked in the desired guest solution in absolute ethanol (15 mL, 3M). After 15 min, crystals are removed from the solution, put during 1 min between two pieces of chromatography paper to remove supernatant solution, and the resulting solid immediately dissolved in D<sub>2</sub>O (for <sup>1</sup>H- and <sup>13</sup>C-NMR experiments) and/or simultaneously subjected to EA/TGA. Single crystals for X-ray diffraction have been collected directly out from ethanol solution.

CH<sub>3</sub>COOH@SPA-2 (15 min): <sup>1</sup>H-NMR (400 MHz, D<sub>2</sub>O, δ ppm): SPA-2 peaks: 8.52 – 8.45 (m, 8H; H<sub>ar</sub>-Tpy), 7.51 – 7.42 (m, 8H; H<sub>ar</sub>-Tpy), 4.80 (s, 8H; CH<sub>2</sub>-Tpy); Guests peaks: 3.57 (q, 3.4H; CH<sub>3</sub>CH<sub>2</sub>OH), 1.99 (s, 6.9 H; CH<sub>3</sub>-acetic acid), 1.10 (t, 5.1H; CH<sub>3</sub>CH<sub>2</sub>OH). <sup>13</sup>C-NMR (400 MHz, D<sub>2</sub>O, δ ppm): SPA-2 peaks: 170.8 (C<sub>ar</sub>-Tpy), 165.4 (C-oxalate), 142.6 (C<sub>ar</sub>-Tpy), 113.4 (C<sub>ar</sub>-Tpy); 67.5 (CH<sub>2</sub>-Tpy); 43.8 (C<sub>quat</sub>-Tpy); Guests peaks: 176.9 (COOH-acetic acid), 57.4 (CH<sub>3</sub>CH<sub>2</sub>OH), 20.5 (CH<sub>3</sub>-acetic acid), 16.8 (CH<sub>3</sub>CH<sub>2</sub>OH). Solid <sup>13</sup>C-NMR HPDec <sup>13</sup>C{<sup>1</sup>H} (400 MHz, δ ppm): 175.3 (COOH-acetic acid); 171.7 (C<sub>ar</sub>-Tpy), 166.5 (C-oxalate), 143.0 (C<sub>ar</sub>-Tpy), 113.60 (C<sub>ar</sub>-Tpy), 69.7 (CH<sub>2</sub>-Tpy), 57.3 (CH<sub>3</sub>CH<sub>2</sub>OH), 43.9 (C<sub>quat</sub>-Tpy), 20.7 (CH<sub>3</sub>-acetic acid), 16.7 (CH<sub>3</sub>CH<sub>2</sub>OH). I.R. (ATR, cm<sup>-1</sup>): 3442(m), 3086(m), 2955(m), 1716(m), 1666(s), 1634(s), 1505(s), 1466(m), 1392(s), 1318(s), 1292(s), 1194(s), 1101(w), 1028(s), 1016(s), 993(m), 946(f), 904(m), 811(s), 798(s), 723(w), 673(w). Elemental Anal. (%) calcd. for [(H<sub>3</sub>Tpy)Al(Ox)<sub>3</sub>]·2.3CH<sub>3</sub>COOH·7.5H<sub>2</sub>O·1.7EtOH (C<sub>39.00</sub>H<sub>61.40</sub>N<sub>4.00</sub>O<sub>29.80</sub>Al<sub>1.00</sub>): C, 42.97; H, 5.68; N, 5.14; Found: C, 42.84; H, 5.90; N, 5.50. TGA: Calculated weight loss for (2.3CH<sub>3</sub>COOH + 7.5H<sub>2</sub>O + 1.7EtOH): 32.2%; Found: 30.1% between TA-245°C (See Figure S23 for TGA trace). <sup>1</sup>H-NMR formula: [(H<sub>3</sub>Tpy)Al(Ox)<sub>3</sub>]·2.3CH<sub>3</sub>COOH·xH<sub>2</sub>O·1.7EtOH; EA formula: [(H<sub>3</sub>Tpy)Al(Ox)<sub>3</sub>]·2.3CH<sub>3</sub>COOH·7.5H<sub>2</sub>O·1.7EtOH; Single crystal X-ray diffraction formula: [(H<sub>3</sub>Tpy)Al(Ox)<sub>3</sub>]·0.5CH<sub>3</sub>COOH·6.25H<sub>2</sub>O·0EtOH

CF<sub>3</sub>COOH@SPA-2 (15 min): <sup>1</sup>H-NMR (400 MHz, D<sub>2</sub>O, δ ppm): SPA-2 peaks: Identical to CH<sub>3</sub>COOH@SPA-2; Guests peaks: 3.57 (q, 3.8H; CH<sub>3</sub>CH<sub>2</sub>OH), 1.10 (t, 5.7H; CH<sub>3</sub>CH<sub>2</sub>OH). <sup>13</sup>C-NMR (400 MHz, D<sub>2</sub>O, δ ppm): SPA-2 peaks: Identical to CH<sub>3</sub>COOH@SPA-2; Guests

peaks: 163.1-162.0 (q, COOH-trifluoroacetic acid), 120.4-111.8 (q, CF<sub>3</sub>-trifluoroacetic acid), 57.4 (CH<sub>3</sub>CH<sub>2</sub>OH), 16.8 (CH<sub>3</sub>CH<sub>2</sub>OH). I.R. (ATR, cm<sup>-1</sup>): 3434(m), 3086(m), 2955(m), 1717(m), 1667(s), 1634(s), 1505(s), 1466(m), 1404(s), 1318(s), 1294(s), 1193(s), 1130 (C–F stretch, m), 1101(w), 1027(s), 1016(s), 995(m), 948(w), 905(m), 811(s), 798(s), 723(w), 673(w). Elemental Anal. (%) calcd. for {[H<sub>3</sub>Tpy)Al(Ox)<sub>3</sub>]·1.5CF<sub>3</sub>COOH·8.5H<sub>2</sub>O·1.9EtOH} (C<sub>37.80</sub>H<sub>56.90</sub>N<sub>4.00</sub>O<sub>29.40</sub>Al<sub>1.00</sub>F<sub>4.50</sub>) : C, 39.47; H, 4.99; N, 4.87; Found: C, 39.31; H, 4.75; N, 5.26. TGA: Calculated weight loss for (1.5CF<sub>3</sub>COOH + 8.5H<sub>2</sub>O + 1.9EtOH): 35.80%; Found: 35.40% between TA-245°C (See Figure S23 for TGA trace). <sup>1</sup>H-NMR formula: {[H<sub>3</sub>Tpy)Al(Ox)<sub>3</sub>]·xCF<sub>3</sub>COOH·yH<sub>2</sub>O·1.9EtOH}; EA formula: {[H<sub>3</sub>Tpy)Al(Ox)<sub>3</sub>]·1.5CF<sub>3</sub>COOH·8.5H<sub>2</sub>O·1.9EtOH}; Single crystal X-ray diffraction formula: {[H<sub>3</sub>Tpy)Al(Ox)<sub>3</sub>]·0.25CF<sub>3</sub>COOH·6H<sub>2</sub>O·0EtOH}.

CCl<sub>3</sub>COOH@SPA-2 (15 min): <sup>1</sup>H-NMR (400 MHz, D<sub>2</sub>O, δ ppm): SPA-2 peaks: Identical to CH<sub>3</sub>COOH@SPA-2; Guests peaks: 3.57 (q, 4H; CH<sub>3</sub>CH<sub>2</sub>OH), 1.10 (t, 6H; CH<sub>3</sub>CH<sub>2</sub>OH). <sup>13</sup>C-NMR (400 MHz, D<sub>2</sub>O, δ ppm): SPA-2 peaks: Identical to CH<sub>3</sub>COOH@SPA-2; Guests peaks: 161.5 (COOH-trichloroacetic acid), 94.4 (CCl<sub>3</sub>-trichloroacetic acid), 57.4 (CH<sub>3</sub>CH<sub>2</sub>OH), 16.8 (CH<sub>3</sub>CH<sub>2</sub>OH). I.R. (ATR, cm<sup>-1</sup>): 3414(m), 3090(m), 2957(m), 1716(m), 1667(s), 1635(s), 1506(s), 1465(m), 1403(s), 1319(s), 1294(s), 1195(s), 1101(w), 1027(s), 1016(s), 995(m), 945(w), 906(m), 811(s), 800(s), 738(w), 675(m). Elemental Anal. (%) calcd. for {[H<sub>3</sub>Tpy)Al(Ox)<sub>3</sub>]·1.25CCl<sub>3</sub>COOH·8H<sub>2</sub>O·2EtOH} (C<sub>37.50</sub>H<sub>56.25</sub>N<sub>4.00</sub>O<sub>28.50</sub>Al<sub>1.00</sub>Cl<sub>3.75</sub>): C, 38.20; H, 4.81; N, 4.75; Found: C, 38.10; H, 4.77; N, 4.75. TGA: Calculated weight loss for (1.25CCl<sub>3</sub>COOH + 8H<sub>2</sub>O + 2EtOH): 37.3%; Found: 35.5% between TA-245°C (See Figure S23 for TGA trace). <sup>1</sup>H-NMR formula: {[H<sub>3</sub>Tpy)Al(Ox)<sub>3</sub>]·xCCl<sub>3</sub>COOH·yH<sub>2</sub>O·2EtOH}.; EA formula: {[H<sub>3</sub>Tpy)Al(Ox)<sub>3</sub>]·1.25CCl<sub>3</sub>COOH·8H<sub>2</sub>O·2EtOH}; Single crystal X-ray diffraction formula: {[H<sub>3</sub>Tpy)Al(Ox)<sub>3</sub>]·0.25CCl<sub>3</sub>COOH·5H<sub>2</sub>O·0EtOH}.

## 2) Sorption kinetics for acetic acid and halogenated analogues:

**General experimental procedure:** Ca 150 mg of freshly prepared as-synthesized SPA-2 crystals are soaked during 4h in absolute ethanol. Resulting crystals, EtOH@SPA-2, are then engaged in sorption experiments, by replacing supernatant EtOH by the desired guest solution in absolute ethanol (15 mL, 3M). After the desired soaking time, crystals engaged in characterizations are removed from the guest solution, pressed during 1 min between two

pieces of chromatography paper to remove supernatant solution, and resulting solid immediately dissolved in D<sub>2</sub>O (for <sup>1</sup>H- and <sup>13</sup>C-NMR experiments) and/or subjected to EA.

EtOH@SPA-2 (4h): <sup>1</sup>H-NMR (400 MHz, D<sub>2</sub>O, δ ppm): **SPA-2 peaks:** 8.52 – 8.45 (m, 8H; H<sub>ar</sub>-Tpy); 7.51 – 7.42 (m, 8H; H<sub>ar</sub>-Tpy); 4.80 (s, 8H; CH<sub>2</sub>-Tpy); *Guests peaks:* 3.57 (q, 14H; CH<sub>3</sub>CH<sub>2</sub>OH); 1.10 (t, 21H; CH<sub>3</sub>CH<sub>2</sub>OH). <sup>13</sup>C-NMR (400 MHz, D<sub>2</sub>O, δ ppm): **SPA-2 peaks:** 170.8 (C<sub>ar</sub>-Tpy), 165.4 (C-oxalate), 142.6 (C<sub>ar</sub>-Tpy), 113.4 (C<sub>ar</sub>-Tpy), 67.5 (CH<sub>2</sub>-Tpy), 43.8 (C<sub>quat</sub>-Tpy), *Guests peaks:* 57.4 (CH<sub>3</sub>CH<sub>2</sub>OH), 16.8 (CH<sub>3</sub>CH<sub>2</sub>OH). Elemental Anal. (%) calcd. for {[<sub>3</sub>(H<sub>3</sub>Tpy)Al(Ox)<sub>3</sub>]·3.5H<sub>2</sub>O·6.7EtOH} (C<sub>44.40</sub>H<sub>74.20</sub>N<sub>4.00</sub>O<sub>26.20</sub>Al<sub>1.00</sub>): C, 48.03; H, 6.74; N, 5.05; Found: C, 47.94; H, 6.48; N, 5.22. <sup>1</sup>H-NMR formula: {[<sub>3</sub>(H<sub>3</sub>Tpy)Al(Ox)<sub>3</sub>]·xH<sub>2</sub>O·7.0EtOH}; EA formula: {[<sub>3</sub>(H<sub>3</sub>Tpy)Al(Ox)<sub>3</sub>]·3.5H<sub>2</sub>O·6.7EtOH}.

CH<sub>3</sub>COOH@SPA-2 (90 min.): <sup>1</sup>H-NMR (400 MHz, D<sub>2</sub>O, δ ppm): **SPA-2 peaks:** identical to EtOH@SPA2; *Guests peaks:* 3.57 (q, 11H; CH<sub>3</sub>CH<sub>2</sub>OH), 1.99 (s, 8.4H; CH<sub>3</sub>-acetic acid), 1.10 (t, 16.5H; CH<sub>3</sub>CH<sub>2</sub>OH). <sup>13</sup>C-NMR (400 MHz, D<sub>2</sub>O, δ ppm): **SPA-2 peaks:** identical to EtOH@SPA2; *Guests peaks:* 176.9 (COOH-acetic acid), 57.4 (CH<sub>3</sub>CH<sub>2</sub>OH), 20.5 (CH<sub>3</sub>-acetic acid), 16.8 (CH<sub>3</sub>CH<sub>2</sub>OH).

Elemental Anal. (%) calcd. for {[<sub>3</sub>(H<sub>3</sub>Tpy)Al(Ox)<sub>3</sub>]·2.80CH<sub>3</sub>COOH·1H<sub>2</sub>O·5.2EtOH} (C<sub>47.00</sub>H<sub>71.40</sub>N<sub>4.00</sub>O<sub>27.80</sub>Al<sub>1.00</sub>): C, 48.49; H, 6.18; N, 4.81; Found: C, 48.16; H, 5.89; N, 5.09. <sup>1</sup>H-NMR formula: {[<sub>3</sub>(H<sub>3</sub>Tpy)Al(Ox)<sub>3</sub>]·2.8CH<sub>3</sub>COOH·xH<sub>2</sub>O·5.5EtOH}; EA formula: {[<sub>3</sub>(H<sub>3</sub>Tpy)Al(Ox)<sub>3</sub>]·2.8CH<sub>3</sub>COOH·1H<sub>2</sub>O·5.2EtOH}.

CF<sub>3</sub>COOH@SPA-2 (90 min.)

<sup>1</sup>H-NMR (400 MHz, D<sub>2</sub>O, δ ppm): **SPA-2 peaks:** identical to EtOH@SPA2; *Guests peaks:* 3.57 (q, 10H; CH<sub>3</sub>CH<sub>2</sub>OH), 1.10 (t, 15H; CH<sub>3</sub>CH<sub>2</sub>OH). <sup>13</sup>C-NMR (400 MHz, D<sub>2</sub>O, δ ppm): **SPA-2 peaks:** identical to EtOH@SPA2; *Guests peaks:* 163.1-162.0 (q, COOH-trifluoroacetic acid), 120.4-111.8 (q, CF<sub>3</sub>-trifluoroacetic acid), 57.4 (CH<sub>3</sub>CH<sub>2</sub>OH), 16.8 (CH<sub>3</sub>CH<sub>2</sub>OH). Elemental Anal. (%) calcd. for {[<sub>3</sub>(H<sub>3</sub>Tpy)Al(Ox)<sub>3</sub>]·1.65F<sub>3</sub>CCOOH·2H<sub>2</sub>O·5EtOH} (C<sub>44.30</sub>H<sub>62.65</sub>N<sub>4.00</sub>O<sub>26.30</sub>Al<sub>1.00</sub>F<sub>4.95</sub>): C, 44.60; H, 5.29; N, 4.70; Found: C, 44.32; H, 4.93; N, 4.62. <sup>1</sup>H-NMR Formula: {[<sub>3</sub>(H<sub>3</sub>Tpy)Al(Ox)<sub>3</sub>]·xF<sub>3</sub>CCOOH·yH<sub>2</sub>O·5EtOH}. EA formula: {[<sub>3</sub>(H<sub>3</sub>Tpy)Al(Ox)<sub>3</sub>]·1.65F<sub>3</sub>CCOOH·2H<sub>2</sub>O·5EtOH}.

Cl<sub>3</sub>CCOOH@SPA-2 (90 min.)

<sup>1</sup>H-NMR (400 MHz, D<sub>2</sub>O, δ ppm): SPA-2 peaks: identical to EtOH@SPA2; Guests peaks: 3.57 (q, 7.9H; CH<sub>3</sub>CH<sub>2</sub>OH), 1.10 (t, 11.8H; CH<sub>3</sub>CH<sub>2</sub>OH). <sup>13</sup>C-NMR (400 MHz, D<sub>2</sub>O, δ ppm): SPA-2 peaks: identical to EtOH@SPA2; Guests peaks: 161.5 (COOH-trichloroacetic acid), 94.4 (CCl<sub>3</sub>-trichloroacetic acid), 57.4 (CH<sub>3</sub>CH<sub>2</sub>OH), 16.8 (CH<sub>3</sub>CH<sub>2</sub>OH). Elemental Anal. (%) calcd. for [(H<sub>3</sub>Tpy)Al(Ox)<sub>3</sub>]·1.5Cl<sub>3</sub>CCOOH·2H<sub>2</sub>O·3.8EtOH (C<sub>41.60</sub>H<sub>55.30</sub>N<sub>4.00</sub>O<sub>24.80</sub>Al<sub>1.00</sub>Cl<sub>4.50</sub>): C, 41.82; H, 4.67; N, 4.69; Found: C, 41.69; H, 4.39; N, 4.58. <sup>1</sup>H-NMR Formula: [(H<sub>3</sub>Tpy)Al(Ox)<sub>3</sub>]·xCl<sub>3</sub>CCOOH·yH<sub>2</sub>O·3.9EtOH; EA formula: [(H<sub>3</sub>Tpy)Al(Ox)<sub>3</sub>]·1.5Cl<sub>3</sub>CCOOH·2H<sub>2</sub>O·3.8EtOH.

Cl<sub>2</sub>CHCOOH@SPA-2 (90 min.)

<sup>1</sup>H-NMR (400 MHz, D<sub>2</sub>O, δ ppm): SPA-2 peaks: identical to EtOH@SPA2; Guests peaks: 5.95 (s, 2H; CH-dichloroacetic acid); 3.57 (q, 9.1H; CH<sub>3</sub>CH<sub>2</sub>OH), 1.10 (t, 13.6H; CH<sub>3</sub>CH<sub>2</sub>OH). <sup>13</sup>C-NMR (400 MHz, D<sub>2</sub>O, δ ppm): SPA-2 peaks: identical to EtOH@SPA2; Guests peaks: 168.9 (COOH-dichloroacetic acid), 67.9 (CHCl<sub>2</sub>-dichloroacetic acid), 57.4 (CH<sub>3</sub>CH<sub>2</sub>OH), 16.8 (CH<sub>3</sub>CH<sub>2</sub>OH). Elemental Anal. (%) calcd. for [(H<sub>3</sub>Tpy)Al(Ox)<sub>3</sub>]2Cl<sub>2</sub>CHCOOH·1.5H<sub>2</sub>O·4.5EtOH (C<sub>44.00</sub>H<sub>61.00</sub>N<sub>4.00</sub>O<sub>26.00</sub>Al<sub>1.00</sub>Cl<sub>4.00</sub>): C, 42.94; H, 5.00; N, 4.55; Found: C, 43.05; H, 4.77; N, 4.60. <sup>1</sup>H-NMR Formula: [(H<sub>3</sub>Tpy)Al(Ox)<sub>3</sub>]·2Cl<sub>2</sub>CHCOOH·xH<sub>2</sub>O·4.6EtOH; EA formula: [(H<sub>3</sub>Tpy)Al(Ox)<sub>3</sub>]·2Cl<sub>2</sub>CHCOOH·1.5H<sub>2</sub>O·4.5EtOH.

ClCH<sub>2</sub>COOH@SPA-2 (90 min.)

<sup>1</sup>H-NMR (400 MHz, D<sub>2</sub>O, δ ppm): SPA-2 peaks: identical to EtOH@SPA2; Guests peaks: 4.07 (s, 4.8H; CH<sub>2</sub>-chloroacetic acid), 3.57 (q, 11.5H; CH<sub>3</sub>CH<sub>2</sub>OH), 1.10 (t, 17.1H; CH<sub>3</sub>CH<sub>2</sub>OH). <sup>13</sup>C-NMR (400 MHz, D<sub>2</sub>O, δ ppm): SPA-2 peaks: identical to EtOH@SPA2; Guests peaks: 172.3 (COOH-chloroacetic acid), 57.4 (CH<sub>3</sub>CH<sub>2</sub>OH), 41.6 (ClCH<sub>2</sub>-chloroacetic acid), 16.8 (CH<sub>3</sub>CH<sub>2</sub>OH). Elemental Anal. (%) calcd. for [(H<sub>3</sub>Tpy)Al(Ox)<sub>3</sub>]·2.4ClCH<sub>2</sub>COOH·0.5H<sub>2</sub>O·5.4EtOH (C<sub>46.60</sub>H<sub>67.60</sub>N<sub>4.00</sub>O<sub>26.70</sub>Al<sub>1.00</sub>Cl<sub>2.40</sub>): C, 45.76; H, 5.57; N, 4.58; Found: C, 45.83; H, 5.93; N, 4.62. <sup>1</sup>H-NMR Formula: [(H<sub>3</sub>Tpy)Al(Ox)<sub>3</sub>]·2.4ClCH<sub>2</sub>COOH·xH<sub>2</sub>O·5.8EtOH; EA formula: [(H<sub>3</sub>Tpy)Al(Ox)<sub>3</sub>]·2.4ClCH<sub>2</sub>COOH·0.5H<sub>2</sub>O·5.4EtOH.

### 3) Competitive sorption of acetic acid and halogenated analogues:

**General experimental procedure:** Ca 150 mg of freshly prepared as-synthesized SPA-2 crystals are soaked during 4h in absolute ethanol. Resulting crystals, EtOH@SPA-2, are then engaged in sorption experiments, by replacing supernatant EtOH by the desired guests' equimolar solution in absolute ethanol (15 mL, acid concentration = 3M). After the desired soaking time, crystals engaged in characterizations are removed from the guest solution, pressed during 1 min between two pieces of chromatography paper to remove supernatant solution, and immediately dissolved in D<sub>2</sub>O for <sup>1</sup>H- and <sup>13</sup>C-NMR experiments.

#### **Reference experiment: CH<sub>3</sub>COOH@SPA-2 (72h)**

<sup>1</sup>H-NMR (400 MHz, D<sub>2</sub>O, δ ppm): SPA-2 peaks: 8.52 – 8.45 (m, 8H; H<sub>ar</sub>-Tpy); 7.51 – 7.42 (m, 8H; H<sub>ar</sub>-Tpy); 4.80 (s, 8H; CH<sub>2</sub>-Tpy); Guests peaks: 3.57 (q, 11.1H; CH<sub>3</sub>CH<sub>2</sub>OH), 1.99 (s, 8.5H; CH<sub>3</sub>-acetic acid), 1.10 (t, 16.7H; CH<sub>3</sub>CH<sub>2</sub>OH). <sup>13</sup>C-NMR (400 MHz, D<sub>2</sub>O, δ ppm): SPA-2 peaks: 170.8 (C<sub>ar</sub>-Tpy), 165.4 (C-oxalate), 142.6 (C<sub>ar</sub>-Tpy), 113.4 (C<sub>ar</sub>-Tpy); 67.5 (CH<sub>2</sub>-Tpy); 43.8 (C<sub>quat</sub>-Tpy); Guests peaks: 176.9 (COOH-acetic acid); 57.4 (CH<sub>3</sub>CH<sub>2</sub>OH), 20.5 (CH<sub>3</sub>-acetic acid); 16.8 (CH<sub>3</sub>CH<sub>2</sub>OH). <sup>1</sup>H-NMR formula: [(H<sub>3</sub>Tpy)Al(Ox)<sub>3</sub>]·2.8CH<sub>3</sub>COOH·xH<sub>2</sub>O·5.5EtOH}.

#### **Competitive sorption between CF<sub>3</sub>COOH and CH<sub>3</sub>COOH (72h)**

<sup>1</sup>H-NMR (400 MHz, D<sub>2</sub>O, δ ppm): SPA-2 peaks: identical to CH<sub>3</sub>COOH@SPA-2; Guests peaks: 3.57 (q, 5.4H; CH<sub>3</sub>CH<sub>2</sub>OH), 1.99 (s, 0.9H; CH<sub>3</sub>-acetic acid), 1.10 (t, 8.1H; CH<sub>3</sub>CH<sub>2</sub>OH). <sup>13</sup>C-NMR (400 MHz, D<sub>2</sub>O, δ ppm): SPA-2 peaks: identical to CH<sub>3</sub>COOH@SPA-2; Guests peaks: 176.9 (COOH-acetic acid), 163.1-162.0 (COOH-trifluoroacetic acid), 120.4-111.8 (q, CF<sub>3</sub>-trifluoroacetic acid), 57.4 (CH<sub>3</sub>CH<sub>2</sub>OH), 20.5 (CH<sub>3</sub>-acetic acid), 16.8 (CH<sub>3</sub>CH<sub>2</sub>OH). <sup>1</sup>H-NMR formula: [(H<sub>3</sub>Tpy)Al(Ox)<sub>3</sub>]·0.3CH<sub>3</sub>COOH·xCF<sub>3</sub>COOH·yH<sub>2</sub>O·2.7EtOH}.

#### **Competitive sorption between Cl<sub>3</sub>CCOOH and CH<sub>3</sub>COOH (72h)**

<sup>1</sup>H-NMR (400 MHz, D<sub>2</sub>O, δ ppm): SPA-2 peaks: identical to CH<sub>3</sub>COOH@SPA-2; Guests peaks: 3.57 (q, 5H; CH<sub>3</sub>CH<sub>2</sub>OH), 1.99 (s, 1H; CH<sub>3</sub>-acetic acid), 1.10 (t, 7.5H; CH<sub>3</sub>CH<sub>2</sub>OH). <sup>13</sup>C-NMR (400 MHz, D<sub>2</sub>O, δ ppm): SPA-2 peaks: identical to CH<sub>3</sub>COOH@SPA-2; Guests peaks: 176.9 (COOH-acetic acid), 161.5 (COOH-trichloroacetic acid), 94.4 (CCl<sub>3</sub>-

trichloroacetic acid), 57.4 ( $\text{CH}_3\text{CH}_2\text{OH}$ ), 20.5 ( $\text{CH}_3$ -acetic acid), 16.8 ( $\text{CH}_3\text{CH}_2\text{OH}$ ).  $^1\text{H-NMR}$  formula:  $\{[(\text{H}_3\text{Tpy})\text{Al}(\text{Ox})_3] \cdot 0.3\text{CH}_3\text{COOH} \cdot x\text{CCl}_3\text{COOH} \cdot y\text{H}_2\text{O} \cdot 2.5\text{EtOH}\}$ .

#### Competitive sorption between $\text{Cl}_2\text{CHCOOH}$ and $\text{CH}_3\text{COOH}$ (72h)

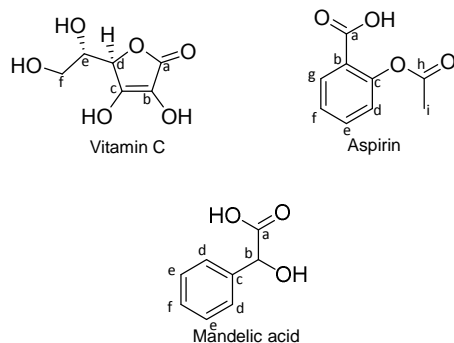
$^1\text{H-NMR}$  (400 MHz,  $\text{D}_2\text{O}$ ,  $\delta$  ppm): **SPA-2 peaks:** identical to  $\text{CH}_3\text{COOH@SPA-2}$ ; *Guests peaks:* 5.98 (s, 1.5 H,  $\text{CH}$ -dichloroacetic acid), 3.57 (q, 6.1H;  $\text{CH}_3\text{CH}_2\text{OH}$ ), 1.99 (s, 1.8H;  $\text{CH}_3$ -acetic acid), 1.10 (t, 9.3H;  $\text{CH}_3\text{CH}_2\text{OH}$ ).  $^{13}\text{C-NMR}$  (400 MHz,  $\text{D}_2\text{O}$ ,  $\delta$  ppm): **SPA-2 peaks:** identical to  $\text{CH}_3\text{COOH@SPA-2}$ ; 176.9 ( $\text{COOH}$ -acetic acid), 168.9 ( $\text{COOH}$ -dichloroacetic acid), 67.9 ( $\text{CHCl}_2$ -dichloroacetic acid), 57.4 ( $\text{CH}_3\text{CH}_2\text{OH}$ ), 20.5 ( $\text{CH}_3$ -acetic acid), 16.8 ( $\text{CH}_3\text{CH}_2\text{OH}$ ).  $^1\text{H-NMR}$  formula:  $\{[(\text{H}_3\text{Tpy})\text{Al}(\text{Ox})_3] \cdot 0.6\text{CH}_3\text{COOH} \cdot 1.5\text{Cl}_2\text{CHCOOH} \cdot y\text{H}_2\text{O} \cdot 3.1\text{EtOH}\}$ .

#### Competitive sorption between $\text{ClCH}_2\text{COOH}$ and $\text{CH}_3\text{COOH}$ (72h)

$^1\text{H-NMR}$  (400 MHz,  $\text{D}_2\text{O}$ ,  $\delta$  ppm): **SPA-2 peaks:** identical to  $\text{CH}_3\text{COOH@SPA-2}$ ; *Guests peaks:* 4.12 (s, 3.9H;  $\text{CH}_2$ -chloroacetic acid) 3.57 (q, 6.6H;  $\text{CH}_3\text{CH}_2\text{OH}$ ), 1.99 (s, 3.1H;  $\text{CH}_3$ -acetic acid), 1.10 (t, 10H;  $\text{CH}_3\text{CH}_2\text{OH}$ ).  $^{13}\text{C-NMR}$  (400 MHz,  $\text{D}_2\text{O}$ ,  $\delta$  ppm): **SPA-2 peaks:** identical to  $\text{CH}_3\text{COOH@SPA-2}$ ; 176.9 ( $\text{COOH}$ -acetic acid), 172.3 ( $\text{COOH}$ -chloroacetic acid), 57.4 ( $\text{CH}_3\text{CH}_2\text{OH}$ ), 41.6 ( $\text{CHCl}_2$ -dichloroacetic acid), 20.5 ( $\text{CH}_3$ -acetic acid), 16.8 ( $\text{CH}_3\text{CH}_2\text{OH}$ ).  $^1\text{H-NMR}$  formula:  $\{[(\text{H}_3\text{Tpy})\text{Al}(\text{Ox})_3] \cdot 1.95 \text{ClCH}_2\text{COOH} \cdot 1\text{CH}_3\text{COOH} \cdot y\text{H}_2\text{O} \cdot 3.3\text{EtOH}\}$ .

## 4) Drugs sorption:

**General experimental procedure:** Ca 150 mg of freshly prepared as-synthesized **SPA-2** crystals is soaked during 4h in absolute ethanol or in acetone. Resulting crystals,  $\text{EtOH@SPA-2}$  or  $\text{Acetone@SPA-2}$ , are then engaged in sorption experiments, by replacing supernatant solution by the desired guests' solution in absolute ethanol (15 mL, for vitamin C, aspirin and mandelic acid) or absolute acetone (15 mL, for aspirin and mandelic acid; Vitamin C is not soluble in this solvent). 0.3M solutions were used, except for Vitamin C for which it was 0.1M because of the lower solubility of this molecule. After the desired soaking time, crystals engaged in characterizations are removed from the guest solution, pressed during 1 min between two pieces of chromatography paper to remove supernatant solution, and resulting solid immediately dissolved in  $\text{D}_2\text{O}$  (for  $^1\text{H}$ - and  $^{13}\text{C}$ -NMR experiments) or subjected to EA.



Vitamin C@**SPA-2** (0.1 M, Ethanol, 3days):

$^1\text{H-NMR}$  (400 MHz,  $\text{D}_2\text{O}$ ,  $\delta$  ppm): 8.52 – 8.45 (m, 8H;  $\text{H}_{\text{ar-Tpy}}$ ); 7.51 – 7.42 (m, 8H;  $\text{H}_{\text{ar-Tpy}}$ ); 4.80 (broad s, 8H;  $\text{CH}_2\text{-Tpy}$  + 1.2H; CH-Vitamin C cycle); 4.01 – 3.96 (m, 1.2H; CHOH-Vitamin C); 3.68 – 3.66 (m, 2.4H;  $\text{CH}_2\text{-Vitamin C}$ ); 3.57 (q, 8.4H;  $\text{CH}_3\text{CH}_2\text{OH}$ ); 1.10 (t, 12.6H;  $\text{CH}_3\text{CH}_2\text{OH}$ ).  $^{13}\text{C-NMR}$  (400 MHz,  $\text{D}_2\text{O}$ ,  $\delta$  ppm): **SPA-2 peaks:** 170.8 ( $\text{C}_{\text{ar-Tpy}}$ ), 165.4 (C-oxalate), 142.6 ( $\text{C}_{\text{ar-Tpy}}$ ), 113.4 ( $\text{C}_{\text{ar-Tpy}}$ ); 67.5 ( $\text{CH}_2\text{-Tpy}$ ); 43.8 ( $\text{C}_{\text{quat-Tpy}}$ ); **Guests peaks:** 173.5 ( $\text{C}_a\text{-Vitamin C}$ ), 156.7 ( $\text{C}_c\text{-Vitamin C}$ ), 117.5 ( $\text{C}_b\text{-Vitamin C}$ ), 76.2 ( $\text{C}_d\text{-Vitamin C}$ ), 67.5 ( $\text{C}_e\text{-Vitamin C}$ ), 62.0 ( $\text{C}_f\text{-Vitamin C}$ ), 57.4 ( $\text{CH}_3\text{CH}_2\text{OH}$ ), 16.8 ( $\text{CH}_3\text{CH}_2\text{OH}$ ). Elemental Anal. (%) calcd. for  $\{[(\text{H}_3\text{Tpy})\text{Al}(\text{Ox})_3] \cdot 1.2\text{Vitamin C} \cdot 3\text{H}_2\text{O} \cdot 4\text{EtOH}\}$  ( $\text{C}_{46.20}\text{H}_{66.60}\text{N}_{4.00}\text{O}_{30.20}\text{Al}_{1.00}$ ): C, 46.70; H, 5.65; N, 4.72; Found: C, 46.40; H, 5.33; N, 4.43.  $^1\text{H-NMR}$  formula:  $\{[(\text{H}_3\text{Tpy})\text{Al}(\text{Ox})_3] \cdot 1.2\text{Vitamin C} \cdot x\text{H}_2\text{O} \cdot 4.2\text{EtOH}\}$ ; EA formula:  $\{[(\text{H}_3\text{Tpy})\text{Al}(\text{Ox})_3] \cdot 1.2\text{Vitamin C} \cdot 3\text{H}_2\text{O} \cdot 4\text{EtOH}\}$ .

Mandelic acid@**SPA-2** (0.3 M, Ethanol, 3days):

$^1\text{H-NMR}$  (400 MHz,  $\text{D}_2\text{O}$ ,  $\delta$  ppm): **SPA-2 peaks:** 8.52 – 8.45 (m, 8H;  $\text{H}_{\text{ar-Tpy}}$ ); 7.51 – 7.42 (m, 8H;  $\text{H}_{\text{ar-Tpy}}$ ); 4.80 (s, 8H;  $\text{CH}_2\text{-Tpy}$ ); **Guests peaks:** 7.36 (m, 7H;  $\text{H}_{\text{ar-Mandelic acid}}$ ); 5.17 (s, 1.4H; CH-Mandelic acid); 3.57 (q, 2.8H;  $\text{CH}_3\text{CH}_2\text{OH}$ ); 1.10 (t, 4.2H;  $\text{CH}_3\text{CH}_2\text{OH}$ ).  $^{13}\text{C-NMR}$  (400 MHz,  $\text{D}_2\text{O}$ ,  $\delta$  ppm): **SPA-2 peaks:** identical to Vitamin C@**SPA-2**; **Guests peaks:** 176.5 ( $\text{C}_a\text{-Mandelic acid}$ ), 138.3 ( $\text{C}_c\text{-Mandelic acid}$ ), 129.0 ( $\text{C}_e\text{-Mandelic acid}$ ), 128.8 ( $\text{C}_f\text{-Mandelic acid}$ ), 127.0 ( $\text{C}_d\text{-Mandelic acid}$ ), 73.1 ( $\text{C}_b\text{-Mandelic acid}$ ), 57.4 ( $\text{CH}_3\text{CH}_2\text{OH}$ ), 16.8 ( $\text{CH}_3\text{CH}_2\text{OH}$ ). Elemental Anal. (%) calcd. for  $\{[(\text{H}_3\text{Tpy})\text{Al}(\text{Ox})_3] \cdot 1.4\text{mandelic acid} \cdot 4\text{H}_2\text{O} \cdot 1.4\text{EtOH}\}$  ( $\text{C}_{45.00}\text{H}_{54.60}\text{N}_{4.00}\text{O}_{25.60}\text{Al}_{1.00}$ ): C, 49.67; H, 5.06; N, 5.15; Found: C, 49.60; H, 4.99; N, 4.88.  $^1\text{H-NMR}$  formula:  $\{[(\text{H}_3\text{Tpy})\text{Al}(\text{Ox})_3] \cdot 1.4\text{Mandelic acid} \cdot x\text{H}_2\text{O} \cdot 1.4\text{EtOH}\}$ ; EA formula:  $\{[(\text{H}_3\text{Tpy})\text{Al}(\text{Ox})_3] \cdot 1.4\text{Mandelic acid} \cdot 4\text{H}_2\text{O} \cdot 1.4\text{EtOH}\}$ .

Acetone@SPA-2 (4h):

<sup>1</sup>H-NMR (400 MHz, D<sub>2</sub>O, δ ppm): SPA-2 peaks: 8.52 – 8.45 (m, 8H; H<sub>ar</sub>-Tpy); 7.51 – 7.42 (m, H; H<sub>ar</sub>-Tpy); 4.80 (s, 8H; CH<sub>2</sub>-Tpy); Guests peaks: 2.15 (s, 24H; CH<sub>3</sub>-acetone). <sup>13</sup>C-NMR (400 MHz, D<sub>2</sub>O, δ ppm): SPA-2 peaks: 170.7 (C<sub>ar</sub>-Tpy), 165.4 (C-oxalate), 142.7 (C<sub>ar</sub>-Tpy), 113.1 (C<sub>ar</sub>-Tpy), 67.6 (CH<sub>2</sub>-Tpy), 43.8 (C<sub>quat</sub>-Tpy), Guests peaks: 215.3 (C=O-Acetone), 30.2 (CH<sub>3</sub>-Acetone). Elemental Anal. (%) calcd. for {(H<sub>3</sub>Tpy)Al(Ox)<sub>3</sub>·6.1H<sub>2</sub>O·4.1Acetone} (C<sub>43.30</sub>H<sub>63.80</sub>N<sub>4.00</sub>O<sub>26.20</sub>Al<sub>1.00</sub>): C, 47.86; H, 5.92; N, 5.16; Found: C, 47.74; H, 5.63; N, 5.28. <sup>1</sup>H-NMR formula: {(H<sub>3</sub>Tpy)Al(Ox)<sub>3</sub>·xH<sub>2</sub>O·4Acetone}; EA formula: {(H<sub>3</sub>Tpy)Al(Ox)<sub>3</sub>·6.1H<sub>2</sub>O·4.1Acetone}.

Aspirin@SPA-2 (0.3 M, Acetone, 3days):

<sup>1</sup>H-NMR (400 MHz, D<sub>2</sub>O, δ ppm): SPA-2 peaks: identical to Acetone@SPA-2; Guests peaks: 7.87 – 7.84 (m, 1H; H<sub>ar</sub>-Aspirin); 7.61 – 7.57 (m, 1H; H<sub>ar</sub>-Aspirin); 7.38 – 7.33 (m, 1H; H<sub>ar</sub>-Aspirin); 7.15 – 7.12 (m, 1H; H<sub>ar</sub>-Aspirin); 2.28 (s, 3.1H; CH<sub>3</sub>-Aspirin), 2.15 (s, 18.5H; CH<sub>3</sub>-acetone). <sup>13</sup>C-NMR (400 MHz, D<sub>2</sub>O, δ ppm): SPA-2 peaks: identical to Acetone@SPA-2; Guests peaks: 215.3 (C=O-Acetone), 173.4 (C<sub>a</sub>-Aspirin), 168.9 (C<sub>h</sub>-Aspirin), 149.2 (C<sub>c</sub>-Aspirin), 134.3 (C<sub>e</sub>-Aspirin), 131.3 (C<sub>g</sub>-Aspirin), 126.8 (C<sub>f</sub>-Aspirin), 123.3 (C<sub>d</sub>-Aspirin), 119.6 (C<sub>b</sub>-Aspirin), 30.2 (CH<sub>3</sub>-Acetone), 20.4 (C<sub>i</sub>-Aspirin). Elemental Anal. (%) calcd. for {(H<sub>3</sub>Tpy)Al(Ox)<sub>3</sub>·0.95Aspirine·2.9H<sub>2</sub>O·3Acetone} (C<sub>48.55</sub>H<sub>58.40</sub>N<sub>4</sub>O<sub>25.70</sub>Al<sub>1.00</sub>): C, 51.32; H, 5.18; N, 4.93; Found: C, 50.95; H, 5.11; N, 4.74. <sup>1</sup>H-NMR formula: {(H<sub>3</sub>Tpy)Al(Ox)<sub>3</sub>·1Aspirine·xH<sub>2</sub>O·3.1Acetone}; EA formula: {(H<sub>3</sub>Tpy)Al(Ox)<sub>3</sub>·0.95Aspirine·2.9H<sub>2</sub>O·3Acetone}.

Mandelic acid@SPA-2 (0.3 M, Acetone, 3days):

<sup>1</sup>H-NMR (400 MHz, D<sub>2</sub>O, δ ppm): SPA-2 peaks: identical to Acetone@SPA-2; Guests peaks: 7.36 (m, 11H; H<sub>ar</sub>-Mandelic acid); 5.17 (s, 2.2H; CH-Mandelic acid); 2.15 (s, 4.2H; CH<sub>3</sub>-acetone). <sup>13</sup>C-NMR (400 MHz, D<sub>2</sub>O, δ ppm): SPA-2 peaks: identical to Acetone@SPA-2; Guests peaks: 215.3 (C=O-Acetone), 176.2 (C<sub>a</sub>-Mandelic acid), 138.0 (C<sub>c</sub>-Mandelic acid), 129.0 (C<sub>e</sub>-Mandelic acid), 128.9 (C<sub>f</sub>-Mandelic acid), 127.0 (C<sub>d</sub>-Mandelic acid), 72.9 (C<sub>b</sub>-Mandelic acid), 30.2 (CH<sub>3</sub>-acetone). Elemental Anal. (%) calcd. for {(H<sub>3</sub>Tpy)Al(Ox)<sub>3</sub>·2.2Mandelic acid·3.5H<sub>2</sub>O·0.6Acetone} (C<sub>50.40</sub>H<sub>55.20</sub>N<sub>4</sub>O<sub>26.70</sub>Al<sub>1.00</sub>): C, 51.69; H, 4.75; N, 4.78; Found: C, 51.32; H, 4.63; N, 4.48. <sup>1</sup>H-NMR formula: {(H<sub>3</sub>Tpy)Al(Ox)<sub>3</sub>·2.2Mandelic acid·xH<sub>2</sub>O·0.7Acetone}; EA formula: {(H<sub>3</sub>Tpy)Al(Ox)<sub>3</sub>·2.2Mandelic acid·3.5H<sub>2</sub>O·0.6Acetone}.

## B. Figures

**Figure S1.** ORTEP view of the asymmetric unit of **SPA-2·HNO<sub>3</sub>**, with ellipsoids cut at the 30% probability level. H<sub>2</sub>O molecules and Hydrogen of Carbon atoms are not represented for sake of clarity. Color codes: C, grey; H, black, N, blue; O, red.

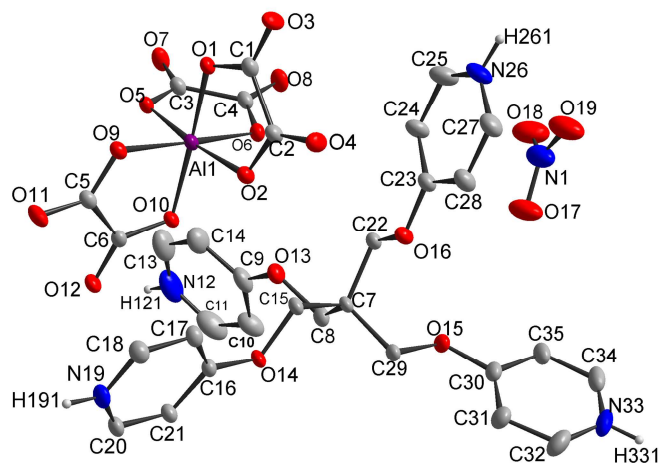


**Figure S2.** Reciprocal H-bonded assemblage between  $[\text{Al}(\text{Ox})_3]^{3-}$  metal-organic units and  $\text{H}_4\text{-Tpy}^{4+}$  cations.

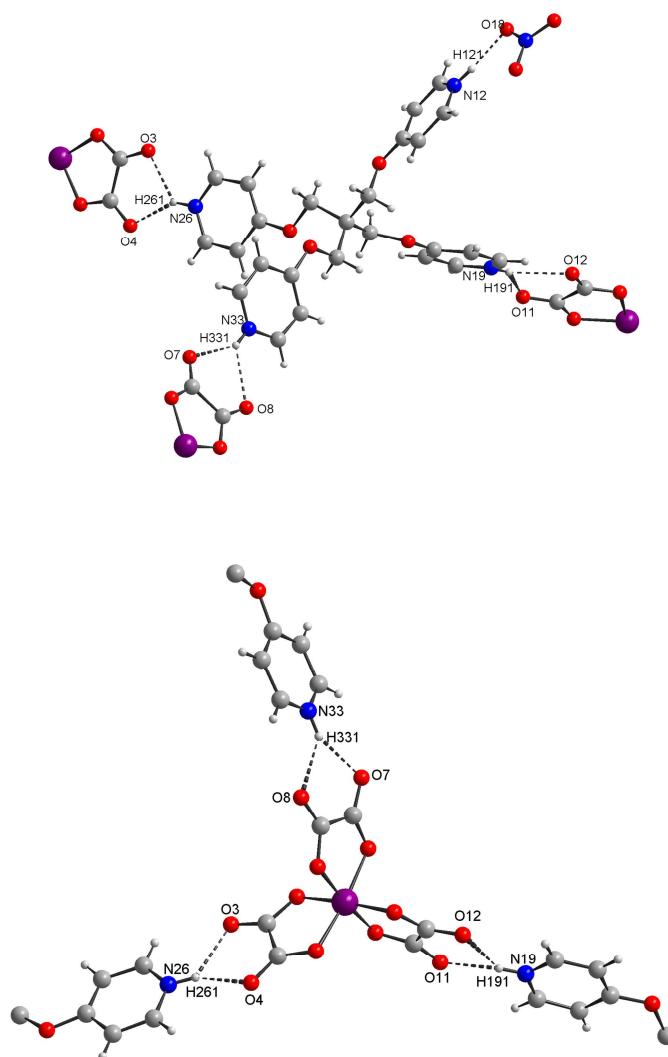
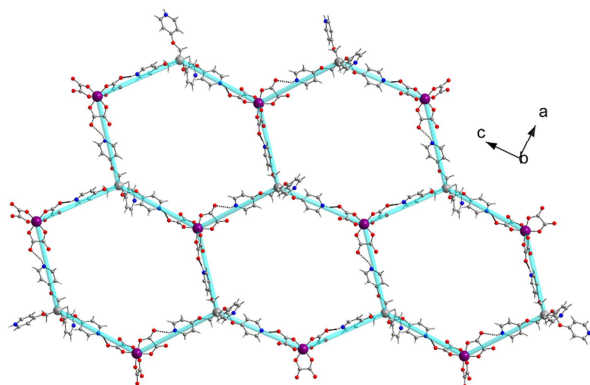


**Figure S3. 2D H-bonded corrugated layers in SPA-2·HNO<sub>3</sub>.** (a) 2D corrugated honeycomb-like layer resulting from the H-bonding between [Al(Ox)<sub>3</sub>]<sup>3-</sup> and (H<sub>4</sub>-Tpy)<sup>3+</sup> units (HNO<sub>3</sub> are omitted for the sake of clarity). (b) Positioning of pyridinium nitrate groups relative to the 2D H-bonded layer.

a)



b)

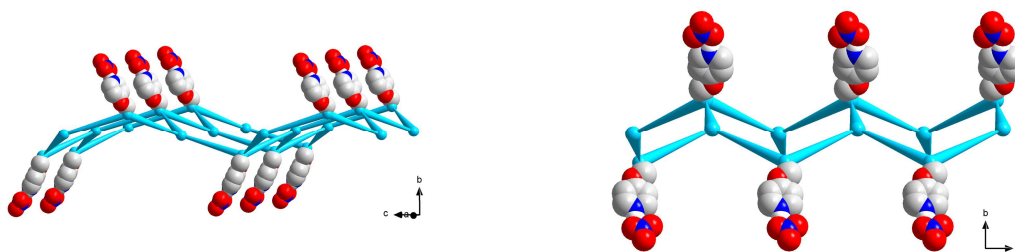


**Figure S4.** (*top*) Schematic representation of the 2D to 3D mutual interpenetration for the two sets of 2D layers existing in SPA-2·HNO<sub>3</sub>. (*bottom*) View showing the angle between the two sets of interpenetrated honeycomb layers; the angle was estimated by measuring the angle between their corresponding virtual planes. Each plane was determined by selecting 6 nodes (forming a closed hexagonal loop) of the corresponding corrugated honeycomb layer. Plane construction and angle determination were done using Diamond<sup>®</sup> software version 3.

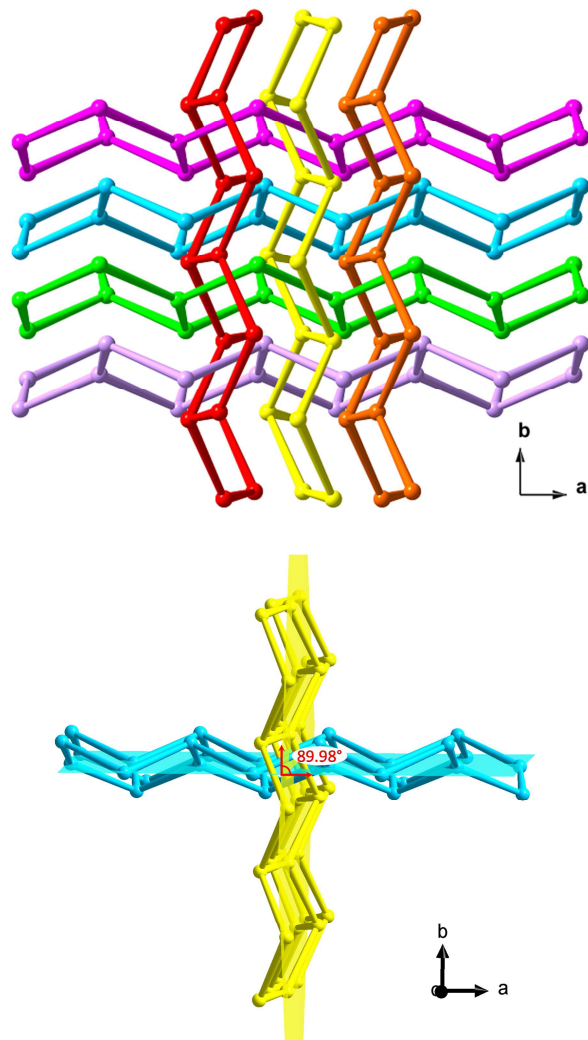


**Figure S5.** (a) Spacefill representation for the supramolecular architecture of SPA-2·HNO<sub>3</sub>. Guest solvent molecules are omitted. (b) Apparent pore size estimation for SPA-2·HNO<sub>3</sub>: vertical arrow, 6Å; horizontal arrow, 4Å. Color codes: C, grey; H, black, N, blue; O, red.

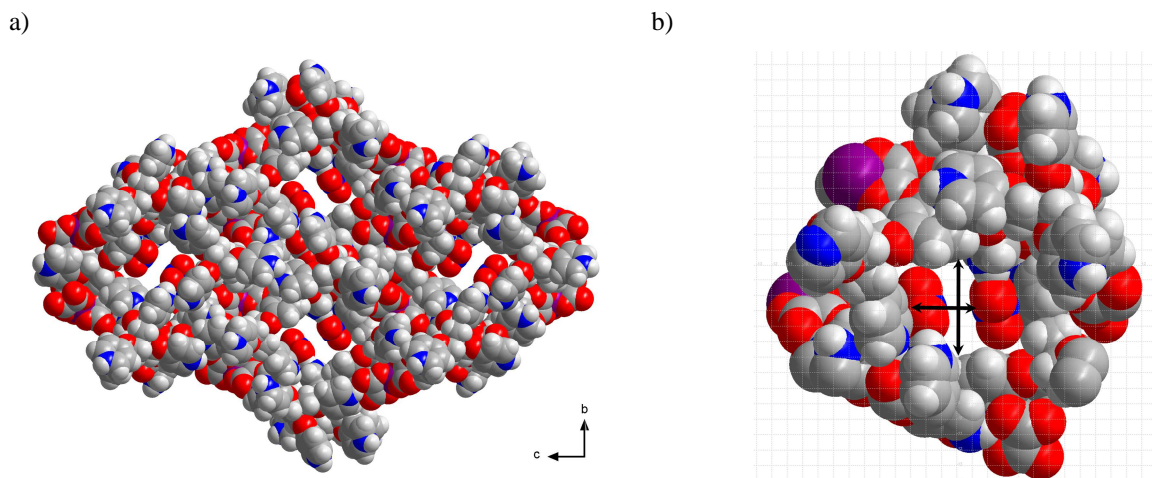


**Figure S6.** Supramolecular interactions (dashed lines) between H-bonded framework and nitrate ions in SPA-2·HNO<sub>3</sub> ( $d(\text{N12}\cdots\text{O18}) = 2.77 \text{ \AA}$ ;  $d(\text{N1}\cdots\text{C24}) = 3.28 \text{ \AA}$ ;  $d(\text{O17}\cdots\text{C23}) = 3.23 \text{ \AA}$ ;  $d(\text{O19}\cdots\text{C25}) = 3.18 \text{ \AA}$ ). Color codes: C, grey; H, black, N, blue; O, red.

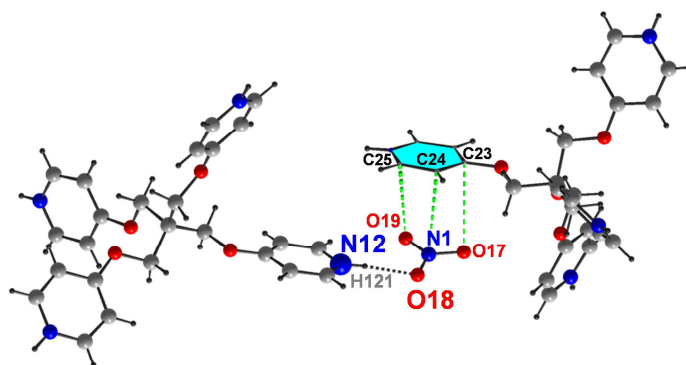


**Figure S7.** Comparison of IR spectra (KBr pellets) registered for **SPA-2·HNO<sub>3</sub>** (blue) and **SPA-2** (black). (a) Full window (3900-700  $\text{cm}^{-1}$ ) and (b) enlarged view for the 1900-1000  $\text{cm}^{-1}$  region. Red arrow tags the nitrate band (1385  $\text{cm}^{-1}$ ) in **SPA-2·HNO<sub>3</sub>**; this band disappears in IR spectrum of **SPA-2**.

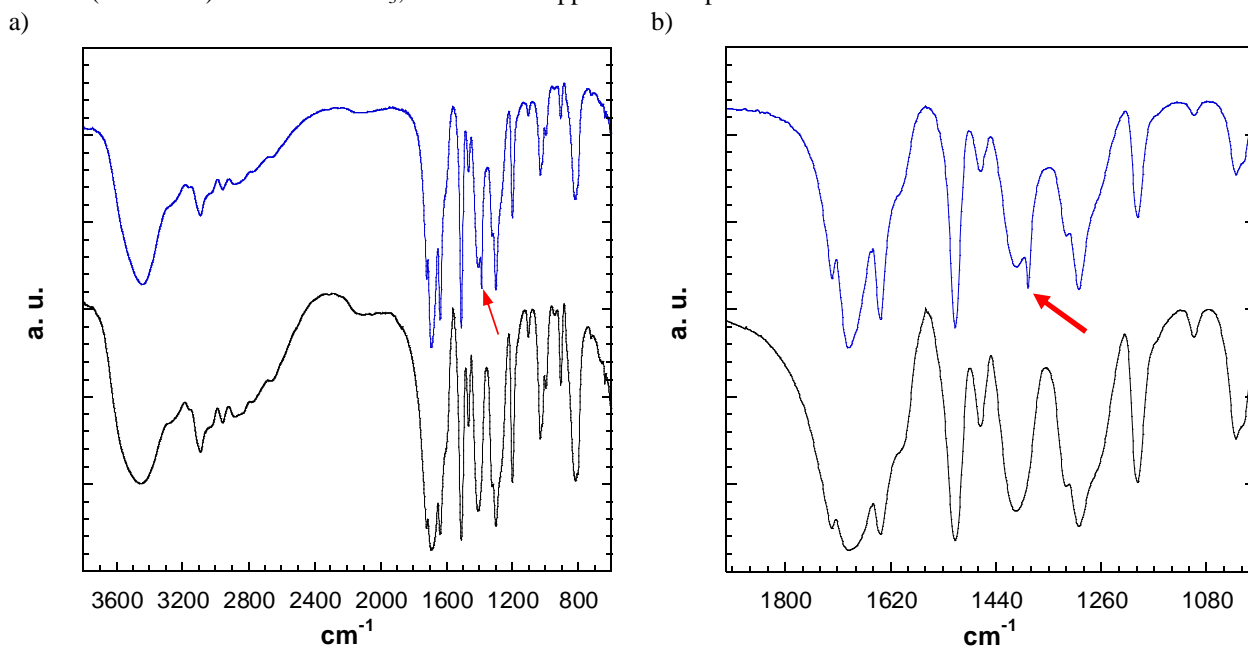


**Figure S8.** TGA traces (RT-600°C) for **SPA-2·HNO<sub>3</sub>** and **SPA-2**. (a) Comparison between TGA traces obtained for as-synthesized **SPA-2·HNO<sub>3</sub>** (blue) and **SPA-2** (black). (b) Enlarged view of TGA trace for **SPA-2·HNO<sub>3</sub>**: ①, 29.1% weight loss (15 H<sub>2</sub>O + 2EtOH); ②, 7.3% weight loss (loss of HNO<sub>3</sub> + 2 H<sub>2</sub>O); ③, EA, IR and <sup>1</sup>H-NMR performed on **SPA-2·HNO<sub>3</sub>** progressively heated to 245°C under nitrogen flux confirmed the chemical integrity of the [(H<sub>3</sub>tpy)Al(Ox)<sub>3</sub>] units and the disappearance of the nitrate ion.

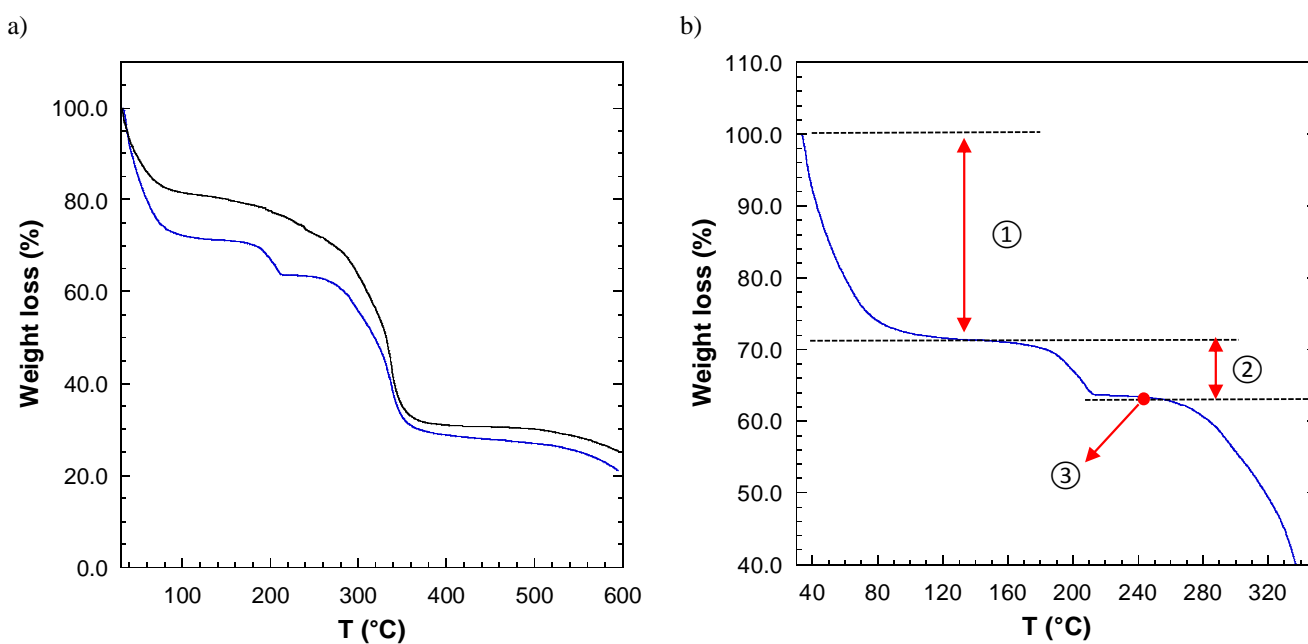


**Figure S9.** (a) Experimental PXRD diffractograms (293K, isolated solids) for **SPA-2**·HNO<sub>3</sub> (black) and **SPA-2** (blue); (b, c) comparison of the experimental diffractograms (black) and the ones calculated (red) from the corresponding crystal structures cif (data collected at 120K) to highlight the effect of the cell changes (see comments below); (c) diffractograms for **SPA-2**·HNO<sub>3</sub> (black) and **SPA-2** (blue) calculated from the respective crystal structures cif.

The diffractograms collected at 293 K for **SPA-2**·HNO<sub>3</sub> (black) and **SPA-2** (blue) are very similar, as do the diffractograms calculated from the cif of the corresponding crystal structures. However, a clear shift of the peaks is found between the experimental and calculated diffractograms. The cell parameters refined on the PXRD of **SPA-2** revealed an increase by ca. 0.5 Å for *a* and *b* whereas *c* is shrunk by same value as compared to the value found at 100 K (see table below). This can be attributed to a deformation of the framework at 293 K as compared to 100 K, a consequence of the release of part of the guest molecules.

	Single crystal 120 K	Powder 293 K
Space group	<i>P4<sub>1</sub>2<sub>1</sub>2<sub>1</sub></i>	<i>P4<sub>1</sub>2<sub>1</sub>2<sub>1</sub></i>
<i>a</i> = <i>b</i> (Å)	18.0205(6)	18.563(1)
<i>c</i> (Å)	38.474(1)	37.965(3)
<i>V</i> (Å <sup>3</sup> )	12493.9(4)	13082(1)

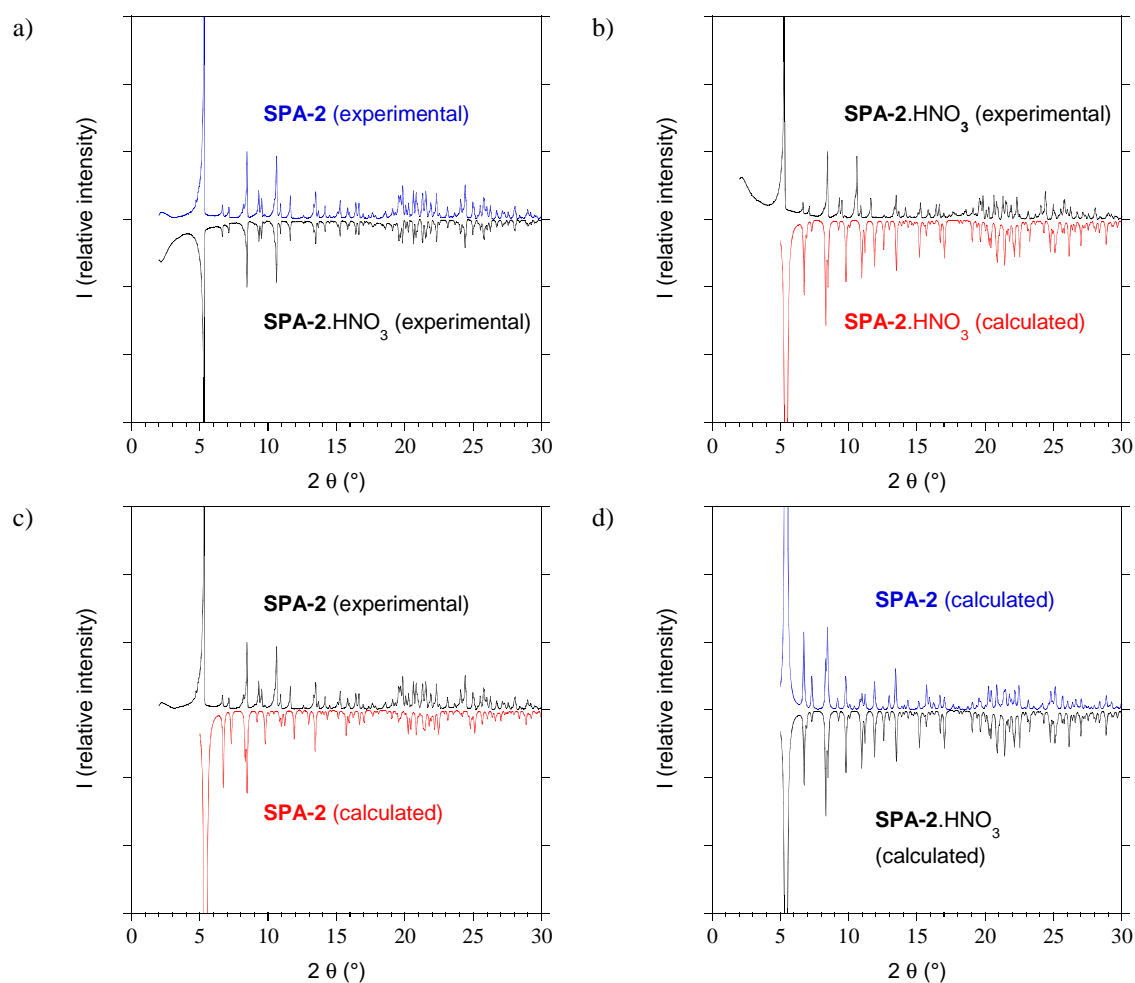


**Figure S10.** ORTEP view of the asymmetric unit of **SPA-2**, with ellipsoids cut at the 30% probability level. H<sub>2</sub>O molecules and Hydrogen of Carbon atoms are not represented for sake of clarity. Color codes: C, grey; H, black, N, blue; O, red.

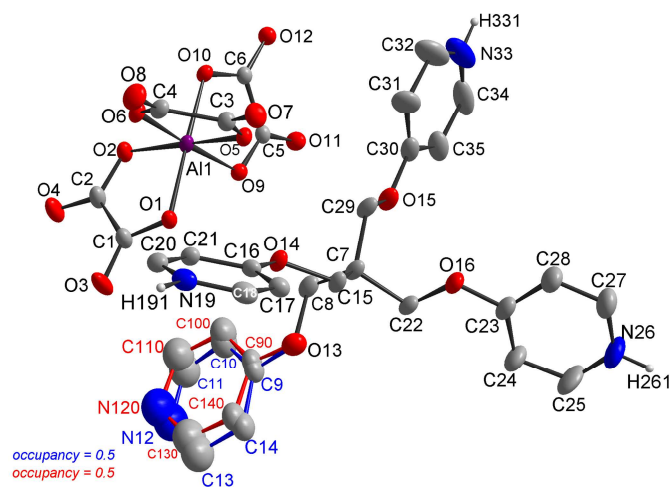
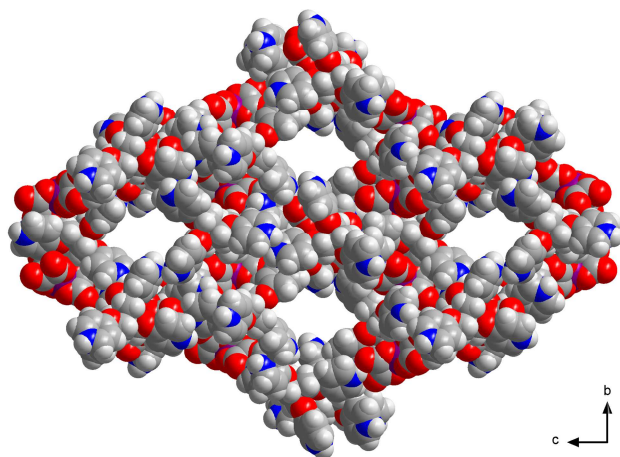


**Figure S11.** (a) Spacefill representation for the supramolecular architectures of **SPA-2**. Guest solvent molecules are omitted. (b) Apparent pore size estimation for **SPA-2**: vertical arrow, 6Å; horizontal arrow, 7.5Å. Color codes: C, grey; H, black, N, blue; O, red.

a)



b)

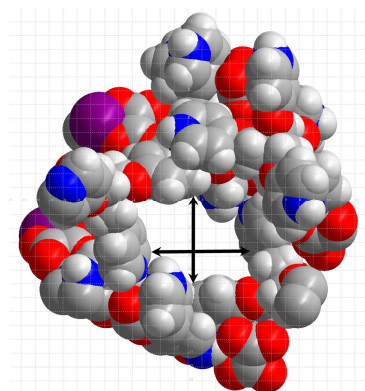


**Figure S12.** (a) Additional pores observed along [111] crystallographic direction after the removal of  $\text{HNO}_3$ . (b) Apparent pore size estimation: vertical arrow, 3Å; horizontal arrow, 6Å. Color codes: C, grey; H, black, N, blue; O, red.

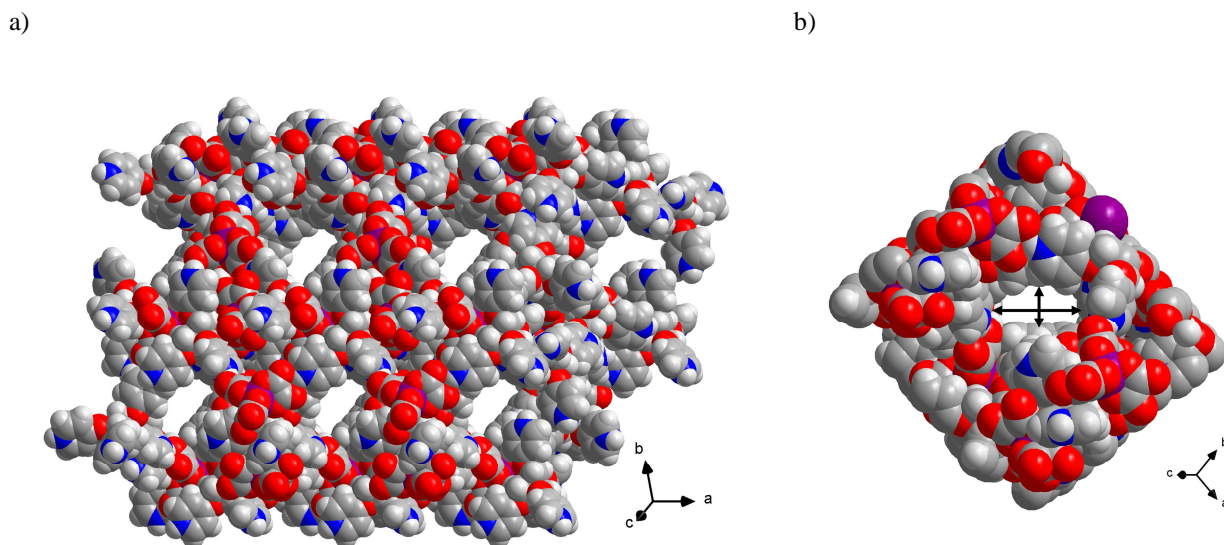


**Figure S13.** Organization of free pyridil groups in the channels of SPA-2. (a) View of one channel along  $a$ . (b) Sectional pore view along  $c$ .  $d_1 = 11.4\text{Å}$ ,  $d_2 = 12.0\text{Å}$  and  $d_3 = 18.0\text{Å}$ . Color codes: C, grey; H, black, N, blue; O, red.

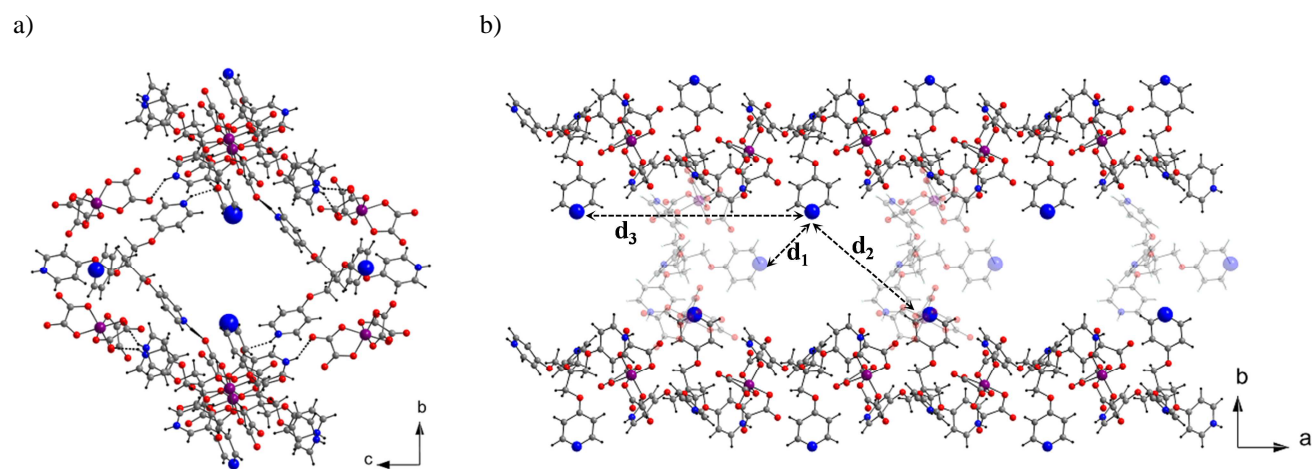


**Figure S14.** PXRD for SPA-2 as-synthesized material (red, registered at RT), SPA-2 stored in air during 1 week before (black, registered at RT) and after soaking in 4:1 EtOH:H<sub>2</sub>O (blue, registered at RT).

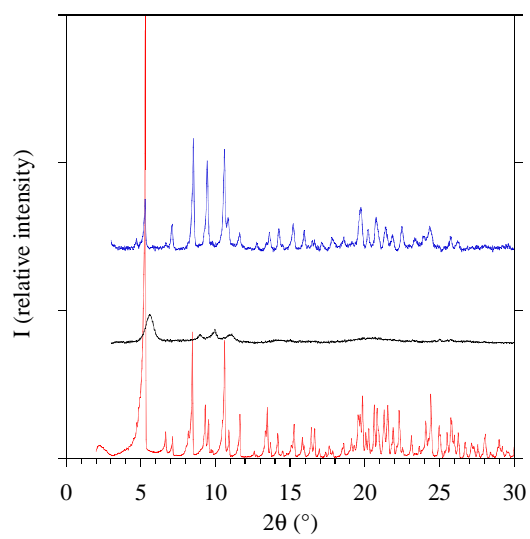


**Figure S15.** Comparison of representative TGA traces (RT-600°C) for as-synthesized SPA-2 (black) and several solvent@SPA-2 materials (red) obtained after 1 month of soaking: (a) acetone@SPA-2, (b) CHCl<sub>3</sub>@SPA-2; (c) EtOH@SPA-2 and (d) iPrOH@SPA-2.

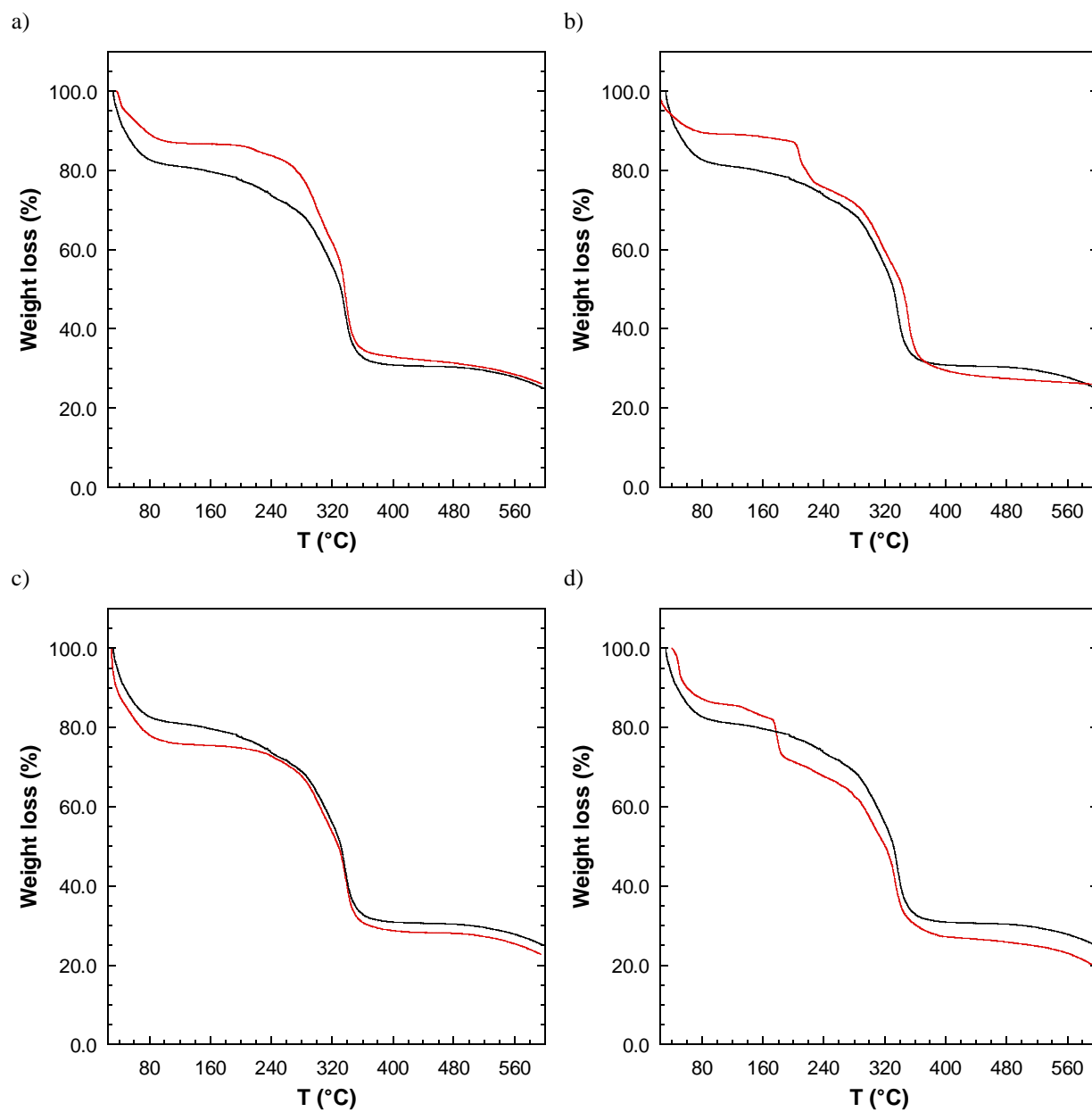


**Figure S16.** PXRD diffractograms calculated from SCXRD data collected at 100K for solvent@**SPA-2** crystals (1 month of soaking). Colour codes for **SPA-2** crystals soaked in: ethanol (black), isopropanol (green), acetone (red),  $\text{CHCl}_3$  (cyan). Reference diffractogram (as-synthesized **SPA-2**) is given in blue.

The crystal structures solved from single crystal diffraction data recorded at 100 K for all solvent@**SPA-2** confirmed an unchanged supramolecular framework but the guest molecules could not be localized in the channels.

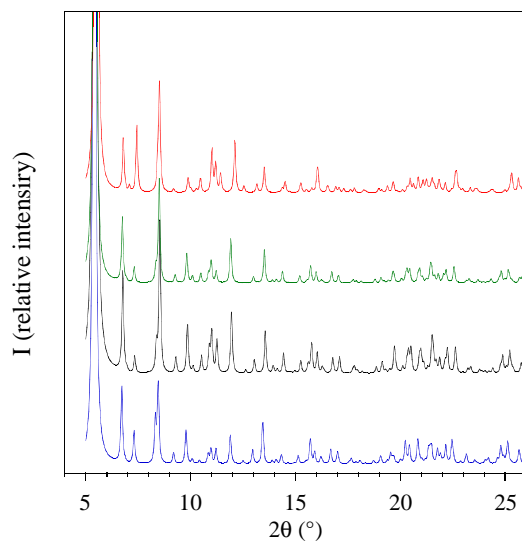


**Figure S17.** D<sub>2</sub>O <sup>1</sup>H-NMR spectra for solvent@SPA-2. Colour codes for SPA-2 crystals soaked in: ethanol (black), methanol (green), isopropanol (pink), acetone (red), THF (blue).

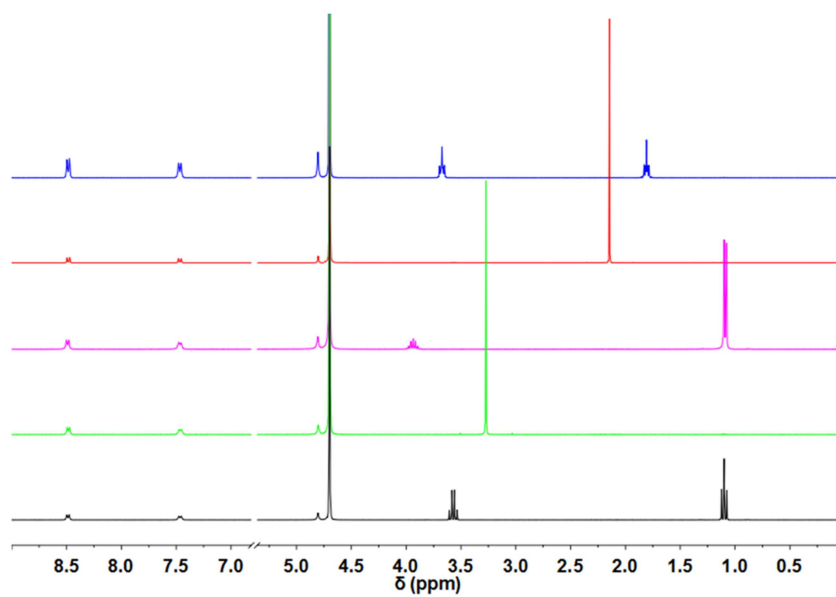


**Figure S18.** ORTEP view of the asymmetric unit of  $\text{CH}_3\text{COOH@SPA-2}$ , with ellipsoids cut at the 30% probability level.  $\text{H}_2\text{O}$  molecules and Hydrogen of Carbon atoms are not represented for sake of clarity. Color codes: C, grey; H, black; N, blue; O, red.

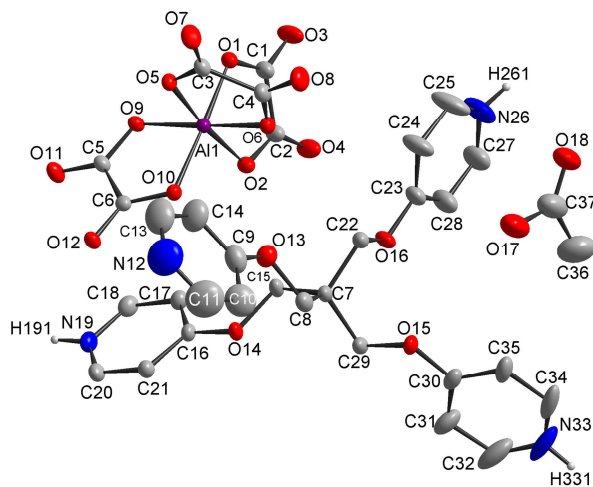


**Figure S19.** ORTEP view of the asymmetric unit of  $\text{CF}_3\text{COOH@SPA-2}$ , with ellipsoids cut at the 30% probability level.  $\text{H}_2\text{O}$  molecules and Hydrogen of Carbon atoms are not represented for sake of clarity. Color codes: C, grey; H, black; N, blue; O, red; F, yellow.

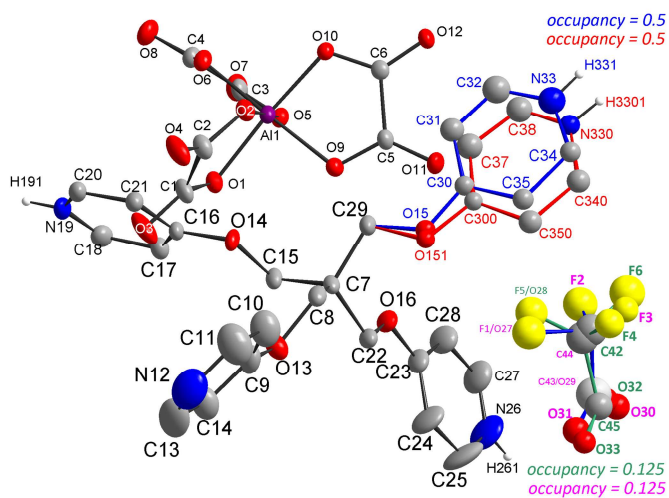
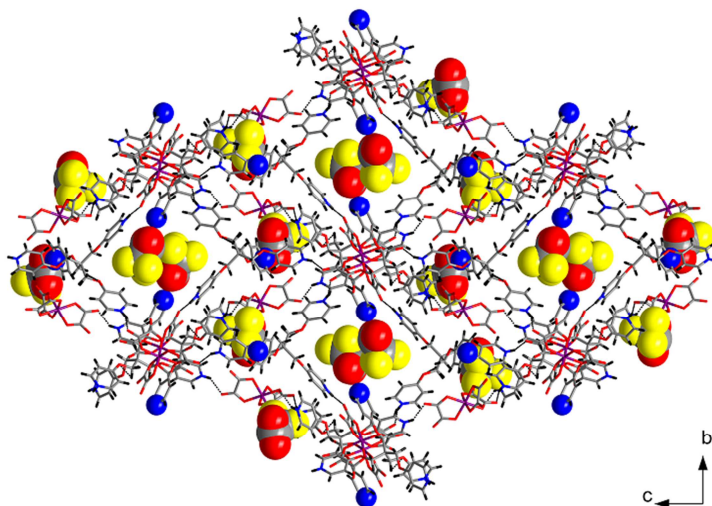


**Figure S20.** Supramolecular architecture of  $\text{CF}_3\text{COOH}@$ **SPA-2**. (a) Ball and stick structure view along the  $a$  crystallographic direction, showing crystallized trifluoroacetic acid guests (spacefill) in the channels. (b) Supramolecular interactions (dashed lines) of crystallized trifluoroacetic acid molecules with the host framework of **SPA-2** ( $d(\text{N12}\cdots\text{O33}) = 2.60 \text{ \AA}$ ;  $d(\text{F5}\cdots\text{C23}) = 3.02 \text{ \AA}$ ).  $\text{H}_2\text{O}$  crystallized solvent molecules are omitted in all cases. Color codes: C, grey; H, black, N, blue; O, red; F, yellow.

a)



b)

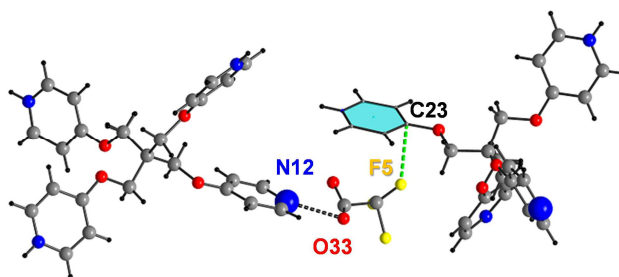


**Figure S21.** ORTEP view of the asymmetric unit of  $\text{CCl}_3\text{COOH}@$ **SPA-2**, with ellipsoids cut at the 30% probability level.  $\text{H}_2\text{O}$  molecules and Hydrogen of Carbon atoms are not represented for sake of clarity. Color codes: C, grey; H, black; N, blue; O, red; Cl, green.

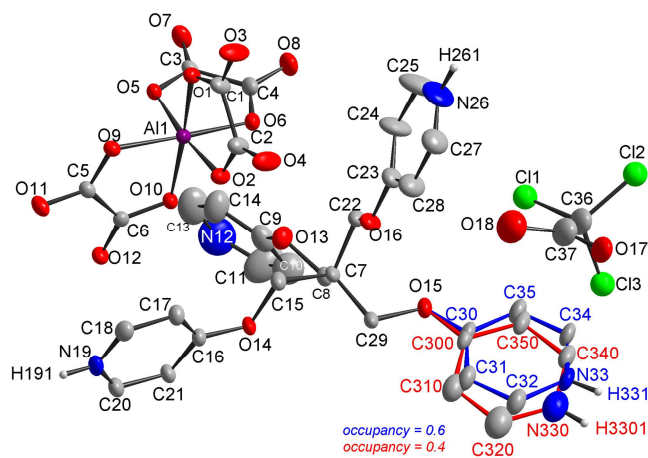


**Figure S22.** Supramolecular architecture of  $\text{CCl}_3\text{COOH}@$ **SPA-2**. (a) Ball and stick structure view along the  $a$  crystallographic direction, showing crystallized trichloroacetic acid guests (spacefill) in the channels. (b) Supramolecular interactions (dashed lines) of crystallized trichloroacetic acid molecules with the host framework of **SPA-2** ( $d(\text{Cl}2\cdots\text{O}4) = 3.26 \text{ \AA}$ ,  $d(\text{Cl}3\cdots\text{O}4) = 3.54 \text{ \AA}$ ,  $d(\text{Cl}3\cdots\text{C}2) = 3.32 \text{ \AA}$ ,  $d(\text{Cl}3\cdots\text{O}2) = 3.27 \text{ \AA}$ ,  $d(\text{Cl}3\cdots\text{O}5) = 3.30 \text{ \AA}$ ).  $\text{H}_2\text{O}$  crystallized molecules are omitted. Color codes: C, grey; H, black; N, blue; O, red; Cl, green.

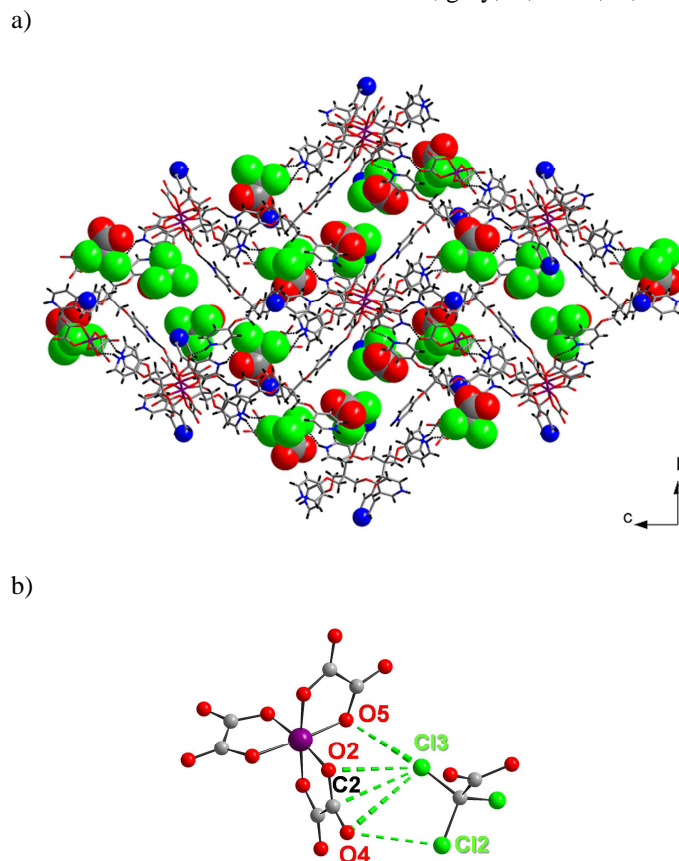
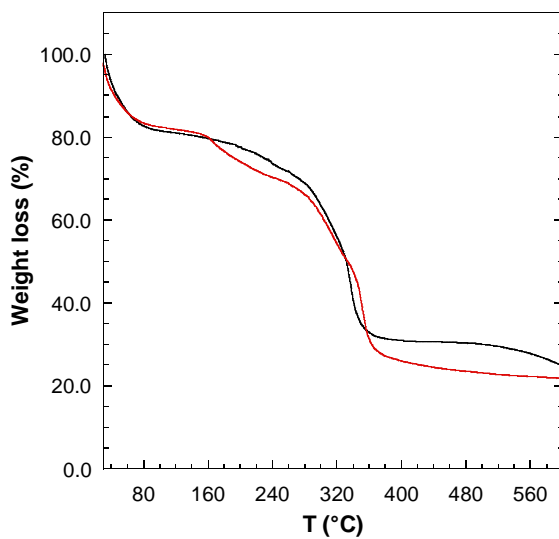
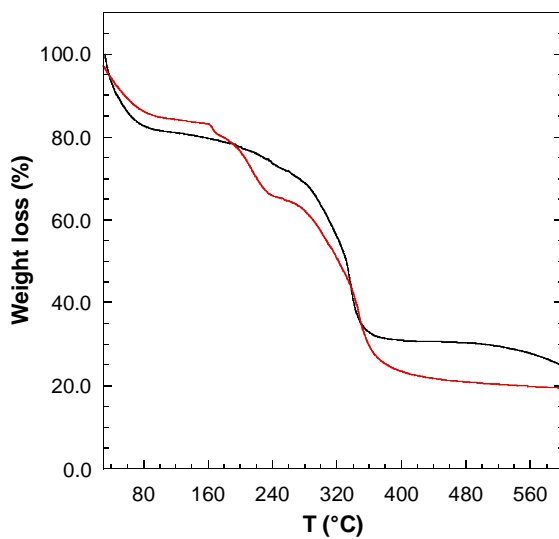


**Figure S23.** Comparison of TGA traces (RT-600°C) for as-synthesized **SPA-2** (black) and acid@**SPA-2** materials (red). (a)  $\text{CH}_3\text{COOH}@$ **SPA-2**, (b)  $\text{CF}_3\text{COOH}@$ **SPA-2** and (c)  $\text{CCl}_3\text{COOH}@$ **SPA-2**.

a)



b)



c)

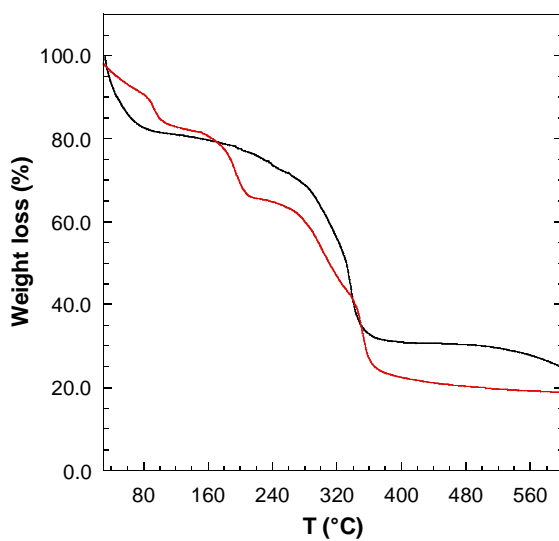


**Figure S24a.** Evolution of the uptake of  $\text{CH}_3\text{COOH}$  by **SPA-2** as a function of the acid concentration (3.0 M-0.3 M - 0.03 M) in EtOH. The number of  $\text{CH}_3\text{COOH}$  molecules per **SPA-2** formula after a given soaking time ( $\circ$ ) was deduced from  $^1\text{H-NMR}$  ( $\text{D}_2\text{O}$ ) of dissolved crystals.

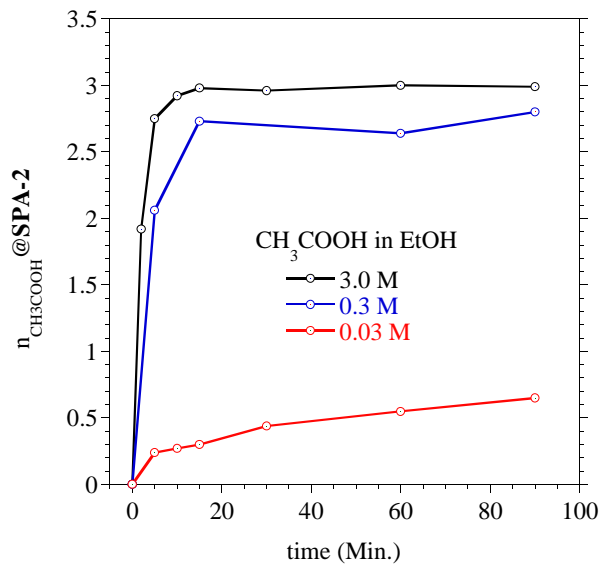


**Figure S24b.**  $^1\text{H-NMR}$  spectra for  $\text{CH}_3\text{COOH@SPA-2}$  crystals dissolved in  $\text{D}_2\text{O}$  before (a) and (b) after crystals washing with ethanol ( $3\times 5$  mL of absolute EtOH, over 15 min). Similar result is obtained in less than 2 minutes when crystals are soaked in 15 mL of absolute ethanol.

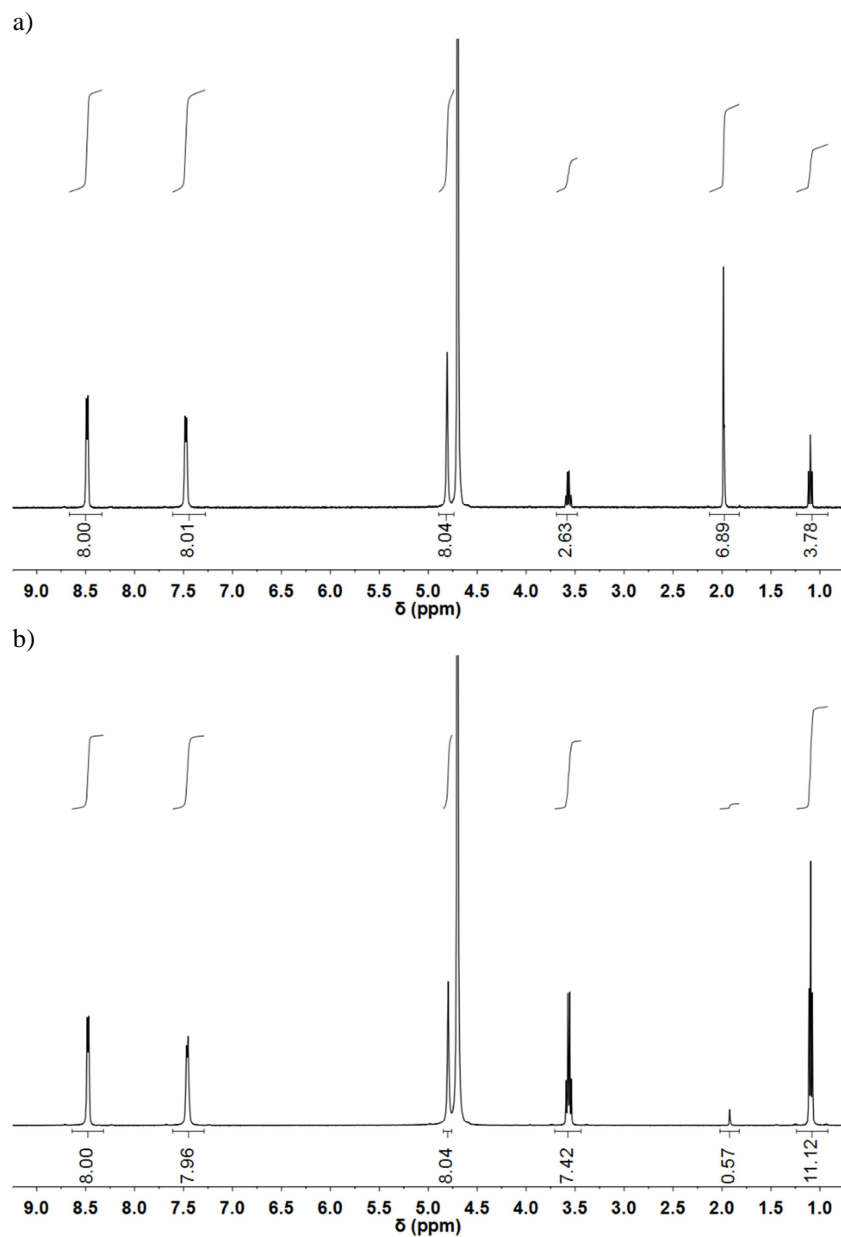


**Figure S25.** Solid state  $^{13}\text{C}$  MAS spectra registered for (a) single crystals of  $\text{CH}_3\text{COOH@SPA-2}$  and for (b)  $\text{CH}_3\text{COOH@SPA-2}$  crystals washed with ethanol. In both a) and b),  $^{13}\text{C}$  MAS experiment with: *top*, direct polarization; *middle*, cross polarization (CP); *bottom*, INEPT polarization (quaternary  $^{13}\text{C}$  atoms are not detected in INEPT experiments). Stars (\*) brand spinning side bands. For  $^{13}\text{C}$  atoms:  $\diamond$ , oxalates;  $\circ$ ,  $\text{H}_3\text{Tpy}^{3+}$ ;  $\square$ , EtOH;  $\bullet$ , acetic acid.

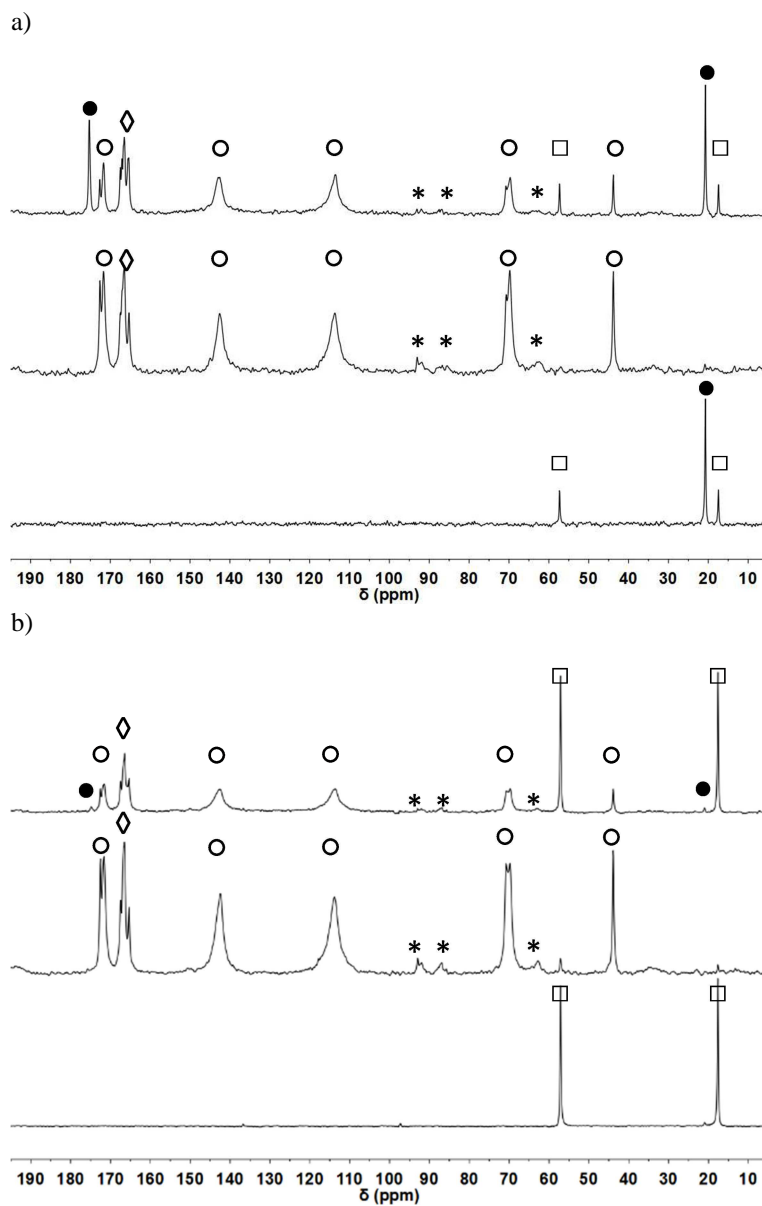


**Figure S26.** Evolution of C-F band ( $1130\text{ cm}^{-1}$ ) intensity observed in IR spectra of  $\text{CF}_3\text{COOH@SPA-2}$  crystals as a function of soaking time in pure EtOH (a) and in Pyridine/EtOH (0.01M, b). In (a) and (b),  $\text{CF}_3\text{COOH@SPA-2}$  starting material IR spectrum is given in green, while **SPA-2** IR spectrum is given in black. In (a), orange spectrum is registered after 124h of soaking. In (b), blue, pink and red spectra are obtained for soaking times of 24h, 48h and 96h, respectively.

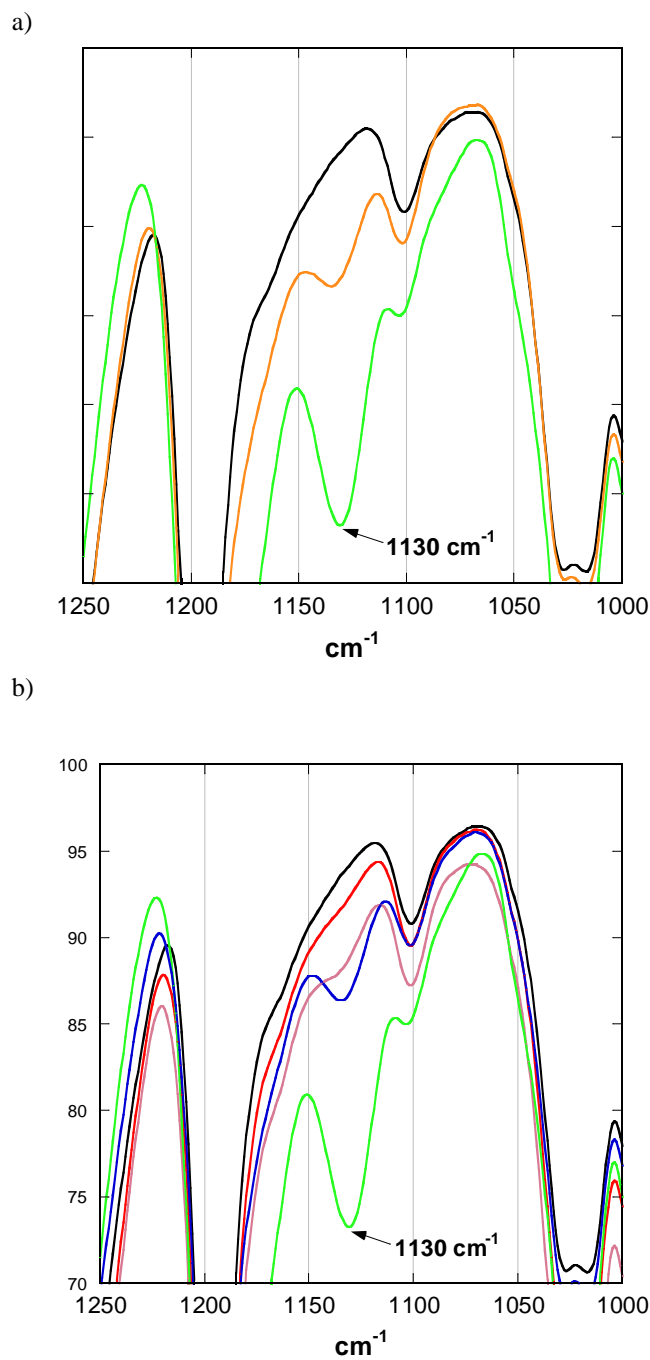


**Figure S27.** D<sub>2</sub>O <sup>1</sup>H-NMR (left) and <sup>13</sup>C NMR (right) spectra for **acid guest@SPA-2**. Spectra are obtained by dissolving crystals of EtOH@SPA-2 starting material (a), CH<sub>3</sub>COOH@SPA-2 (b) and CF<sub>3</sub>COOH@SPA-2 (c) after 90 min of soaking. When visible (CCl<sub>3</sub>- and CF<sub>3</sub>-COOH are <sup>1</sup>H-NMR silent in D<sub>2</sub>O), signals corresponding to the acid guest are tagged with circles (O), while EtOH signals are tagged with squares (□).

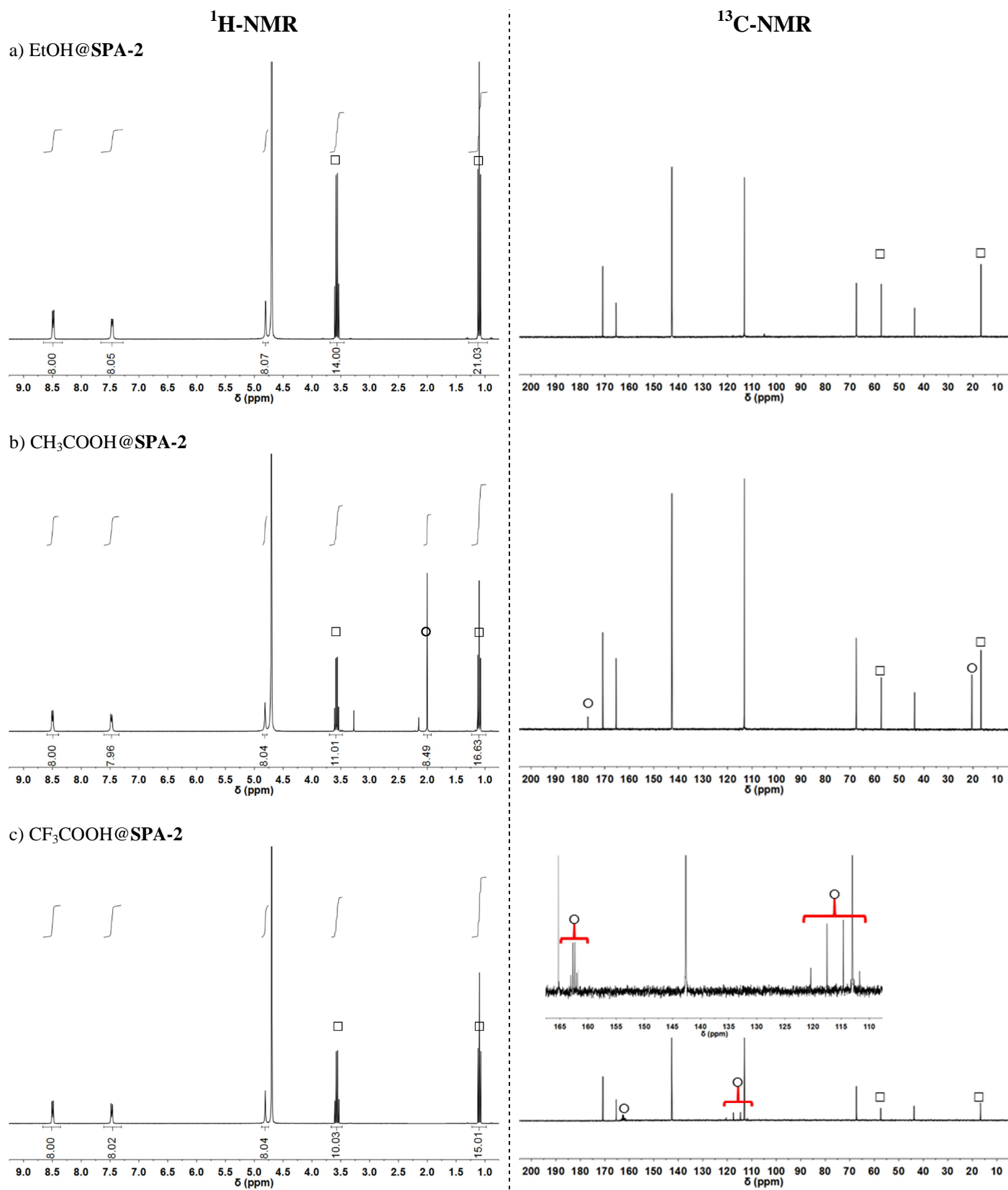


**Figure S28.** D<sub>2</sub>O <sup>1</sup>H-NMR (left) and <sup>13</sup>C NMR (right) spectra for **acid guest@SPA-2**. Spectra are obtained by dissolving crystals of Cl<sub>3</sub>CCOOH@SPA-2 (a), Cl<sub>2</sub>CHCOOH@SPA-2 (b), and ClCH<sub>2</sub>COOH@SPA-2 (c) 2 after 90 min of soaking. When visible (CCl<sub>3</sub>- and CF<sub>3</sub>-COOH are <sup>1</sup>H-NMR silent in D<sub>2</sub>O), signals corresponding to the acid guest are tagged with circles (○), while EtOH signals are tagged with squares (□).

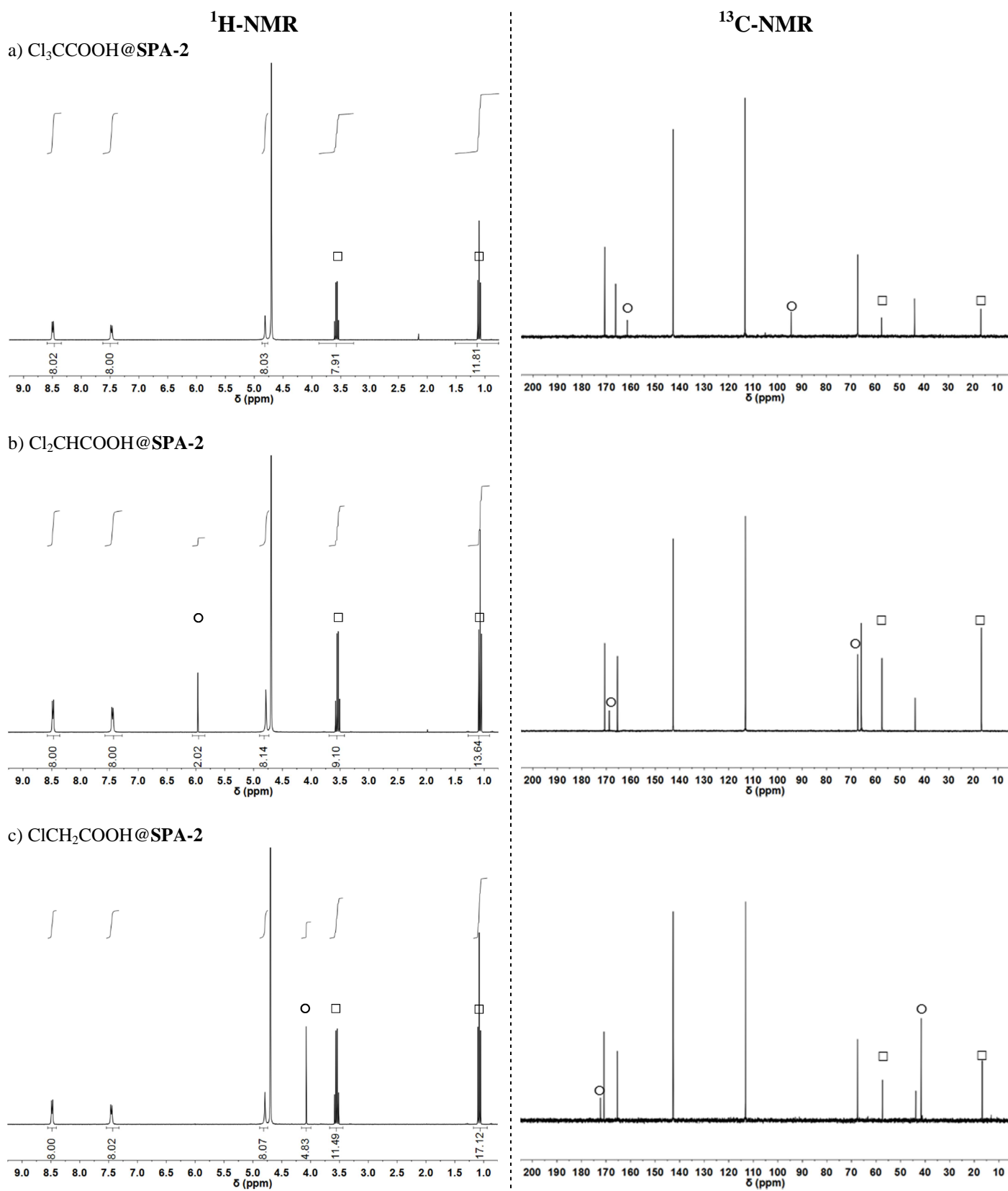


**Figure S29.** D<sub>2</sub>O <sup>1</sup>H-NMR (left) and <sup>13</sup>C NMR (right) spectra for acid@SPA-2 materials obtained through **competitive sorption of acetic acid and its halogenated analogues**. Spectra are obtained by dissolving crystals of SPA-2 soaked 72h in: (a) 3M acetic acid ethanol solution (reference experiment); (b) 3M equimolar trifluoroacetic-/acetic-acid solution; (c) 3M equimolar trichloroacetic-/acetic-acid solution. Ethanol signals are tagged with squares (□), acetic acid signals with open circles (O), and competitive guest signals (when visible) with black circles (●).

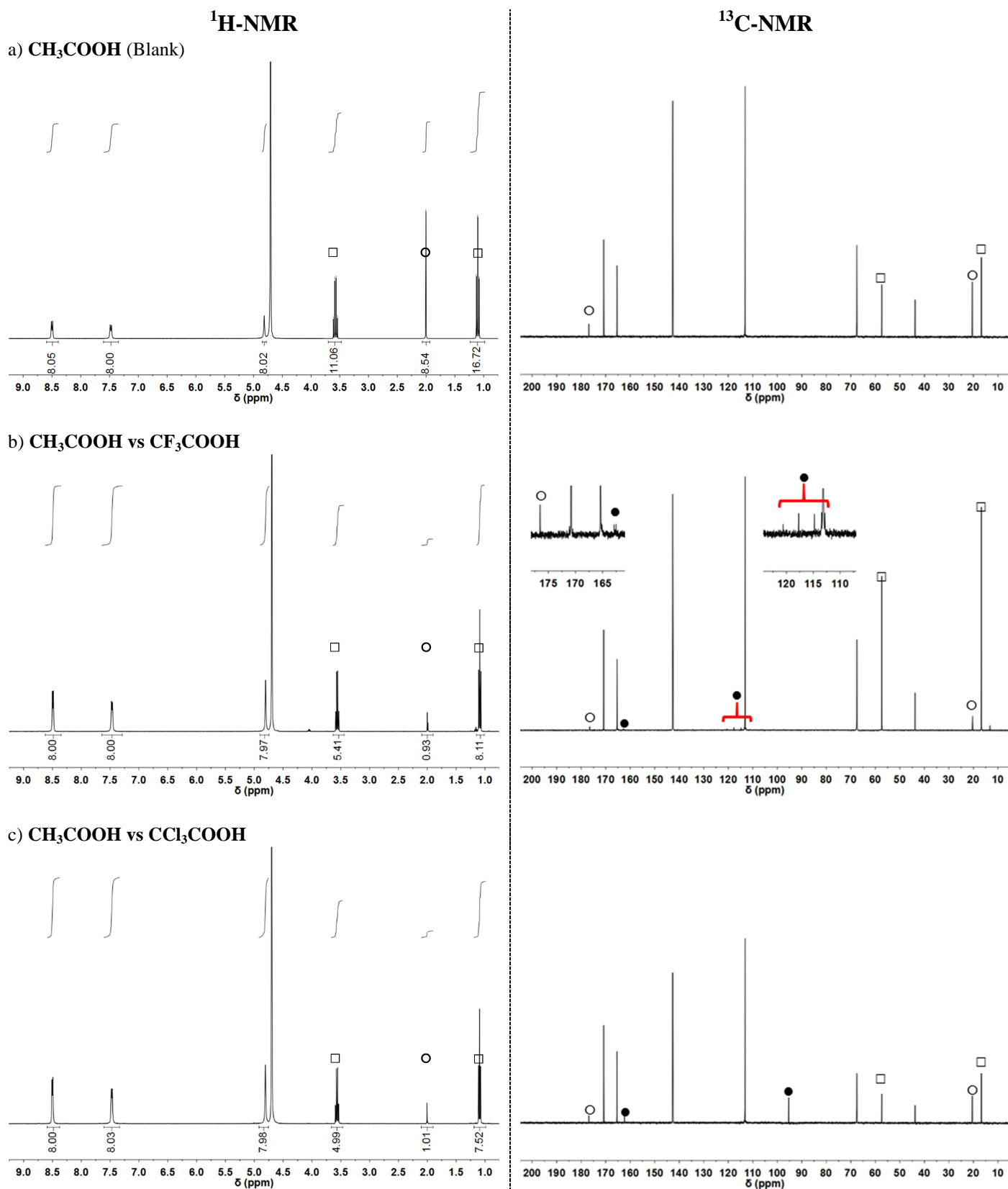


**Figure S30.** D<sub>2</sub>O <sup>1</sup>H-NMR (left) and <sup>13</sup>C NMR (right) spectra for acid@SPA-2 materials obtained through **competitive sorption of acetic acid and its halogenated analogues**. Spectra are obtained by dissolving crystals of SPA-2 soaked 72h in: (a) 3M acetic acid ethanol solution (reference experiment); (b) 3M equimolar dichloroacetic-/acetic-acid solution; (c) 3M equimolar chloroacetic-/acetic-acid solution. Ethanol signals are tagged with squares (□), acetic acid signals with open circles (O), and competitive guest signals (when visible) with black circles (●).

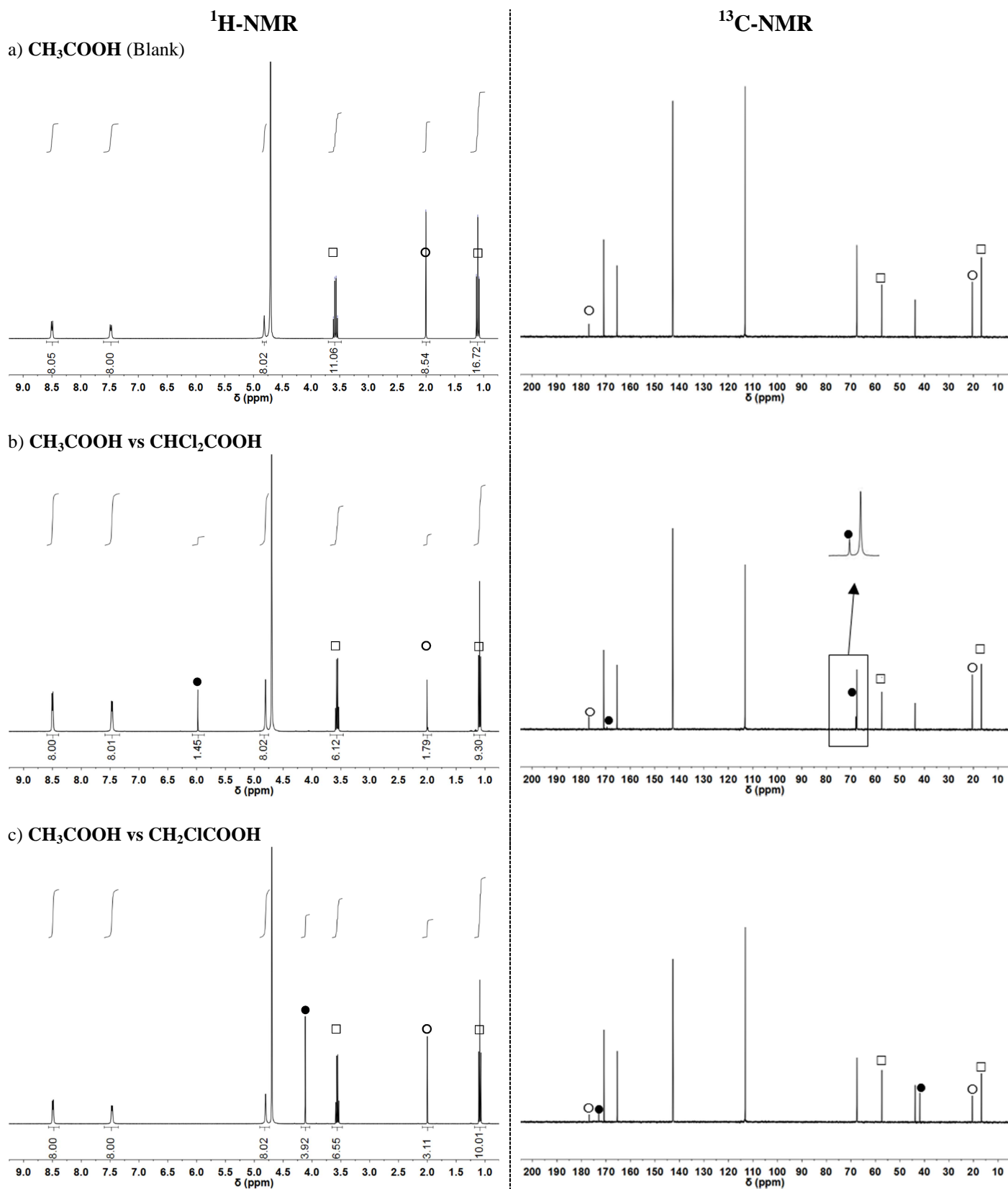


**Figure S31.** D<sub>2</sub>O <sup>1</sup>H-NMR (left) and <sup>13</sup>C NMR (right) spectra for **drug@SPA-2 materials** obtained from **ethanol solutions**. Spectra are obtained by dissolving crystals of: (a) EtOH@SPA-2 starting material; (b) Vitamin C@SPA-2; (c) Mandelic acid@SPA-2. Ethanol signals are tagged with squares (□); guest signals with open circles (○).

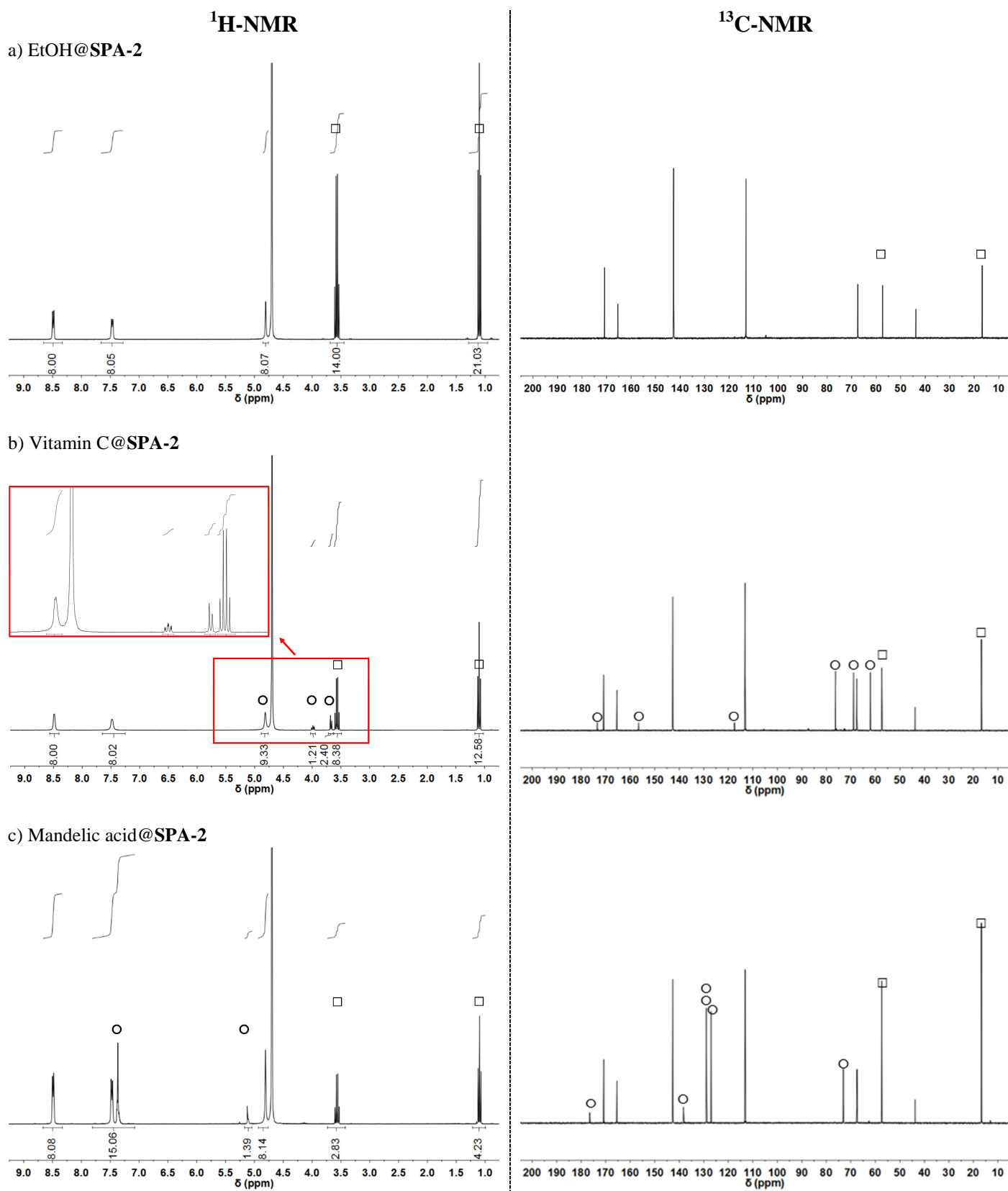


**Figure S32.** D<sub>2</sub>O <sup>1</sup>H-NMR (left) and <sup>13</sup>C NMR (right) spectra for **drug@SPA-2 materials** obtained from **acetone solutions**. Spectra obtained by dissolving crystals of: (a) Acetone@SPA-2 starting material; (b) Aspirin @SPA-2; (c) Mandelic acid@SPA-2. Acetone signals are tagged with squares (□); guest signals with open circles (○).

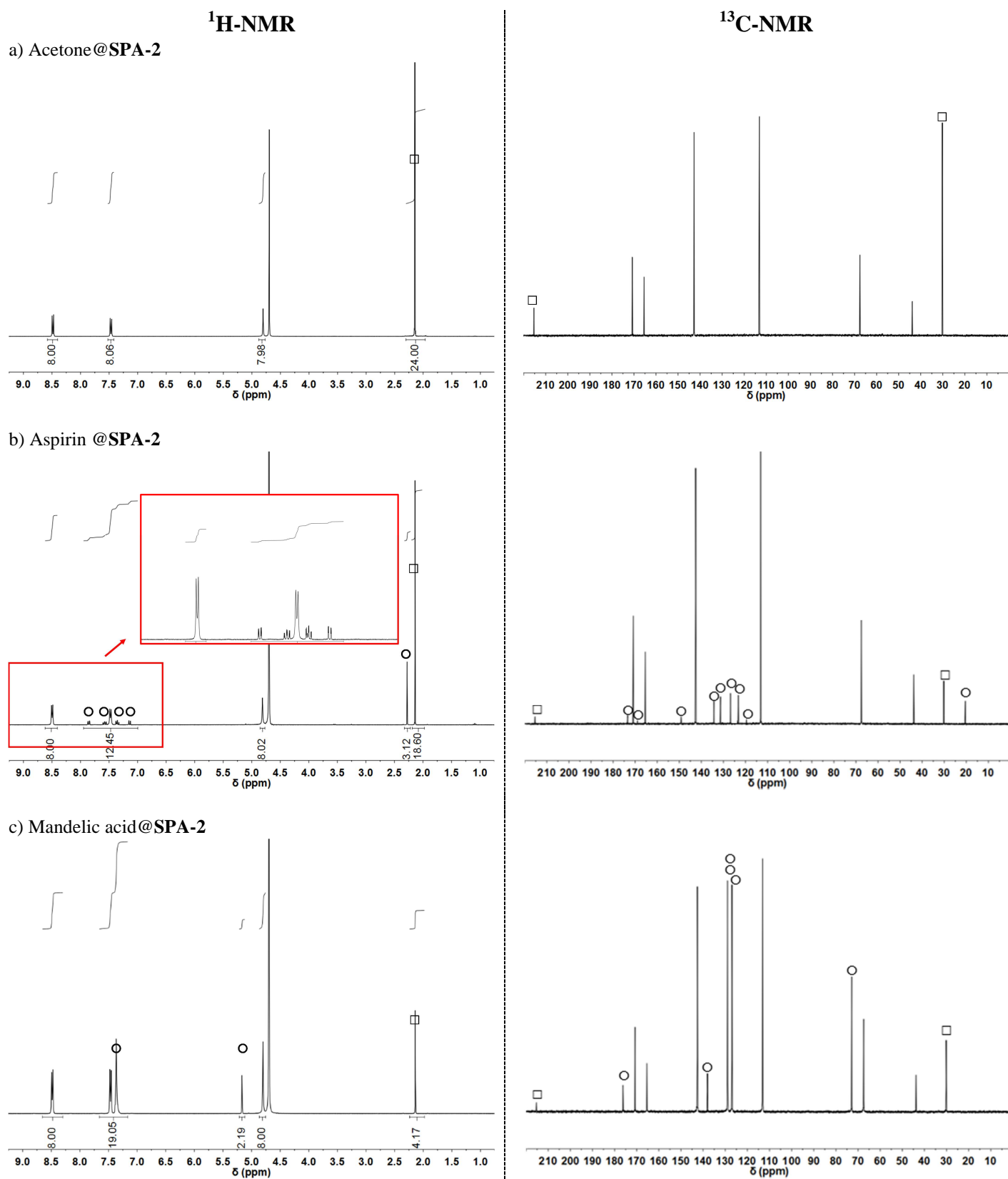


**Figure S33.** Solid state  $^{13}\text{C}$ -MAS spectra registered for single crystals of Vitamin C@SPA-2.  $^{13}\text{C}$  MAS experiment with *top*, direct polarization; *middle*, Cross polarization (CP) ; *bottom*, INEPT polarization (quaternary  $^{13}\text{C}$  atoms are not detected in INEPT experiments). For  $^{13}\text{C}$  atoms:  $\diamond$ , oxalates;  $\circ$ ,  $\text{H}_3\text{Tpy}^{3+}$ ;  $\square$ , EtOH;  $\bullet$ , Vitamin C.

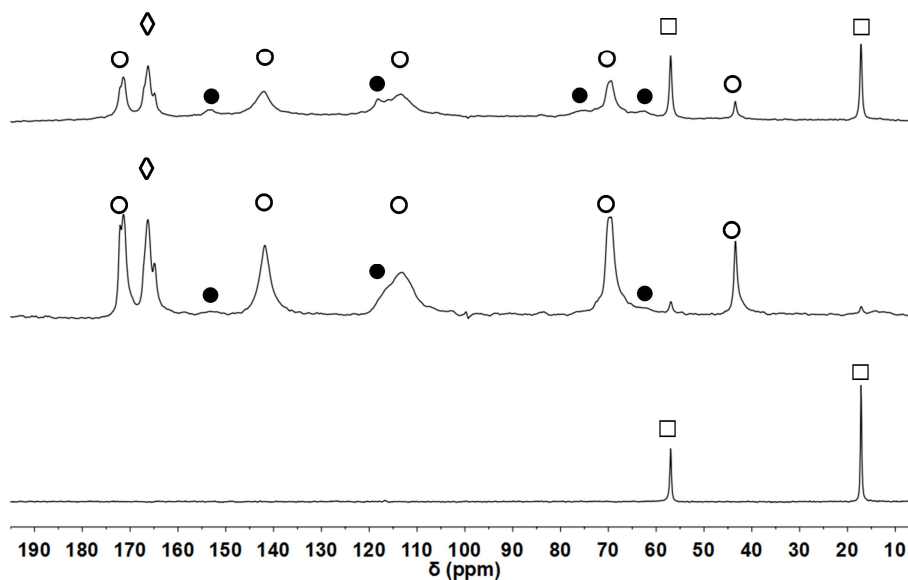


**Figure S34.** Solid state  $^{13}\text{C}$ -MAS spectra registered for single crystals of Aspirin@SPA-2.  $^{13}\text{C}$  MAS experiment with *top*, direct polarization; *middle*, Cross polarization (CP) ; *bottom*, INEPT polarization (quaternary  $^{13}\text{C}$  atoms are not detected in INEPT experiments). For  $^{13}\text{C}$  atoms:  $\diamond$ , oxalates;  $\circ$ ,  $\text{H}_3\text{Tpy}^{3+}$ ;  $\square$ , Acetone;  $\bullet$ , Aspirin.

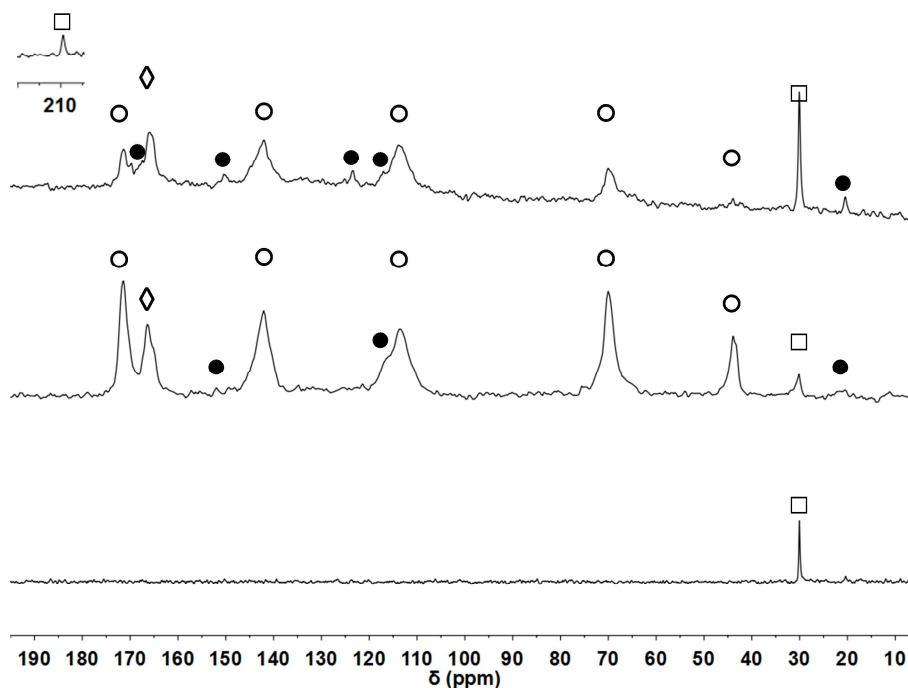


**Figure S35.** Solid state  $^{13}\text{C}$ -MAS spectra registered for single crystals of Mandelic acid@SPA-2.  $^{13}\text{C}$  MAS experiment with *top*, direct polarization; *middle*, Cross polarization (CP) ; *bottom*, INEPT polarization (quaternary  $^{13}\text{C}$  atoms are not detected in INEPT experiments). For  $^{13}\text{C}$  atoms:  $\diamond$ , oxalates;  $\circ$ ,  $\text{H}_3\text{TPy}^{3+}$ ;  $\square$ , Acetone;  $\bullet$ , Mandelic acid.

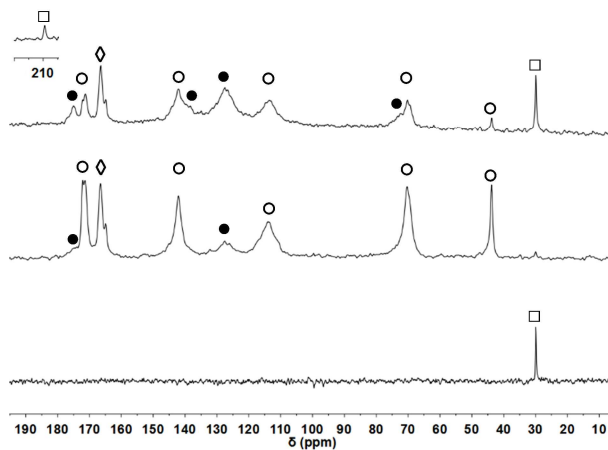


**Figure S36.** PXRD patterns calculated for SPA-2 (red), Vitamin C@SPA-2 (black), Aspirin@SPA-2 (blue) and Mandelic acid@SPA-2 (pink) from cif of respective the compounds. The crystal structures were solved from single crystal diffraction data collected at 110 K for crystals soaked during one week in a drug solution. None of these structures allowed to localize the guest molecules.

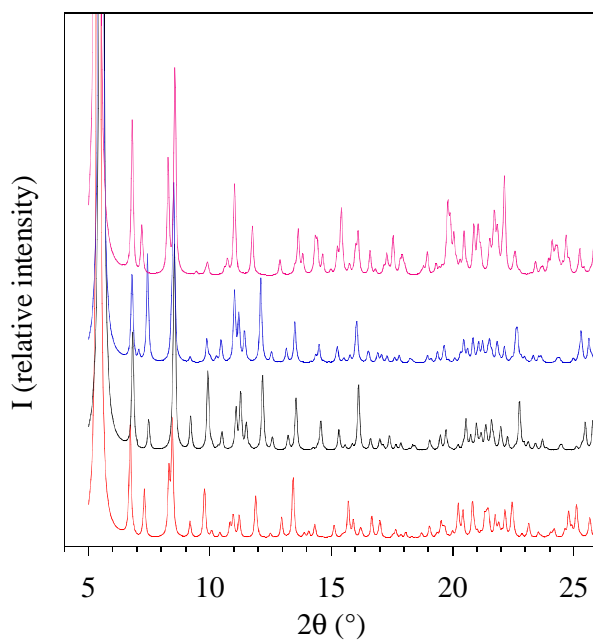
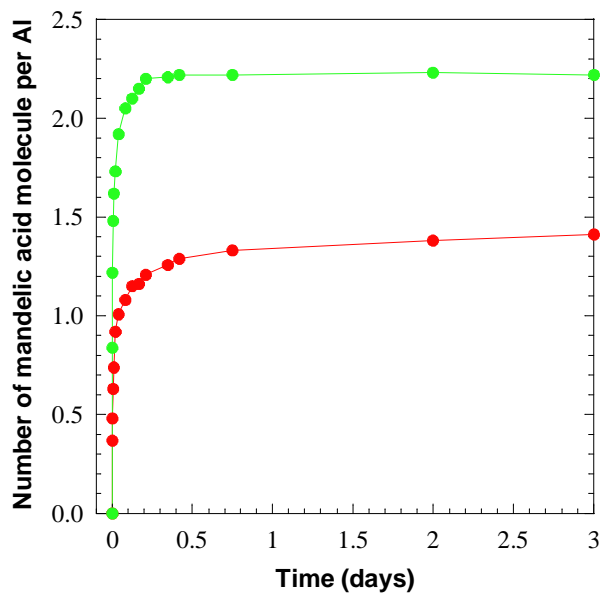


**Figure S37.** Sorption of Mandelic acid in the supramolecular framework of **SPA-2** (up to 3d) from 0.3M ethanol solution (green) and from 0.3M acetone solution (red).



## C. Tables

**Table S1.** Crystallographic data, details of data collection and structure refinement parameters.

Compound	SPA-2·HNO <sub>3</sub>	SPA-2	CH <sub>3</sub> COOH@SPA-2	CF <sub>3</sub> COOH@SPA-2	CCl <sub>3</sub> COOH@SPA-2
Empirical formula	C <sub>31</sub> H <sub>57.50</sub> AlN <sub>5</sub> O <sub>33.75</sub>	C <sub>31</sub> H <sub>48</sub> AlN <sub>4</sub> O <sub>26.50</sub>	C <sub>32</sub> H <sub>42</sub> AlN <sub>4</sub> O <sub>23.50</sub>	C <sub>31.50</sub> H <sub>40.75</sub> AlF <sub>0.75</sub> N <sub>4</sub> O <sub>23.25</sub>	C <sub>31.50</sub> H <sub>38.75</sub> AlCl <sub>0.75</sub> N <sub>4</sub> O <sub>22.25</sub>
Formula weight (g·mol <sup>-1</sup> )	1067.29	927.72	885.68	847.433	882.99
λ (Å)	1.54180	0.71073	1.54180	1.54180	1.54180
Temperature (K)	120	100	100	100	100
Crystal system	Tetragonal	Tetragonal	Tetragonal	Tetragonal	Tetragonal
Space group	<i>P</i> 4 <sub>3</sub> 2 <sub>1</sub> 2	<i>P</i> 4 <sub>1</sub> 2 <sub>1</sub> 2	<i>P</i> 4 <sub>1</sub> 2 <sub>1</sub> 2	<i>P</i> 4 <sub>3</sub> 2 <sub>1</sub> 2	<i>P</i> 4 <sub>3</sub> 2 <sub>1</sub> 2
<i>a</i> = <i>b</i> (Å)	18.04217(16)	18.0205(6)	17.88268(7)	17.81191(16)	17.7691(2)
<i>c</i> (Å)	38.2056(4)	38.4736(13)	38.4329(2)	38.7208(5)	38.7809(6)
Volume (Å <sup>3</sup> )	12436.69(13)	12493.9(4)	12290.48(7)	12284.71(15)	12244.68(18)
<i>Z</i>	8	8	8	8	8
Calc. Density (g·cm <sup>-3</sup> )	1.141	0.996	0.957	0.916	0.958
Absorption coefficient (mm <sup>-1</sup> )	1.040	0.099	0.844	0.691	1.125
Theta range for data collection (°)	3.37-71.29	1.92-26.83	3.38-70.60	3.37-60.61	3.37-71.51
Reflections collected	118999	303826	142422	75622	88941
Independent reflections	12037	13396	11753	9235	11841
<i>R</i> (int)	0.056	0.047	0.025	0.033	0.032
Data/restraints/parameters	10632/2/687	10102/0/554	11209/0/564	8581/21/561	10564/13/554
Goodness-of-fit	0.904	0.956	0.943	1.006	0.975
Refinement on	<i>F</i>	<i>F</i>	<i>F</i>	<i>F</i>	<i>F</i>
Final <i>R</i> indices [ <i>I</i> > 3σ( <i>I</i> )]	0.0722	0.0749	0.0745	0.0842	0.0888
Final <i>wR</i> indices [ <i>I</i> > 3σ( <i>I</i> )]	0.0880	0.0814	0.0808	0.0915	0.0967
Flack parameter, nb Friedel-pairs	-0.02(5), 5239	0.0(2), 5873	0.02(4), 5113	0.04(6), 3967	0.01(4), 5133
Largest diff. Peak and hole (e Å <sup>-3</sup> )	0.90 and -0.33	0.74 and -0.33	0.94 and -0.40	0.61 and -0.40	0.81 and -0.15
CCDC reference	1537662	1537663	1537661	1537660	1537659

**Table S2.** Selected Hydrogen bonds. (H-bonds involving nitrate and acid guests are given in blue).

Atoms D–H...A	Dist. D–H (Å)	Dist. H–A (Å)	Dist. D–A (Å)	Angle D–H ... A (°)
<b>SPA-2·HNO<sub>3</sub></b>				
N19–H191...O11a	0.852	2.045	2.793(4)	146.0
N19–H191...O12a	0.852	2.245	2.887(3)	131.2
N26–H261...O3b	0.868	2.144	2.795(4)	131.4
N26–H261...O4b	0.868	2.123	2.882(4)	145.0
N33–H331...O7c	0.852	1.996	2.756(4)	148.2
N33–H331...O8c	0.852	2.288	2.921(4)	131.3
N12–H121...O18d	0.866	1.904	2.765(7)	172.3
<b>SPA-2</b>				
N19–H191...O11e	0.875	2.112	2.816(4)	136.9
N19–H191...O12e	0.875	2.134	2.846(3)	138.1
N26–H261...O3f	0.861	2.215	2.863(6)	130.0
N26–H261...O4f	0.861	2.022	2.810(6)	148.2
N33–H331...O7g	0.872	2.176	2.856(7)	134.5
N33–H331...O8g	0.872	2.053	2.803(6)	143.7
<b>CH<sub>3</sub>COOH@SPA-2</b>				
N19–H191...O11h	0.876	2.061	2.786(3)	139.6
N19–H191...O12h	0.876	2.216	2.881(3)	132.5
N26–H261...O3b	0.866	2.280	2.858(5)	124.2
N26–H261...O4b	0.866	2.078	2.823(5)	143.7
N33–H331...O7c	0.843	2.104	2.802(6)	139.9
N33–H331...O8c	0.843	2.177	2.860(5)	138.0
N12...H...O18d	-	-	2.993(1)	-
<b>CF<sub>3</sub>COOH@SPA-2</b>				
N19–H191...O11i	0.858	2.092	2.820(4)	142.1
N19–H191...O12i	0.858	2.169	2.851(4)	136.3
N26–H261...O3j	0.862	2.279	2.895(6)	128.5
N26–H261...O4j	0.862	2.036	2.821(7)	151.0
N33–H331...O7k	0.858	2.502	3.051(1)	122.6
N33–H331...O8k	0.858	1.822	2.634(1)	157.3
N330–H3301...O7k	0.859	1.995	2.730(8)	142.9
N330–H3301...O8k	0.859	2.300	2.977(9)	135.9
N12...H...O31l	-	-	2.673(2)	-
N12...H...O33l	-	-	2.603(3)	-
<b>CCl<sub>3</sub>COOH@SPA-2</b>				
N19–H191...O11h	0.859	2.074	2.809(4)	143.1
N19–H191...O12h	0.859	2.199	2.875(3)	135.4
N26–H261...O3m	0.860	2.263	2.879(6)	128.6

N26–H261…O4m	0.860	2.057	2.826(7)	148.4
N33–H331…O7n	0.854	1.879	2.679(5)	155.2
N33–H331…O8n	0.854	2.412	2.973(5)	123.8
N330–H3301…O7n	0.858	2.326	2.930(1)	127.7
N330–H3301…O8n	0.858	1.728	2.491(1)	146.7

*Symmetry operations:* (a)  $1-y, 1-x, 0.5-z$ ; (b)  $y, x, 1-z$ ; (c)  $y, 1+x, 1-z$ ; (d)  $0.5-y, 0.5+x, -0.25+z$ ; (e)  $1.5-y, 0.5+x, -0.25+z$ ; (f)  $0.5+y, 1.5-x, -0.25+z$ ; (g)  $-0.5+y, 1.5-x, -0.25+z$ ; (h)  $1-y, 1-x, 1.5-z$ ; (i)  $0.5+y, 1.5-x, 0.25+z$ ; (j)  $0.5-y, -0.5+x, -0.25+z$ ; (k)  $1.5-y, -0.5+x, -0.25+z$ ; (l)  $0.5+y, 0.5-x, 0.25+z$ ; (m)  $1+y, -1+x, 1-z$ ; (n)  $y, -1+x, 1-z$ .

## D. HRMAS $^1\text{H}$ NMR

**Experimental details :**  $\text{CH}_3\text{COOH}@SPA-2$  was prepared and isolated according to the procedure given in section A-2 above using a microcrystalline powder of **SPA-2**. Same sample of **SPA-2** was used for the High Resolution (HR)MAS  $^1\text{H}$  NMR of that compound.

HRMAS NMR experiments were recorded on a Bruker AvanceII 500 MHz spectrometers. All chemical shifts are relative to TMS. Samples were packed into 4 mm zirconia rotors and spun at 4 kHz at 293K. For  $^1\text{H}$  MAS, small flip angle of  $30^\circ$  were used with recycle delays of 3 s. All pulsed field gradient HRMAS measurements were collected with a stimulated echo sequence with bipolar and spoil gradient pulses. Different diffusion delays between 80 to 500 ms and gradient pulse duration between 1.6 to 4 ms were used in order to measure the high, intermediate and low diffusion coefficients. The strength of the gradient (56.0 Gauss/cm at a current of 10A) was calibrated by measuring the self-diffusion of a pure  $\text{H}_2\text{O}$  solution at 293K ( $2.02 \times 10^{-9} \text{ m}^2 \cdot \text{s}^{-1}$ ). For PGSE-NMR experiments, after Fourier transformation and baseline correction, the diffusion dimension was processed with mono or bi-exponential analysis involving least-squares fitting (Topspin software).

**Figure S38.**  $^1\text{H}$  HRMAS NMR (4 kHz, 293 K) spectra for (top)  $\text{CH}_3\text{COOH}@SPA-2$  and (bottom) **SPA-2**.

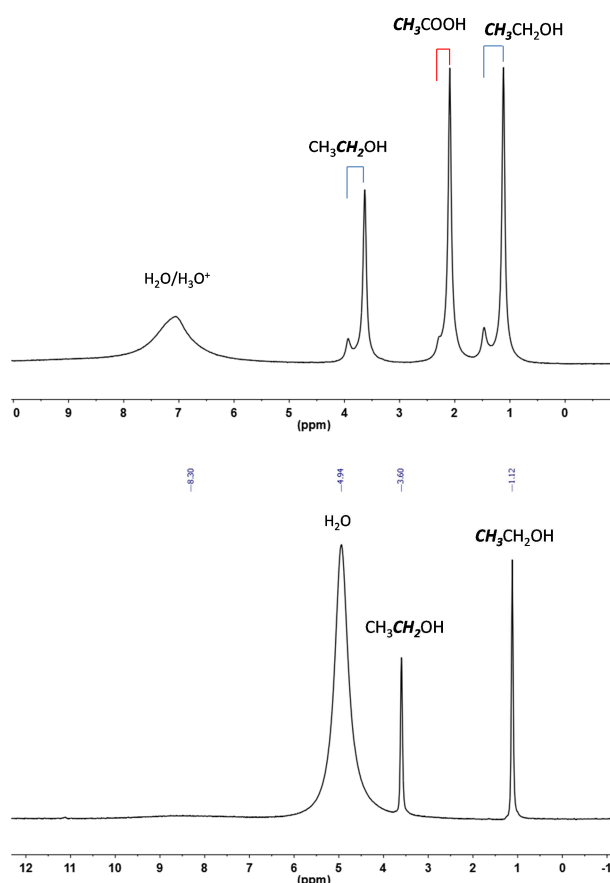


**Figure S39.**  $^1\text{H}$  PFG HRMAS NMR spectra (293 K, 4 kHz) for (top)  $\text{CH}_3\text{COOH@SPA-2}$  and (bottom) for **SPA-2**, showing the intensity variation of the signals for EtOH and for  $\text{CH}_3\text{COOH}$  with the gradient strength.

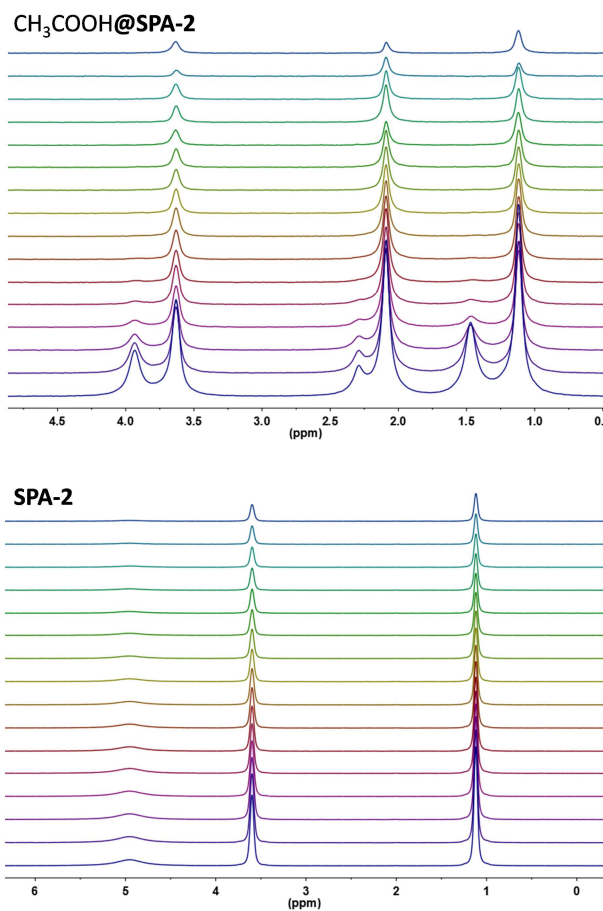
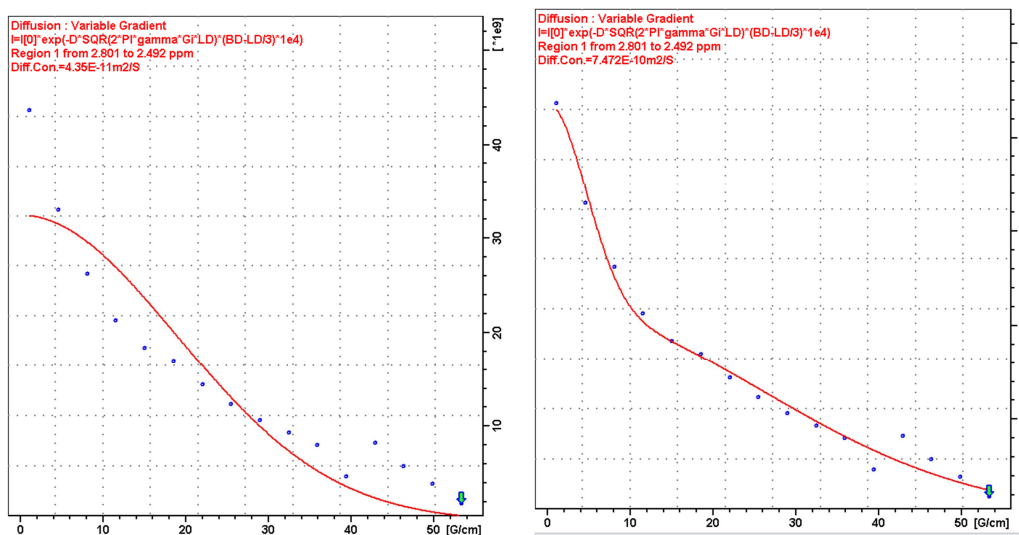


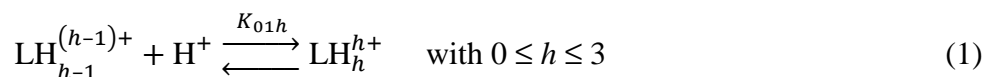
**Figure S40.** Example of single-exponential least-squares fitting analysis (*left*) and bi-exponential analysis least-square fitting (*right*) for the D signal of CH<sub>3</sub>COOH@SPA-2 (Fig. 5, main text). A bi-exponential analysis is obviously required to fit the experimental data.



## E. Acid-Base Properties of the Tpy

**Experimental Potentiometry procedure.** Protonation constants were determined by potentiometric titrations of carefully weighted ( $\pm 0.01$  mg) amounts of compounds dissolved in 10 mL of supporting electrolyte solution (MeOH/H<sub>2</sub>O 8:2 v/v containing 0.2 M KCl in order to maintain the ionic strength and the activity coefficients approximately constant). Temperature was set to 298.2(1) K by circulating water through the jacketed titration vessel. To avoid the ingress of CO<sub>2</sub>, the cell was kept under a blanket of argon that was humidified by bubbling the gas through an identical solution of supporting electrolyte. Standardized reagents (0.2 M KOH and HCl solutions) were prepared in the binary solvent mixture form Titrisol ampoules (Merck) and analytical-grade methanol (Carlo Erba) and kept under argon. The experimental setup and general procedure were identical to those described elsewhere in detail.<sup>1</sup> Prior to each experiment, the glass-electrode was soaked for at least 30 min in the supporting electrolyte solution and then calibrated in concentration units by performing a strong acid-strong base titration ( $p[H] = -\log [H^+]$ ). The autoprotolysis constant of water in the methanolic medium ( $pK_w = 14.10$ ,  $I = 0.2$  M KCl,  $T = 298.2(1)$  K) was determined independently by the method of Fischer and Byé.<sup>2</sup> The titration data were analyzed using the HYPERQUAD 2013 program.<sup>3</sup>

**Acid-Base Properties of the Tpy Building Block.** The tetrapyrnidinium cation  $[H_4Tpy]^{4+}$  (Tpy stands for tetrakis(4-pyridyloxymethyl)methane)) of tetrahedral geometry is one of the key component of the supramolecular porous architecture **SPA-2** described herein. As pyridyl moieties are well known to act as weak bases, it appeared crucial to investigate the acid-base properties of the conjugated free-base Tpy. For solubility reasons, potentiometric titrations were carried out in a methanol-rich binary solvent mixture with water (MeOH/H<sub>2</sub>O 80:20 v/v). Ionic strength ( $I = 0.2$  M KCl) and temperature ( $T = 298.2(1)$  K) were strictly controlled during each experiment, while CO<sub>2</sub> was excluded from the headspace of the titration vessel by maintaining it under a slight overpressure of argon. Upon adding a slight excess of base (0.2 M KOH), the titration curves recorded by incremental addition of a standardized 0.2 M HCl solution display two sharp inflection points, corresponding to the neutralization of the added strong base and to the addition of 4 equivalents of acid per molecule of Tpy, respectively. Thus, the tetrapyrnidyl derivative Tpy behaves, as expected, as a tetraprotic base, with four stepwise-protonation constants ( $K_{01h}$ ,  $h = 1-4$ , eq 1-2) lying closely together in the range accessible to a glass-electrode.



$$K_{01h} = \frac{[LH_h^{h+}]}{[LH_{h-1}^{(h-1)+}][H^+]} \quad (2)$$

$$\beta_{01h} = \prod_{i=1}^h K_{01i} \quad (3)$$

Their numerical values were deduced from the global equilibrium constants  $\beta_{01h}$  (eq 3) refined using the nonlinear least squares program HYPERQUAD 2013.<sup>3</sup> Their average corresponding to four independent titrations, together with their associated standard deviation, are listed in Table S3. Accordingly, it can be concluded that Tpy behaves a weak base prevailing at more than 99% above pH 7.8, while  $[\text{H}_4\text{Tpy}]^{4+}$  is formed at more than 99% below pH 2.33 in the 80:20 v/v methanol/water mixture.

**Table S3.** Apparent Stepwise Protonation Constants ( $K_{01h}$ ) of Tpy and Model Ligands Determined by potentiometry in MeOH/H<sub>2</sub>O 80:20 v/v,  $I = 0.2$  M KCl,  $T = 298.2(1)$  K.

Ligand	log $K_{011}$	log $K_{012}$	log $K_{013}$	log $K_{014}$
Tpy	5.8(2)	5.04(7)	4.8(1)	4.3(1)
Pyridine	3.87(1)			
	5.21, <sup>a</sup> 5.24 <sup>b</sup>			
(4-MeO)Pyridine	6.47, <sup>c</sup> 6.58 <sup>d</sup>			

<sup>a</sup> Solvent: pure MeOH,  $T = 298.2(1)$  K.<sup>4</sup> <sup>b</sup> Solvent: water,  $I = 0.1$  M KCl,  $T = 298.2(1)$  K.<sup>5</sup>

<sup>c</sup> Solvent: water,  $I \sim 0$ ,  $T = 298.2(1)$  K.<sup>6</sup> <sup>d</sup> Solvent: water,  $I \sim 0$ ,  $T = 298.2(1)$  K.<sup>7</sup>

For comparison purposes, the protonation constant of pyridine has also been determined under the same experimental conditions. The experimental  $K_{011}$  value is about 1.3 logarithmic units lower compared to those reported in the literature for both pure solvents. This observation follows a general trend among amines, as their protonation constants drop by up to about 1.2 log units with increasing amounts of methanol until a minimum is reached for alcohol contents of about 70–80%.<sup>8</sup> Hence, a decrease of similar magnitude of log  $K_{011}$  is expected for the model compound, 4-methoxypyridine, with respect to the values reported in aqueous media (log  $K_{011} \sim 6.5$ –6.6).<sup>6</sup> Owing to the electron donating character of a methoxy group, 4-methoxypyridine is more basic than the unsubstituted heterocycle, with an estimated log  $K_{011}$  of ca. 5.2 in 80% methanol. Interestingly, this value falls very close to the average of the four protonation constants measured for Tpy (log  $K_{av} = 5.0$ ).

As this compound possesses four strictly identical chains, it is worthwhile to discuss the relative magnitude of the free-energy cost of protonating a pyridyl group in the neighborhood of positively charged pyridinium moieties, which is reflected by the  $\Delta_{ij}$  parameter ( $\Delta_{ij} = \log K_{01i} - K_{01j}$  with  $j = i + 1$ ). As encountered for the vast majority of systems, the stepwise binding constants decrease steadily as the number of protons taken up by the ligand increases, a phenomenon classically referred to non-cooperativity (i.e. binding of an additional substrate cost more and more energy). Compounds that derogate from that rule, also called cooperative systems, are extremely seldom as far as protonation is concerned.<sup>9</sup> Two main contributions usually account for the gradual decrease in basicity: the ever-increasing electronic repulsion energy between positively charged species and the

statistical factor. The latter effect, which relates to the probability of the entering substrate to find an unoccupied binding site, can be easily factored out for a polytopic receptor having  $t$  identical and independent sites (i.e. statistical binding). For a  $t = 4$  as encountered herein, it can be demonstrated that statistical binding events result in an affinity decrease in the order of  $4Q < {}^3/2Q < {}^2/3Q < {}^1/4Q$ , where  $Q$  is the site-specific or intrinsic binding constant which equals the average the four stepwise binding constants.<sup>10</sup> Under such circumstances, it follows that  $\Delta_{1,2} = \Delta_{3,4} = \log {}^8/3 \sim 0.426$  and  $\Delta_{2,3} = \log {}^9/4 = 0.352$ . Larger differences between experimental stability constants than those corresponding to the aforementioned statistical factors can therefore be assigned to coulombic effects. For Tpy, the observed gaps between the apparent protonation constants ( $\Delta_{1,2} = 0.8$ ,  $\Delta_{2,3} = 0.2$ , and  $\Delta_{3,4} = 0.5$ ) come close to these threshold values, highlighting the rather independent behavior of each pyridyl arm.

## REFERENCES

- (1) a) Cuenot, F.; Meyer, M.; Espinosa, E.; Bucaille, A.; Burgat, R.; Guillard, R.; Marichal-Westrich, C., *Eur. J. Inorg. Chem.*, **2008**, 267; b) Meyer, M.; Frémond, L.; Tabard, A.; Espinosa, E.; Vollmer, G. Y.; Guillard, R.; Dory, Y., *New J. Chem.*, **2005**, 29, 99; c) Ranyuk, E.; Uglov, A.; Meyer, M.; Bessmertnykh-Lemeune, A.; Denat, F.; Averin, A.; Beletskaya, I.; Guillard, R., *Dalton Trans.*, **2011**, 40, 10491.
- (2) Fischer, R.; Byé, J., *Bull. Soc. Chim. Fr.*, **1964**, 2920.
- (3) Gans, P.; Sabatini, A.; Vacca, A., *Talanta*, **1996**, 43, 1739.
- (4) Augustin-Nowacka, D.; Makowski, M.; Chmurzynski, L., *Anal. Chim. Acta*, **2000**, 418, 233.
- (5) Martell, A. E.; Smith, R. M.; Motekaitis, R. J.; 8.0 ed.; NIST Standard Reference Database No. 46: Gaithersburg, MD, 2004.
- (6) Murmann, R. K.; Basolo, F., *J. Am. Chem. Soc.*, **1955**, 77, 3484.
- (7) *Handbook of Chemistry and Physics*; 85 ed.; Lide, D. R., Ed.; CRC Press: Boca Raton, 2005.
- (8) Rorabacher, D. B.; MacKellar, W. J.; Shu, F. R.; Bonavita, M., *Analytical Chemistry*, **1971**, 43, 561.
- (9) a) Chambron, J.-C.; Meyer, M., *Chem. Soc. Rev.*, **2009**, 38, 1663; b) Graf, E. Ph-D, Université L. Pasteur, 1979; c) Meyer, M.; Frémond, L.; Espinosa, E.; Brandès, S.; Vollmer, G. Y.; Guillard, R., *New J. Chem.*, **2005**, 29, 1121; d) Potvin, P. G.; Wong, M. H., *Can. J. Chem.*, **1988**, 66, 2914.
- (10) Perlmutter-Hayman, B., *Acc. Chem. Res.*, **1986**, 19, 90.